Micro to Macro: Improving the Resolution for Monitoring of Cyanobacteria in Small Urban Lake

Thesis

Presented in Partial Fulfillment of the Requirements for the Degree Master of Science in the Graduate School of The Ohio State University

By

Kendall Preston Byrd

Graduate Program in Environmental Science

The Ohio State University

2023

Thesis Committee

Dr. Jiyoung Lee, Advisor

Dr. Motomu Ibaraki

Dr. Rongjun Qin

Dr. Joseph Ortiz

Abstract

As increases in frequency, duration, intensity, and geographical location of cyanobacterial harmful algal blooms (HABs) have been observed, more timely monitoring and targeted treatment of HABs and their cyanotoxins are crucial for freshwater bodies that are used for drinking water, recreation, and food production sources. To combat this, new management practices with tools that can handle the spatial and temporal variability of HABs are needed for water treatment plants and other sectors to ensure human health and ecosystem health. Unmanned Aerial Vehicles (UAVs), also known as drones, serve as one solution for near real-time monitoring of HABs. Recently, UAVs have gained increasing interest in research and development due to their many applications, efficiency in data collection, and the ability to customize these systems to specific needs.

While research has shown that UAVs can accurately estimate chl-a and phycocyanin values -HAB indicators- little research has been conducted analyzing UAV imagery in parallel with microbiome data. In chapter 1, major relevant topics are summarized related to cyanoHABs, public health, and UAV systems. This provides a holistic view of current knowledge, methods, and limitations in cyanoHAB monitoring and detection. Chapter 2 seeks to explore the microbial community in parallel with environmental data, by analyzing seasonal dynamics, composition, and interactions

within the microbial community in a hypereutrophic urban lake. In chapter 3, the feasibility and accuracy of using an UAV system for monitoring a hypereutrophic, urban water body was assessed. Objectives of this chapter include 1) proposing an UAV system and imagery processing framework that can be utilized by non-geospatial experts, 2) assess the accuracy of UAV derived chlorophyll-a values by regressing ground sampled fluorometer values and remotely sensed values, and 3) determine what algorithms and buffer sizes perform the best for cyanobacteria quantification.

To accomplish this, fourteen field sampling campaigns were conducted at an urban lake in Columbus, OH, USA from April 2022 through September 2022. During each field visit aerial imagery, water samples, meteorological data, and water quality data were collected. Microcystin quantification was employed utilizing ELISA kits to evaluate cyanotoxin levels for each visit. Microbial source tracking (MST) was utilized to evaluate major fecal contamination sources (human, canine, and geese). Droplet digital PCR was utilized to quantify the level of MST host contamination. 16S and 18S rRNA gene sequencing was conducted so shifts in the microbial community could be analyzed. All data was analyzed and correlations between UAV aerial imagery, microbial community, and water quality/meteorological data were discovered. Results found that microbial community composition changes seasonally, including the cyanobacteria community. This study shows that UAV imagery is an efficient tool for monitoring HABs, but more research needs to be conducted to better understand factors negatively affecting the accuracy of UAV derived chlorophyll-a values.

Dedication

I would like to dedicate this body of work to my undergraduate mentors, Dr. Zachary Felix and Keith Ray. Without their guidance I do not believe I would have found my passions in life or pursued them. They molded me into a better student, but more than that they taught me how to find and explore the hidden beauties in nature. They planted a seed of appreciation for the natural world in me and when needed, reminded me to never lose sight of what I really want out of life. To never sacrifice my true desires, no matter the offer. For their guidance and friendship, I will forever be grateful.

Acknowledgments

I would like to begin by thanking my advisor, Dr. Jiyoung Lee. Her work ethic, consistency, and knowledge within our field of study is admirable and incomparable. Without her example and guidance, I would not have experienced the academic growth I have had in the past two years. Additionally, I would like to thank all my lab mates for their help, guidance, and friendship over the past two years. Without their help, this research would not have been possible. Next, I would like to thank my committee members Dr. Motomu Ibaraki, Dr. Rongjun Qin, and Dr. Joseph Ortiz. Each of these provided guidance and expertise throughout the project. Lastly, I would like to thank my family and friends for their support throughout my work. To my family, Ronnie, Jennifer, Walker, and Foster, thank you for the encouragement and support during this portion of my academic journey. To my friends Michael Carew, Jonathan Ragsdale, Jordan Pitt, Cy Marchese, and others, thank you for pushing me and constantly reminding me of my purpose. Through the highs and lows that come with research, you were there and for that I am thankful.

Vita

May 2016…… H.S. Diploma, Model High School

May 2020…… B.S. Biology, Reinhardt University

2017…… Undergraduate Research Assistant, Reinhardt University

2017-2018…….... Kennel Assistant, Riverstone Animal Hospital

2020…… Service Coordinator, Aquatic Environmental Services

2021……... Contracted Drone Pilot, SkyTec LLC

2021-Current……... Graduate Research Assistant, The Ohio State University

Publications

Lancaster, E., Byrd, K., Ai, Y., & Lee, J. (2022). Socioeconomic status correlations with confirmed COVID-19 cases and SARS-CoV-2 wastewater concentrations in small-medium sized communities. Environmental Research, 215, 114290. https://doi.org/10.1016/j.envres.2022.114290

Fields of Study

Major Field: Environmental Sciences

Research Department: Environmental Health Sciences, College of Public Health

Table of Contents

List of Tables

List of Figures

Chapter 1. Introduction

1. Cyanobacteria, Harmful Algal Blooms, and Water Quality

1.1 Introduction to Cyanobacteria

Cyanobacteria, also referred to as blue-green algae, are an ancient phylum of prokaryotic microorganisms, with fossil evidence dating back approximately 3.5 billion years (Schopf, 1987, Barwant, 2022). The term "blue-green algae" is derived from their characteristic blue-green pigmentation, which is a result of the presence of a unique pigment known as phycocyanin (PC) (Hachicha et al., 2022). Cyanobacteria are oxygenic phototrophs, meaning they perform oxygenic photosynthesis, a process that utilizes sunlight to convert carbon dioxide into organic compounds, while releasing oxygen as a byproduct (Sánchez-Baracaldo & Cardona, 2020). It is believed that these microorganisms played a critical role in the first major oxygenation event on Earth, allowing for the emergence and evolution of aerobic organisms such as plants and animals (Lyons et al., 2014). Cyanobacteria are extremely adaptable microorganisms, occupying many different environments, including freshwater systems, marine environments, ice caps, and hot springs. This adaptability has resulted in cyanobacteria occupying almost every habitable environment on Earth (Díez & Ininbergs, 2014). In addition to the historical roles filled by cyanobacteria, they still play crucial ecological roles today such as global carbon and nutrient cycling. In fact, these organisms account for 20-30% of Earth's photosynthetic productivity (Lee et al., 2017). Some species can fix atmospheric nitrogen, converting it into biologically available

forms useful to other microorganisms. This aids in the growth and proliferation of these other microorganisms (Sahu et al., 2012).

Beyond their ecological roles, cyanobacteria have recently attracted industrial interest, due to their potential applications as a new biotechnology in many fields. Researchers have explored cyanobacterial cell mass and their associated pigments as a source of biofuel, biofertilizers, pharmaceuticals, cosmetics, food colorants, food sources, and antibody labeling (Gierhart n.d., Nagarkar et al. nn.d., Rastogiet al., 2016). Currently, many researchers are focused on enhancing the variety, productivity, and concentration of cyanobacteria derived products by utilizing metabolically and genetically engineered strains (Saini et al., 2018). Despite these beneficial attributes of cyanobacteria, many challenges still exist in harnessing their full potential. In addition, climate change and anthropogenic impacts, such as over nutrification, due to agricultural runoff, dumping, and effluent from sewage treatment plants have led to an increase in cyanobacterial harmful algal blooms (cyanoHABs) (Brown et al., 2021). This results in negative impacts within aquatic ecosystems, local economies, and public health.

1.2 Freshwater CyanoHABs: Bloom Formation, Persistence, and Impacts

1.2.1 Formation

Due to anthropogenic impacts and climate change, increases in frequency, duration, intensity, and geographical location of cyanoHABs have been observed (Shi et al., 2019). This has resulted in freshwater cyanoHABs becoming a growing concern worldwide, due to their negative effects on aquatic ecosystems, local economies, and human health. Cyanobacterial cyanoHABs are defined as abundances of cyanobacterial biomass that are significantly higher than a water bodies' average bacterial population. Simply put, cyanoHABs are the excessive

growth of cyanobacteria in water (Cheung et al., 2013). Due to their extensive evolutionary history, cyanobacteria have many traits enabling them to adapt to climatic and anthropogenic impacts on water systems such as eutrophication, changing water levels, and salinization (Paerl & Otten, 2013). For example, many species can fix atmospheric nitrogen (dinitrogen) during aerobic conditions in response to certain environmental cues (Herrero et al., 2001). This provides cyanobacteria with a competitive advantage when the ratio of nitrogen and phosphorus is low and nitrogen availability is the limiting factor for phytoplankton growth (Dolman et al., 2012).

The formation of cyanoHABs is influenced by a combination of physical, chemical, and biological factors. Although still an ongoing area of research, it is thought that nutrient loadings, light intensity, temperature, oxidative stressors, and interactions with other microbiota all contribute to cyanoHAB formation (Cheung et al., 2013). While cyanoHAB formation is complex, research has shown that high nutrient concentrations are required for cyanobacteria to obtain high biomasses. Specifically, phosphorus and nitrogen have been shown to be limiting factors in cyanoHAB formation (Andersson et al., 2015). It has been known for some time that phosphorus is essential for cyanoHAB formation, but more recently nitrogen has been shown to be a limiting nutrient in freshwater systems. Especially in water systems harboring cyanobacteria species without the ability to fix atmospheric nitrogen, including *Microcystis* and *Planktothrix* (Paerl & Otten, 2013). Additionally, research has shown that nitrogen is essential for cyanotoxin production (Chaffin et al., 2018). This has led to many researchers advocating for management of both phosphorus and nitrogen in cyanoHAB mitigations strategies (McCarthy et al., 2016). These nutrients can originate from various sources such as agricultural runoff, urban stormwater,

and wastewater discharges. Figure 1.1 illustrates the many interacting environmental variables contributing to CyanoHAB formation and proliferation within water systems.

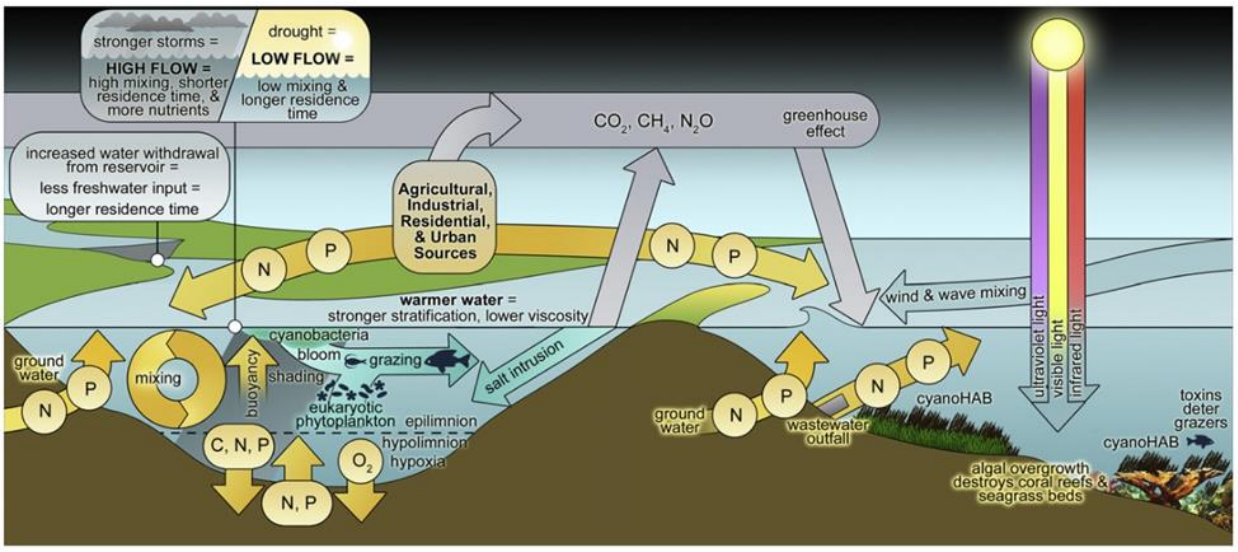

Figure 1.1 Factors involved include nutrient availability, water column transparency, water column mixing, temperature, and grazing (Retrieved from (Paerl & Paul, 2012)).

1.2.2 Persistence and Influence of Climate Change

In addition to increased nutrient loadings, research indicates climate change is another catalyst for cyanoHAB formation. This is because global warming has caused water temperatures and heavy precipitation events to increase globally (Paerl et al., 2017). Cyanobacteria are adapted for warm water conditions and have optimal growth rates at relatively high-water temperatures (25° C) and continue to show high growth rates at temperatures beyond this. In eutrophic waters, this provides cyanobacteria an advantage over nutrient-loving eukaryotic organisms, when competition is highest. As eukaryotic organisms' growth rates begin to decline in response to higher water temperatures, cyanobacteria growth rates reach their

optima (Paerl & Otten, 2013). In addition, warmer water temperatures intensify and lengthen periods of vertical stratification, resulting in stratification occurring earlier in the spring and continuing longer into the fall (Peeters et al., 2007). Vertical stratification refers to the layering of water based on chemical and physical properties, such as temperature, dissolved oxygen, and density, relative to depth. In a typical freshwater system, vertical stratification consists of three main layers, these being the epilimnion, metalimnion, hypolimnion. The epilimnion is the uppermost layer of the water column and is directly exposed to sunlight. It is characterized by warmer water temperatures and higher dissolved oxygen levels. This layer supports primary productivity and is typically occupied by species of phytoplankton, such as cyanobacteria (Dodds, 2019). Many cyanoHAB forming species can exploit stratified water conditions by controlling their buoyancy using gas vesicles. This allows the formation of dense surface blooms, providing cyanobacteria access to high levels of irradiance, optimizing photosynthesis. Also, surface-dwelling cyanobacteria contain photoprotective pigments and UV absorbing compounds allowing for long term survival under intense irradiance conditions (Paerl & Paul, 2012). Additionally, cyanobacteria may locally increase water temperatures due to their photosynthetic and photoprotective pigments. Both Ibelings et al. 2003 and Kahru et al. 1993 found that surface water temperatures were higher than surrounding water temperatures when blooms were present. Besides water temperatures increasing globally, climate change has also increased the number and intensity of heavy precipitation events globally. These events trigger the movement of nutrients across land, leading to elevated nutrient loadings in surrounding water systems. In addition, extreme precipitation events can cause rapid influxes of water, resulting in short term dilution and flushing of cyanoHABs. Nonetheless, as discharge diminishes, water will

remain in these bodies for longer durations, allowing accumulated nutrient loads to be captured and circulated, increasing the potential of cyanoHAB formation (Paerl & Paul, 2012).

1.2.3 Ecological and Economical Impacts

The formation of cyanoHABs can have negative impacts on both aquatic ecosystems and local economies. Ecologically, cyanoHABs can disrupt the balance of freshwater ecosystems, negatively impacting the organisms living within them. One of the most common consequences of cyanoHABs in ecosystem is the depletion of dissolved oxygen (Yan et al., 2022). As cyanoHABs proliferate rapidly, dense mats can be formed on the water's surface, preventing sunlight from penetrating to deeper depths (Anderson et al., 2000). This leads to a decrease in photosynthetic activity of submerged plants and other phytoplankton, resulting in hypoxic conditions. Also, as cyanoHABs decompose, this fuels respiration in other species of bacteria, further exacerbating oxygen loss. Large fish kills can be a direct result of hypoxic layers, or due to changes in fish behavior in which hypoxic layers are avoided at the cost of reduced food sources and growth (Scavia et al., 2014). Additionally, some cyanoHABs can produce cyanotoxins that can be released into the water. These can be harmful to many aquatic organisms, such as other invertebrates, fish, and amphibians. These toxins can bioaccumulate within the tissues of other organisms, potentially posing risks to organisms further up the food chain (Zhang et al., 2007). Furthermore, as cyanoHABs dominate a freshwater system, they outcompete native plant species, leading to a reduction in plant habitat, and consequently biodiversity (Amorim & Moura, 2021). This can have cascading effects for the entire ecosystem, affecting all organisms that rely on the water system for survival.

Beyond the ecological impacts of cyanoHABs, these blooms can negatively impact local economies, including costs associated with fisheries, tourism, recreation, real estate, water treatment, and public health. Fisheries and other aquaculture industries are negatively affected by cyanoHABs due to large fish kills, which directly impact fish populations, and consequently the livelihoods of fisherman and fish farmers (Qin et al., 2010). Even non-toxic cyanoHABs can cause oxygen depletion resulting in hypoxic environments, or clog fish gills (Munir et al., 2022). This results in a reduction of catches, fish quality, and profits for fishing communities and seafood industries. Additionally, recreation and tourism can be negatively impacted due to cyanoHAB occurrences. Recreational waterbodies used for swimming, boating, fishing, and other water activities may be closed due to health risks associated with cyanotoxin exposure. Closure of these areas results in lost revenue for local businesses dependent on tourism, such as hotels, waterfront restaurants, and touring services. Furthermore, waterfront property values may decrease if cyanoHABs become persistent (Hamilton et al., 2013). Blooms can produce foul odors, limit recreational use, and ruin the aesthetics associated with owning a waterfront property. The reduction in water quality and associated health risks could deter potential buyers, resulting in a reduction in property value. Water treatment facilities may incur increased treatment costs as well. As cyanoHABs decompose, organic matter and toxins may be released, affecting the taste, odor, and overall quality of the drinking water. These can also increase the amount of chemical needed for adequate treatment, microbial growth within water supply lines, and disinfection by-product formation (Cheung et al., 2013). To combat this, water treatment facilities must invest in additional monitoring and water treatment technologies, to ensure effective removal of cyanobacterial cells and toxins (Anderson et al., 2000). These new additions

result in increased water treatment costs, leading to higher water bills for consumers. Besides the economic impacts already discussed, public health costs can be increased due to cyanoHAB events. Exposure to cyanotoxins can cause many negative short-term and long-term health effects (Lee et al., 2017). In cases of severe symptoms or complications, individuals may require hospital visits, hospitalization, treatment, and further monitoring. If treatment is required, over the counter or prescription medications contribute to overall healthcare expenses. To assess and mitigate future cyanoHABs, public health surveillance and monitoring programs must be established. These programs involve routine sampling and analysis for recreational bodies of water, contributing to overall public health expenses (Shi et al., 2019). Additionally, educating the public about the associated health risks of cyanoHABs is crucial for preserving public health. The costs associated with creating education materials and facilitating outreach events contribute to public health expenses as well.

1.2.4 Effects on Microbial Communities

Aquatic microbiomes are complex and dynamic communities of microorganisms that play a critical role in maintaining the health of freshwater ecosystems. For example, aquatic microbiomes shape the biogeochemistry of aquatic systems by processing and recycling both organic and inorganic matter (Marmen et al., 2021). These microbiomes are highly dependent on environmental conditions, such as water temperature and nutrient availability. In general, more diverse microbial communities have increased productivity, higher temporal stability, and longer nutrient retention. Therefore, biodiversity loss diminishes aquatic ecosystem's benefits and services (Amorim & Moura, 2021). That said, the formation of cyanoHABs can negatively impact microbial communities by altering chemical and physical water features (Toporowska &

Pawlik-Skowrońska, 2014). CyanoHABs can cause increases in pH and redox potential, while decreasing light penetration through the water column, resulting in microbial biodiversity reduction. Besides altering environmental conditions, cyanoHABs can impact phytoplankton and zooplankton dynamics, by blocking energy transfer from primary producers to zooplankton (Tian et al., 2017). Also, grazing of zooplankton of phytoplankton can be interrupted during cyanoHABs due to the presence of cyanotoxins, formation of large colonies, and lower nutritional availability (Amorim & Moura, 2021). Additionally, Grey et al., 2000 showed that if the dominant phytoplankton taxa shift to be cyanobacteria, carbon assimilation by zooplankton is hindered, resulting in a carbon limited community. These disruptions cause imbalances within the microbial community, having cascading effects on aquatic ecosystem and ultimately human health.

2. CyanoHABs and Implications for Human Health

2.1 Exposure Pathways

Figure 1.2 illustrates the main routes of exposure to cyanotoxins, which are through ingestion of cyanoHAB affected waters, inhalation of bioaerosols, and dermal contact (Lee et al., 2017). Routes of exposure represented include ingestion (water and food), inhalation (recreational water activities and bathing), and dermal (recreation, bathing, and aquaculture).

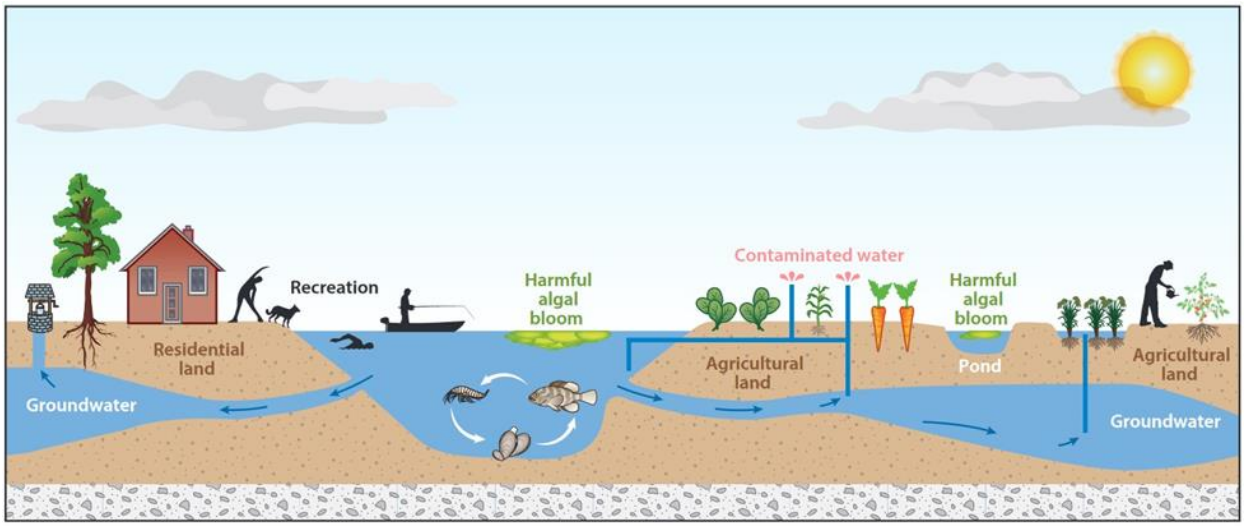

Figure 1.2 Visual representation of the different routes of exposure to cyanotoxins for humans in freshwater environments. Retrieved from (Lee et al., 2017).

2.1.1 Ingestion

Ingestion is the most common route of exposure for humans to cyanotoxins. Ingestion of cyanotoxins can occur during recreational activities, consumption of contaminated drinking water, and food (Cheung et al., 2013). Individuals participating in recreational activities such as swimming, boating, or skiing can accidentally ingest contaminated water, although ingestion of contaminated drinking water and food is a more frequent route for cyanotoxin intake. If a water treatment facility is utilizing surface waters during a cyanoHAB event, it is possible that drinking water could contain cyanotoxins even after treatment. In locations without adequate water treatment technology, individuals could ingest both extracellular and intracellular cyanotoxins, providing a route for both short-term and long-term exposure (Drobac et al., 2013). Additionally, cyanotoxins are known to bioaccumulate in both aquatic invertebrates and vertebrates such as zooplankton, mollusks, crustaceans, and fish (Corbel et al., 2014). Bioaccumulation of

cyanotoxins in zooplankton could lead to the transfer of these toxins through the food web, although few studies have provided evidence of this (Lehman et al., 2010, Ferrão-Filho et al., 2002, Ibelings et al., 2005). Bioaccumulation within the other organisms mentioned can lead to human ingestion, resulting in negative health effects. For example, microcystins have been detected in both freshwater shrimps and red crayfish (Chen & Xie, 2005, Chen & Xie, 2005). Additionally, cyanotoxins can accumulate within the liver, muscles, gills, guts, and kidneys of fish (Drobac et al., 2013). Kozlowsky-Suzuki et al., 2012 found that zooplanktivorous fish had exceptionally high microcystin concentrations compared to others, indicating these are of highest concern. Furthermore, the accumulation of cyanotoxins in agricultural crops is of recent concern. Spraying crops with water sourced from locations experiencing cyanoHABs could lead to the uptake and accumulation of cyanotoxins within plants (Corbel et al., 2014). Although research is ongoing, studies have suggested this is possible and warrants further investigation (Ai et al., 2020).

2.1.2 Inhalation and Dermal Contact

Although inhalation and dermal contact are lesser routes of exposure for cyanotoxins these should not be ignored. Swimmers and individuals participating in water contact sports are most susceptible, with cases reported from Japan, Hawaii, Florida, and Australia. Surface cyanobacterial mats can be broken apart by waves. These filaments can then accumulate in swimmers bathing suits, having acute and negative effects. Additionally, exposure to cyanotoxins can occur via inhalation. Cyanobacterial mats can be broken apart by waves, releasing cyanoHAB associated aerosols. These aerosols have been shown to have negative health effects in animal models and can be transported long distances dependent on weather

conditions (Bilyeu et al., 2022). Also, recreational activities such as water skiing could result in contaminated water entering through the nasal cavity. This is of concern because intranasal administration of cyanotoxins in mice showed 10 times the sensitivity when compared to oral exposure. Therefore, the potential for cyanotoxin inhalation during recreational activities should not be ignored (Drobac et al., 2013).

2.2 Cyanotoxins and Human Health Impacts

CyanoHABs are known to produce a variety of different toxins, with several being some of the most toxic compounds known (Table 1.1) (Cheung et al., 2013). These can be harmful to microorganisms, plants, animals, and humans. Many different cyanobacteria taxa can produce toxins, and the same toxins can be produced by different taxa (Cheung et al., 2013). Also, some taxa can produce multiple types of cyanotoxins. Cyanotoxins can be placed into five distinct categories, these are: 1) hepatotoxins; 2) neurotoxins; 3) dermatotoxins; 4) cytotoxins and 5) irritant toxins (Lee et al., 2017). Cyanotoxins are placed into these categories based on their mechanism of toxicity. In addition to the different types of cyanotoxins, each one has structural variants.

Table 1.1 LD_{50s} (ppb) of different cyanotoxins for rodents (24-h intraperitoneal) in comparison to other well-known toxins. LD_{50} refers to the median lethal dose. Table adapted from (Hudnell 2010, Cheung et al., 2013).

Cyanotoxin	**LD_{50} (Cyanotoxin)**	**Comparison**	**LD_{50} (Comparison)**
Microcystin-LR	50	Sarin	218
Cylindrospermopsin	300/180	Strychnine	2500/980
Anatoxin-a	200	Curare	500
Anatoxin-a(s)	20	Cobra Venom	185
Saxitoxin	10	Ricin	22

2.2.1 Hepatotoxins

The most common cyanotoxin encountered globally, a cyclic heptapeptide hepatotoxin known as microcystin (MC), has more than 240 structural variants (Spoof & Catherine, 2016). Out of these, the best known and most toxic variant is MC-LR, which has leucine and arginine residues in amino acid positions 2 and 4 (Svirčev et al., 2017). Microcystins are produced by many different cyanobacterial taxa, including *Microcystis, Dolichospermum, Planktothrix, Anabaenopsis, Nostoc*, and *Aphanizomenon*. Cylindrospermopsin is another common hepatotoxin, and is a tricyclic alkaloid, consisting of a tricyclic guanidine moiety, hydroxymethyluracil, and sulfate. These are characterized as being water soluble and stable when exposed to UV light (Westrick et al., 2010). Cylindrospermopsin is produced by *Cylindrospermopsis, Aphaznizomenon, Dolichospermum, Lyngbya, Phaphidiopsis,* and *Umezakia* (Lee et al., 2017). A third hepatotoxin, referred to as nodularins, are cyclic pentapeptides containing d-MeAsp, L-arginine, Adda, D-glutamate and N-methyldehydrobutyrine (Ufelmann et al., 2012, Mazur-Marzec et al., 2006). These toxins are mainly reported in Australia, New Zealand, and the Baltic Sea. The biosynthesis of nodularins is performed non-ribosomally, like mechanisms involved in MC production. Currently, 9 variants of this toxin have been identified, with these only being produced by *Nodularia spumigena* (Merel et al., 2013).

The health effects associated with cyanoHAB exposure are dependent on the concentration of cyanotoxin, route of exposure, and type of cyanotoxin. Additionally, cyanotoxins can have both acute and chronic effects on human health (Cheung et al., 2013). In the United States, the first documented cases of human illnesses due to cyanoHAB exposure took

place in Charleston, West Virginia in 1931, where 5000–8000 people experienced gastroenteritis after using water sourced from the Ohio River (Svirčev et al., 2017). The cyanotoxin responsible for this was a hepatotoxin, microcystin. Generally, cyanobacterial hepatotoxins are unable to penetrate vertebrate cell membranes. This requires the toxins be taken up via the bile acid transport system found in liver cells and cells lining the inside of the small intestine (Runnegar et al., 1991). Due to this, the toxicity of these cyanotoxins is confined to organs that have the organic anion transporter expressed on their cell membranes, such as the liver (Corbel et al., 2014). This results in symptoms, such as weakness, diarrhea, vomiting, abdominal pain, liver inflammation, pneumonia, dermatitis, and liver failure leading to death (Lee et al., 2017, Lopez et al., 2008). Batista et al. 2003 found that treating human liver cells with microcystins led to blebbing and separation. Additionally, there is evidence that microcystins aid in the formation of reactive oxygen species causing DNA damage, promote tumor growth, and have negative impacts on reproduction via disruption of the endocrine system (Zegura et al. 2003, Li et al. 2016, Chen et al. 2016). Studies conducted on chronic exposure of microcystins have shown high correlations between microcystin exposure and liver or colon cancer incidents (Lee et al., 2017). Additionally, a study conducted by Zhang et al. 2015 revealed that the risk of non-alcoholic liver disease deaths was significantly correlated with cyanoHAB bloom coverage in the United States. Cylindrospermopsin, another hepatotoxin produced by cyanoHABs, also affects the liver. Following ingestion, the toxin primarily affects the liver by inducing irreversible inhibition of protein synthesis, ultimately culminating in cell death. The most famous instance of cylindrospermopsin intoxication occurred in Australia in 1979. Algaecide was used to eradicate a cyanoHAB in a water treatment facilities source water. This inadvertently led to the release of

intracellular toxins. Consequently, over 100 children were admitted to the nearby hospital and treated for gastroenteritis (Merel et al., 2013).

2.2.2 Neurotoxins

In addition to hepatotoxins, cyanoHABs can produce neurotoxins. Three neurotoxins associated with cyanoHABs are anatoxin-a, saxitoxins, and β-N-methylaminoL-alanine (BMAA). Anatoxin-a is a bicyclic secondary amine, has the smallest molecular mass of all cyanotoxins, contains two functional groups susceptible to oxidation, is soluble in most natural water systems, and unstable in most environments with a half-life less than 24 hours (Westrick et al., 2010). This toxin can be produced by *Dolichospermum, Planktothrix, Aphanizomenon, Cylindrospermopsis, and Oscillatoria* (Lee et al., 2017). Although this toxin is extremely potent, comparable to cobra venom or curare (Table 1.1), it is studied less than other toxins due to its instability in natural environments (Cheung et al., 2013). Saxitoxins are neurotoxins produced by both freshwater and saltwater cyanobacteria. These toxins are commonly associated with "red tides" and shellfish poisonings in saltwater environments. Saxitoxins are tricyclic and can be non-sulphated, monosulfonated, or disulfonated (Merel et al., 2013). In freshwater systems, cyanobacteria taxa that perform biosynthesis of these include *Aphanizomenon, Dolichospermum, Lyngbya,* and *Cylindrospermopsis* (Westrick et al., 2010). These toxins are water soluble and can persist in freshwater environments for over 90 days. High water temperatures can chemically alter these toxins into more toxic variants (Merel et al., 2013). A third neurotoxin produced by cyanoHABs, BMAA, is a nonproteinogenic amino acid and is far less potent than anatoxins or saxitoxins (Sivonen and Jones, 1999). While research on BMAA is limited, recent research

indicates that this toxin may be produced by every recognized cyanobacterium group (Merel et al., 2013).

Acute exposure to cyanobacterial neurotoxins can cause death within a few minutes to hours, depending on the weight and overall health of the organism (Lee et al., 2017). Anatoxin-a, a common cyanobacterial neurotoxin, is a potent neuromuscular blocking agent that affects both nicotinic and muscarinic acetyl cholineacetylcholine receptors (Corbel et al., 2014). This toxin mimics acetylcholine but is not broken down by acetylcholinesterase, leading to overstimulation of muscles and consequently, muscle paralysis. If respiratory muscles are affected, respiratory arrest can occur, starving the brain of oxygen and leading to death (Corbel et al., 2014, Lee et al., 2017). Saxitoxins, produced by both marine and freshwater cyanobacteria, block sodium channels along nerve cells, inhibiting the transmission of nerve impulses. This results in the under stimulation of muscles, including those required for respiration, inducing respiratory paralysis (Christensen & Khan, 2020). Other less acute effects associated with saxitoxin exposure include nausea and weakness. Additionally, Sun et al., 2021 evaluated the neurotoxicity effects of long-term low-dose saxitoxin exposure via drinking water in mice. The results of this study showed that exposed mice had decreased neuronal cells and thinner pyramidal cell layers in the hippocampal CA1 region when compared to control mice, suggesting brain neuronal damage. In addition, a total of 29 proteins were significantly altered, some of which indicated that chronic, low dose saxitoxin exposure can cause neurol inhibition, resulting in spatial memory impairment. However, the chronic effects of saxitoxin exposure, specifically carcinogenic and reproductive effects, are understudied (Lee et al., 2017). When compared to other cyanotoxin toxicity levels, saxitoxin is the most potent freshwater cyanotoxin, causing an

annual estimated 2000 cases of paralytic shellfish poisoning globally, with a mortality rate of 15% (Pearson et al., 2010). Reports of illnesses related to saxitoxin contaminated food are increasing globally, with many human intoxications resulting in numbness, complete, paralysis, and even death (Lee et al., 2017, Kuiper-Goodman et al., 1999). However, no intoxication through drinking water has been documented so far (Merel et al., 2013). BMAA is an additional neurotoxin associated with cyanoHABs. In humans, BMAA mostly acts as a glutamate agonist, altering neural communication, regulation, and memory formation (Corbel et al., 2014). In addition, it could catalyze neurodegeneration through misfolding of intraneuronal proteins (Banack et al., 2010). BMAA is known to cause different neurodegenerative disorders, including the amyotrophic lateral sclerosis/parkinsonism dementia complex in Guam, and Alzheimer's disease (Merel et al., 2013). For example, cycad plants produce BMAA and are consumed by flying fox bats in Guam. The Chamarro people of Guam consume flying fox bats regularly in their diet. As a result, many Chamarro have developed Parkinsonism dementia (Cox et al. 2005, Lee et al., 2017). However, BMAA is understudied, and more research is needed to understand its presence in human diets globally (Lee et al., 2017).

2.2.3 Dermatotoxins, Cytotoxins, and Irritant Toxins

Additional toxins produced by cyanoHABs include dermatotoxins, cytotoxins, and irritant toxins. Dermatoxins are mainly produced by *Lyngbya, Oscillatoria, and Schizothrix.* These include both aplysiatoxins and lyngybyatoxins and have only been detected in marine waters (Merel et al., 2013). These toxins are acute, and mainly affect swimmers coming into contact with benthic cyanobacteria species, causing severe dermatitis (Sivonen and Jones, 1999). Cytotoxins include additional toxins produced by cyanobacteria that are harmful to cells. These

are not only effective against eukaryotic cells, but also effective against viruses and other bacteria, including cyanobacteria. This group of toxins has a variety of different chemical structures and new bioactive compounds are still being found (Sivonen and Jones, 1999). Irritant toxins, also referred to as lipopolysaccharides, are found in the outer membranes of cyanobacterial cell walls. Research is ongoing, but the few results available suggest that cyanobacterial lipopolysaccharides are equal to, or less toxic than lipopolysaccharides found in other bacteria such as *Salmonella* spp and *Escherichia coli* (Lee et al., 2017). Additionally, research has shown that most of the lipopolysaccharides present during cyanoHABs originate from bacteria other than cyanobacteria (Sivonen and Jones, 1999).

These toxins are usually characterized as having acute effects. For example, swimmers encountering dermatotoxins producing cyanoHABs develop severe contact dermatitis rapidly. Within a few minutes to a few hours itching a burning of the skin occurs, followed by visible redness and dermatitis (Drobac et al., 2013). Additionally, oral and gastrointestinal inflammation can occur causing diarrhea in exposed individuals (Merel et al., 2013). Lipopolysaccharides can have many negative effects in humans such as allergies, endotoxemia, gastrointestinal disease, and autoimmune disease (Lee et al., 2017). Also, research has shown that lipopolysaccharides are significantly associated with type 2 diabetes and obesity (Cani et al., 2007). Furthermore, these toxins are thought to have a tumor promoting factor and can cause liver damage resulting in decreased liver function (Lee et al., 2017). These results indicate that increases in cyanoHABs globally and their associated toxins can have negative effects for human health.

3. Current Regulations and Guidelines

Due to the increased frequency and duration of cyanoHABs and associated toxins in waterways globally, the World Health Organization (WHO) has established guidelines for cyanobacteria and cyanotoxin levels in recreational waters (see Table.1.2). WHO derived microcystin levels based on cyanobacterial cell density.

Table 1.2 WHO established guidelines for cyanobacteria and cyanotoxin levels in recreational waters. Adapted from (Recommended Human Health Recreational Ambient Water Quality Criteria or Swimming Advisories for Microcystins and Cylindrospermopsin, 2019).

Relative Probability of Acute Health Effects	**Cyanobacteria (Cells/mL)**	**Chl-a (µg/L)**	**Estimated Microcystin Levels (µg/L)**
Low	< 20,000	< 10	< 10
Moderate	20,000-100,000	10-50	10-20
High	>100,000-10,000,000	50-50,000	20-2,000
Very High	> 10,000,000	>5,000	> 2,000

These guidelines are based on cyanobacterial cell counts and chlorophyll-a (chl-a) levels (US EPA, 2018). Soon after, other countries and states created their own guidelines to better suit their unique situations. For example, in the United States, the 1996 Safe Drinking Water Act (SDWA), requires that the US EPA publish a list of contaminants every five years that are known to occur and may need regulation in public water systems. This list of contaminants is called the Contaminant Candidate List (CCL) and is used to identify and prioritize contaminants for regulatory decision making and data collection needs (US EPA, 2016). In 1998, the US EPA listed cyanobacteria on CCL1 (1998) and CCL2 (2005). For CCL3 (2009), CCL4 (2016), and CCL5 (2022) cyanotoxins were added, including microcystins, cylindrospermopsin, anatoxin-a,

and saxitoxin (US EPA, 2016). Furthermore, in the United States, national and state water quality agencies have developed monitoring and management frameworks to mitigate the hazardous effects of cyanoHABs and associated toxins for the protection of public health. In 2015, the United States Environmental Protection Agency (EPA) established health advisories for the cyanotoxins cylindrospermopsin and microcystins in drinking water (Mehinto et al., 2021). These advisories are based on a 10-day exposure period and are accepted as adequate for mitigating the potential health effects of cyanotoxin exposure. For microcystins and cylindrospermopsins, the 10-day thresholds for bottle-fed infants and pre-school children are 0.7 µg/L and 0.3 µg/L respectively. For school age children and adults, these thresholds are slightly higher, with thresholds of 3.0 µg/L for cylindrospermopsins and 1.6 µg/L for microcystins (US EPA, 2018). Several years later, in 2019, the EPA set water quality thresholds for recreational waters for microcystins and cylindrospermopsins at 8 µg/L and 15 µg/L respectively (US EPA, 2019). However, these guidelines vary from state to state. To view all state recreational advisory thresholds, including those set in Ohio, see Table A.1. Due to the health risks linked to the exposure of cyanotoxins, the Ohio EPA continually monitors all public water systems (PWS) for the protection of public health.

4. Detection and Monitoring Techniques

4.1 Cyanobacteria Detection and Monitoring

4.1.1 Traditional Methods and On-site Monitoring Networks

Generally speaking, there are four main ways that HABs are monitored: 1) ground sampling and analysis, 2) on-site monitoring network systems 3) satellite remote sensing and 4) airborne remote sensing (Lyu et al., 2017). Each of these has benefits and shortcomings, so a

multi-scale and multi-modal approach is best for adequate cyanoHAB monitoring (Figure 1.3). Ground sampling and lab analysis is the traditional monitoring method for HABs. This method requires an individual to collect a water sample, transport the sample to a laboratory, and perform analysis. The most common analyses include quantification of chlorophyll-a (chl-a) and cyanotoxins using high performance liquid chromatography (HPLC) and immunoassays (most common assay is ELISA) respectively (Chorus, 2021). This process requires transportation, vehicle costs, tools for sample collection, shipping costs, lab supplies, waste generation, and multiple days to analyze the samples (Silvarrey Barruffa et al., 2021). There is general consensus among water resource managers that traditional ground sampling methods do not provide an adequate number of samples or frequency of sampling to accurately assess risks posed by HABs (Zhang et al., 2019). However, traditional water sampling methods do allow for cyanotoxin identification and quantification. Additionally, some methods, such as liquid chromatography tandem mass spectrometry can quantify specific cyanotoxin congeners with minimal interference (Douglas Greene et al., 2021). On-site monitoring network systems utilize automatic monitoring technology, such as monitoring buoys with chl-a and PC sensors, to collect water quality data. This method has the advantage of being automated, but the data collected only represents water quality near that station and is not representative of the entire water body.

4.1.2 Satellite and Airborne Remote Sensing

Satellite remote sensing utilizes satellites equipped with multispectral or hyperspectral sensors for measuring indicative parameters of water quality such as chl-a, PC, and color dissolved organic matter (CDOM). Although satellites can handle the spatial variability of HABs, unlike the other methods mentioned previously, there are two main limitations when

utilizing satellites. The first is that satellites cannot provide the necessary temporal flexibility to adequately monitor HABs. This is because atmospheric effects (i.e. extensive cloud cover, sun position, shadows) can negatively affect satellite image quality, resulting in inaccurate estimations of the desired water quality parameter. This is a significant problem for high latitude areas because nearly 50% of the year is cloudy and water bodies are covered with snow for approximately seven months of the year (El-Alem et al., 2021). In addition, satellites have routine revisitation times, meaning users are unable to acquire imagery as needed. Popular satellite platforms such as Moderate Resolution Imaging Spectroradiometer (MODIS) and Medium Resolution Imaging Spectrometer (MERIS) have revisitation times of 16 and 35 days, respectively (Wu et al., 2019). This results in water resource managers having no information for extended periods of time (Cillero Castro et al., 2020). The second disadvantage of satellite imagery is that the resolution can be too coarse for monitoring smaller bodies of water. The fourth way that HABs are currently monitored is using airborne remote sensing. Traditionally this method requires the use of a manned aerial vehicle equipped with the necessary sensor. Manned aerial vehicles can collect imagery at much higher resolutions than satellites and can fly at lower altitudes to avoid negative effects on data acquisition caused by atmospheric conditions. Although airborne remote sensing has these advantages, their use is limited due to high costs, the level of intrusion on wildlife, associated dangers due to abrupt changes in weather conditions, and the absence of a robust operational infrastructure. In recent years, unmanned aerial vehicles (UAVs) have emerged as a low-cost, safe, and flexible option in airborne remote sensing (Gaffey & Bhardwaj, 2020). UAVs can be deployed as needed, can collect imagery with spatial resolutions at centimeter scale, and fly at lower altitudes avoiding negative atmospheric effects

such as cloud cover. In addition, UAVs can be equipped with many different attachments Red/Green/Blue cameras (RGB), thermal, Light Detection and Ranging (LiDAR), multispectral, hyperspectral, sampling devices, water quality sensors, etc.) per monitoring needs. However, UAVs have the disadvantages of water image processing being difficult, a lack of standardized methods, and limited spatial coverage when compared to other remote sensing techniques (El-Alem et al., 2021). Nonetheless, in recent years UAVs have increasingly been used in HAB research and assessed as an early warning monitoring system for protecting public health.

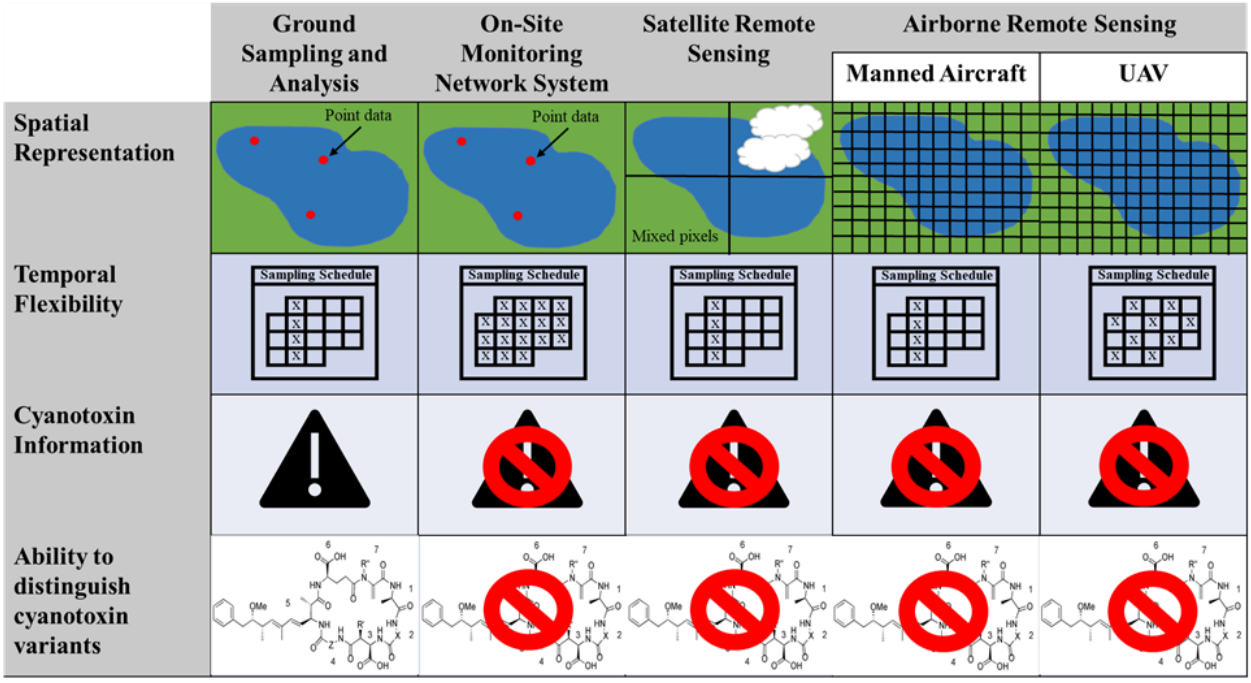

Figure 1.3 Summary of current cyanobacteria monitoring techniques. The advantages and disadvantages of each are highlighted. Figure design adapted from (Douglas Greene et al., 2021).

4.2 Cyanotoxin Detection and Monitoring

4.2.1 Biological Approaches

A wide range of methods are available for detecting and quantifying cyanotoxins in environmental samples, each varying widely in sensitivity, rapidity, cost, and level of expertise required to implement the method (Bone, 2019). Methods available can be placed into two distinct categories, these being biological and physicochemical approaches. Biological approaches include immunological and biochemical assays (Kaushik & Balasubramanian, 2013, Merel et al., 2013). Currently, a popular method for detection and quantification of cyanotoxins is the use of commercially available immunological assays such as Enzyme-Linked ImmunoSorbant Assay (ELISA) (Bone, 2019). The benefits of this method are that it is extremely sensitive and can distinguish between different types of toxins (Kaushik & Balasubramanian, 2013). However, detection methods based on ELISA have some limitations such as the inability to distinguish between cyanotoxin variants and interference from other compounds in the sample can result in overestimation of cyanotoxins (Fayad et al., 2015). Another biological approach for cyanotoxin quantification are biochemical assays. This approach takes advantage of microcystins and nodularins being potent inhibitors of protein phosphatase and is referred to as a protein phosphate inhibition assay (PPIA) (Moore et al., 2016). ELISA kits are available for this method, but the toxin detection technique differs. For ELISA kits using immunological assays, toxins are detected and measured through antibody screening, while ELISA kits utilizing PPIA measure the rate of formation of p-nitrophenol and measures all protein phosphatases inhibitors present in a sample. To do this, an aliquot of the sample being tested is exposed to the enzyme and then incubated with the relevant substrate. Absorbance of

the mixture is then measured at a designated wavelength, allowing detection of the substrate and enzymatic activity. Enzymatic activity is inversely related to toxin concentrations (Merel et al., 2013). Benefits of this method are that it allows for toxin detection in many samples within a few hours and is very sensitive. Some drawbacks to this method are that it can only detect microcystins and nodularins but cannot distinguish between them (Sundaravadivelu et al., 2022). Additionally, it is not possible to distinguish between toxin variants. Furthermore, PPIA measurements can be influenced by other compounds within the sample of interest, leading to under or overestimation of cyanotoxins (Koreivienė & Belous, 2012). Research has shown that on average, PPIA results for microcystin concentrations are lower than those measured using ELISA (Gaget et al., 2017). It is suggested to use a combination of biological approaches to ensure accurate results regarding cyanotoxin concentrations (Bone, 2019).

4.2.2 Physiochemical Approaches

Physiochemical approaches for detecting cyanotoxins include the use of UV absorbance/fluorescence and mass spectrometric techniques. Before conducting either of these, it is common to perform some type of separation technique, allowing distinction between several different toxins in a single analysis (Merel et al., 2013). Common separation techniques include liquid (LC) or gas chromatographic (GC) techniques (Koreivienė & Belous, 2012). Out of the separation methods, liquid chromatographic techniques are the most common (Sundaravadivelu et al., 2022). Once separation is complete, an option for cyanotoxin quantification is the use of absorbance or fluorescence techniques. This method was one of the first techniques implemented for cyanotoxin detection, and measures cyanotoxins using characteristic absorbances. UV absorbance offers limited sensitivity and low specificity since the UV spectra of some

cyanotoxins are very similar (Sundaravadivelu et al., 2022). Furthermore, as with some of the biological techniques mentioned previously, compounds within samples can affect quantification accuracy (Merel et al., 2013). To improve sensitivity, detection by fluorescence can be used. Although, a drawback to this method is that a derivatizing reagent must be added before sample analysis since cyanotoxins do not fluoresce naturally (Kaushik & Balasubramanian, 2013, Sundaravadivelu et al., 2022). This adds an additional step during sample preparation. A more current physiochemical approach used for cyanotoxin quantification are mass spectrometric methods (MS). These methods directly measure the concentrations of toxins, by comparing target compounds with analytical standards. Methods that use LC combined with MS can precisely and accurately quantify specific cyanotoxin congeners if standards are available, with minimal sample matrix interference (Bone, 2019). Currently, mass spectrometric methods are the physicochemical method of choice for quantitative analysis of cyanobacterial toxins within complex matrices due to their specificity, sensitivity, and rapidity. Out of these, liquid chromatography-tandem mass spectrometry (LC–MS/MS) is the most common chromatographic method used for cyanotoxin detection (Sundaravadivelu et al., 2022). This is a method developed by the EPA for detection of cyanotoxins in drinking water (EPA Method 544). This method reduces the chances of false positive identifications, by utilizing compounds' features, such as charge and mass, as well as fragmentation patterns (Bone, 2019). Drawbacks to this method are that it requires expensive equipment, highly qualified staff, and a relatively long analysis time (Koreivienė & Belous, 2012). Although many techniques are available for cyanotoxin quantification, there is a need for automated sampling and detection. A promising solution to this is the use of biosensors, but currently these are fluorescence-based like remote sensing systems,

and not mature enough to replace traditional methods (Kaushik & Balasubramanian, 2013, Miglione et al., 2021).

5. UAVs as a New Tool for HAB Monitoring

5.1 Applications of Drones for Protecting Public Health

UAVs have been applied for monitoring of HABs in many ways due to their flexibility, relatively low costs, and ease in data collection. Table A.2 summarizes studies from 2017-present that utilized UAVs for HAB monitoring. In addition, the potential of each studies' results for informing public health policies is discussed. Studies are listed in chronological order. UAVs were utilized in research globally, with South Korea being the most popular. Figure 1.4 shows the geographical locations for all the studies discussed here. In addition to the differing geographical locations, many different water bodies were assessed using UAVs, including both saltwater and freshwater sources. Figure 1.5 shows the different types of water bodies assessed. The various areas of study and objectives of the studies included here highlight the broad range of applications for UAVs. For example, many of the studies were focused on accurately quantifying photosynthetic pigments related to cyanobacteria presence, but the pigment of choice varied between studies. Photosynthetic pigments selected include chl-a, PC, color dissolved organic matter, total suspended solids, lutein, fucoxanthin, and zeaxanthin (Pyo et al., 2022). Some of these studies combined UAV imagery data with water quality data to create predictive models (Hong et al., 2021). Almost all these studies mentioned different techniques used during image correction and analysis and stated that a standardized processing workflow is needed. (Windle & Silsbe, 2021) focused on this need and evaluated four different approaches for removing sun glint in UAV imagery, with the goal of improving UAV derived chl-a estimates.

Other studies were focused on combining UAV imagery data with more traditional remote sensing methods, such as satellite imagery, to create a multi-scale monitoring tool (Cillero Castro et al., 2020, El-Alem et al., 2021). This framework allows for both regional and local monitoring. Satellite imagery provides regional data while UAV imagery provides local data on HABs. A few studies utilized UAVs for collecting environmental samples such as water and aerosol samples. These studies reported that UAVs drastically reduced the time needed for sample collection (Bilyeu et al., 2022, Hanlon et al., 2022, Kimura et al., 2019). Other, less prominent areas of research utilized UAVs to designate sampling locations or to validate data acquired using novel methods of HAB detection (Stoyneva-Gärtner et al., 2020, Son et al., 2020). A single study utilized a UAV to detect, determine the direction, and velocity of HABs near a desalination plant (Kim et al., 2019). This provided the desalination plant with a real-time monitoring tool, allowing the plant to make better informed decisions. To assess the extent of HABs, UAVs were applied in many ways. Some studies had multiple uses for the UAV, while others did not. Figure 1.6 represents the different purposes of UAVs in these studies. If a study used an UAV for multiple purposes, all purposes were included. The most popular application of UAVs in these studies was for chl-a estimation.

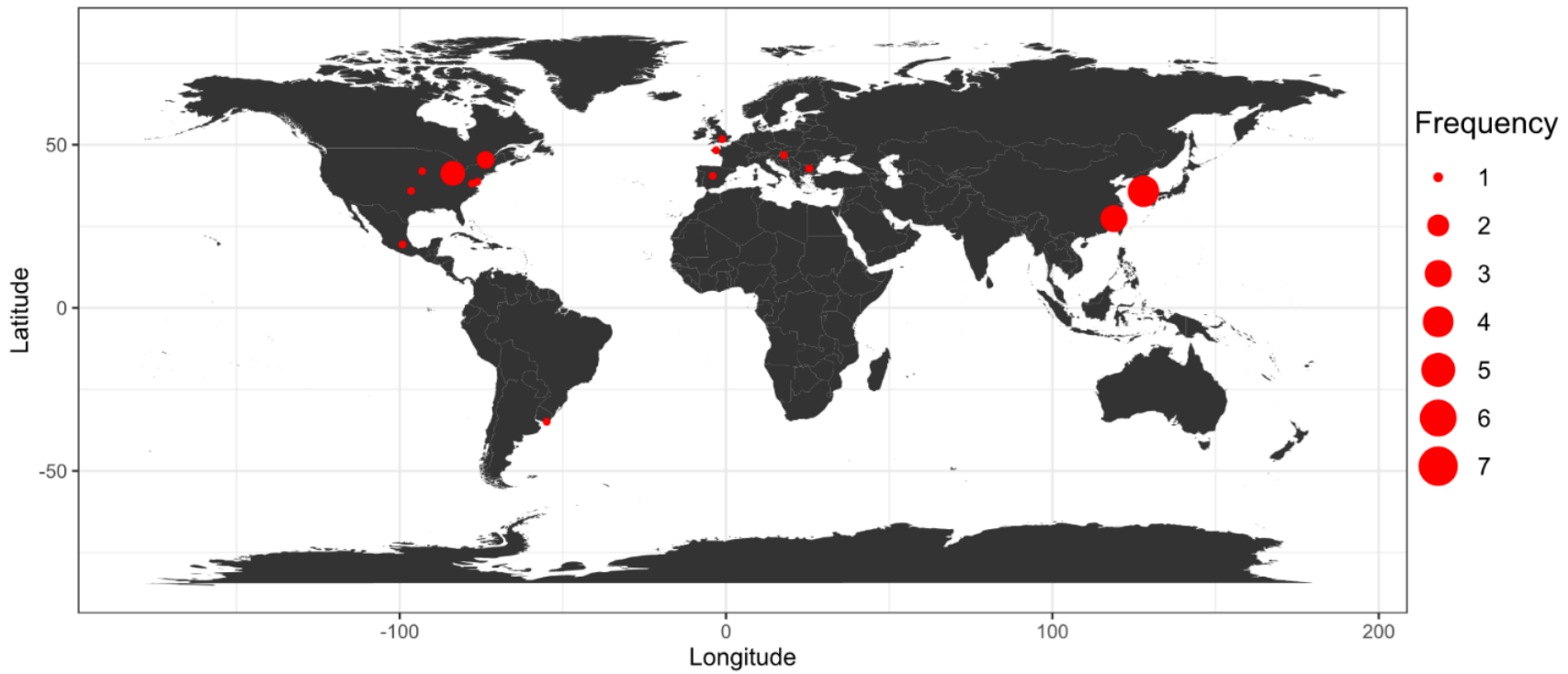

Figure 1.4 Geographical distribution of studies utilizing UAVs for HAB research.

Figure 1.5 The different types of water bodies researched in the studies. “WW Lagoon” stands for “Waste-water Lagoon”. If a study conducted research on multiple types of water bodies, all were included.

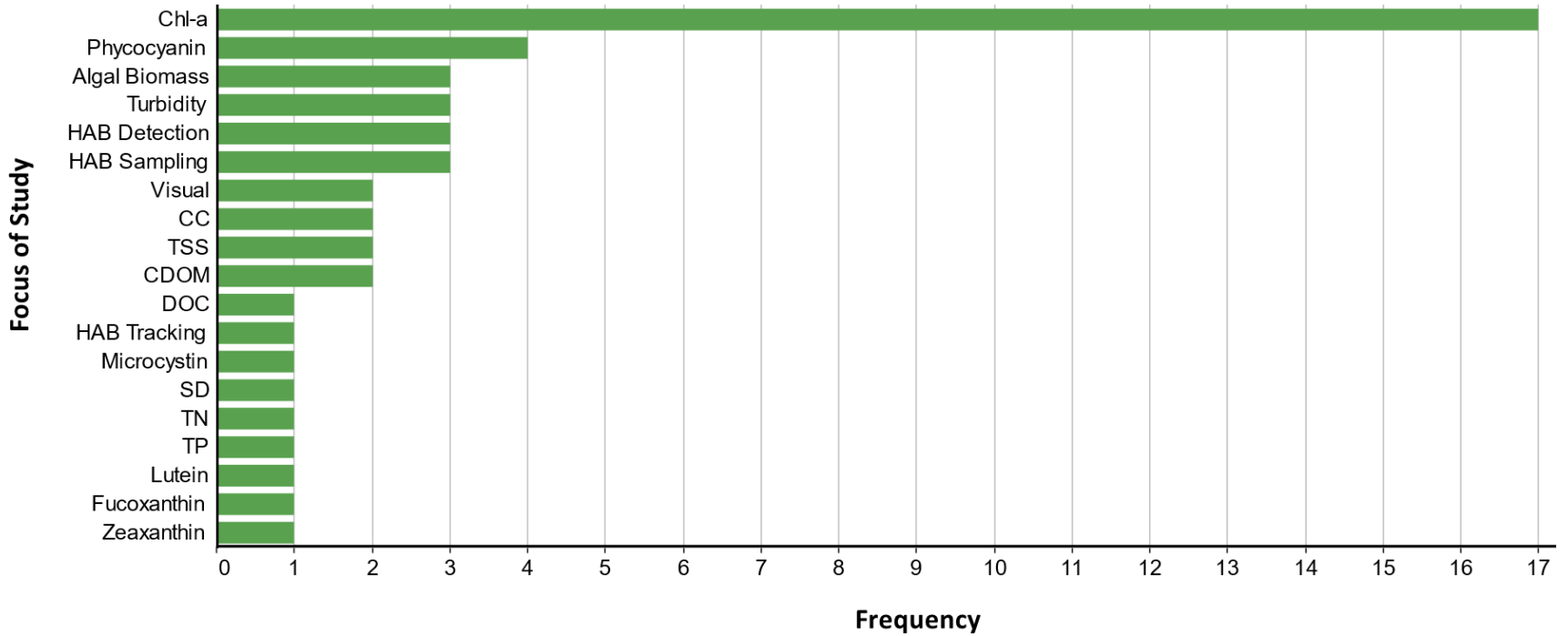

Note: CDOM stands for “color dissolved organic matter”, CC for “cyanobacteria concentration”, TSS for “total suspended solids”, DOC for “dissolved organic carbon”, SD for “secchi disk depth”, TN for “total nitrogen”, and TP for “total phosphorus”.

Figure 1.6 Represents the different research areas from all studies included. If a paper had multiple areas of focus, all were included.

5.1.1 Studies Focused on Chl-a

Chl-a estimation was by far the most common application for UAVs in HAB research, despite the lack of standardization and difficulties in image processing. Out of the 27 studies included, 16 performed some type of chl-a analysis. Of those 16, seven focused solely on chl-a estimation and did not assess other parameters using an UAV. As mentioned previously, there is a need to standardize UAV imagery processing, so a few studies implemented novel techniques to retrieve chl-a estimations based on corrected reflectance measurements. (Shang et al., 2017) developed a novel approach for obtaining remote sensing reflectance (Rrs) in a nearshore environment when using UAVs equipped with spectroradiometers. Simply put, this approach reduces the error in derived Rrs by accounting for environmental interference within the imagery (i.e atmospheric scattering, wave white caps, moving clouds). Before deriving Rrs, a two-step quality control method was performed to remove outliers, by first implementing wavelet transform (Ebadi & Shafri, 2015) and then removing land data. A novel radiometric technique was also implemented by (Cheng et al., 2020) when using UAVs equipped with RGB digital cameras. Raw digital number (DN) values were converted to corrected DN utilizing a calibration panel. These values were then used to derive chl-a concentrations. (Shang et al., 2017) converted UAV derived Rrs to chl-a concentrations utilizing an empirical algorithm. The difference between UAV estimates and in situ measurements was <20%. This deviation was much lower than that between MODIS and in situ measurements, which had an average error of 136%. (Cheng et al., 2020) derived chl-a concentrations based on a linear, power, and exponential regressions between in situ chl-a concentrations and water reflectance ratios between two bands.

Six band ratio combinations were evaluated. The results showed that red/blue is the optimal band ratio for estimation of chl-a when using a RGB digital camera. In addition, the model's prediction is less satisfactory for chl-a concentrations greater than 15-20 μg/L. Both studies concluded that UAVs are promising tools for more effective HAB early warning systems and provide a basis for risk assessment during HAB outbreaks. Future research should focus on standardizing and validating imagery processing workflows.

Three studies focused on chl-a estimations utilizing UAVs equipped with multispectral cameras. The first created a chl-a estimation algorithm using the relationship between Rrs of each wavelength observed by the multispectral sensor on the UAV and in-situ chl-a measurements (Baek et al., 2019). This relationship was derived using a multiple linear regression model. Once the new chl-a estimation algorithm was applied to the UAV imagery, UAV and in-situ chl-a values had high agreement. The correlation between these values was 0.94 and had a root mean square error (RMSE) of approximately 0.8 μg L-1. Another study used a linear regression model to examine the relationship between chl-a concentrations and the normalized difference vegetation index (NDVI) (Choo et al., 2018). The results showed that in-situ chl-a concentrations agreed well with NDVI values, with R^2 of 0.7. The third study defined algal concentrations with three camera outputs, light level, irradiance, and reflectance (Tóth et al., 2021). Chl-a concentrations were determined using blue/green and near infrared (NIR)/red ratios. A first order equation was established between the two ratios and laboratory derived chl-a values. A multiplier that would produce a perfectly accurate lab result was obtained and applied to all camera output and ratio combinations. The deviation from the laboratory and UAV derived chl-a values was analyzed. It is important to note, this study was evaluating multiple water

bodies with different physical characteristics. This required the measurements be split into 5 distinct areas and fitting the model for each of these areas. Results showed that the highest correlation coefficient was obtained when using blue/green ratio-based light levels. This study also highlighted the UAVs efficiency, showing approximately a 50% reduction in required time between UAV and laboratory measurements. All three studies concluded that UAVs are beneficial tools for water quality monitoring, but that future research is needed to validate these techniques.

Optical sensors with the ability to estimate chl-a values are gaining popularity in water resource management but are limited by data availability and locality when developing models. Most models need to be reparametrized from water body to water body. With this knowledge, (El-Alem et al., 2021) developed a UAV data-based model for chl-a estimation and applied it to Sentinel-2 imagery without reparameterization. To do this, an ensemble-based system algorithm was used to train the model. Three lakes with different trophic statuses underwent in-situ sampling, to provide a wide range of in situ chl-a measurements for model calibration. In addition, a blind dataset was created using 94 chl-a data sampling points across 89 waterbodies. This approach was evaluated at both a local and regional scale utilizing cross-validation and the blind dataset respectively. It is important to note, UAV imagery underwent unique pre-processing steps to make it comparable to Sentinel-2 imagery. Briefly, these steps were 1) geometric and radiometric correction 2) upscaling UAV imagery to equal Sentinel-2 imagery resolution 3) Sentinel-2 band simulation and 4) Sentinel bands reflectance computation. In another study, a multi-scale and multi-sensor monitoring tool was developed using multiple multispectral satellite sensors, UAV equipped with multispectral sensor, and in situ sampling.

Empirical models were developed for retrieving chl-a values for all types of imagery. Linear relationships between Rrs at different wavelengths and in situ chl-a data were derived. Sixteen different spectral band combinations were evaluated (Cillero Castro et al., 2020). To statistically evaluate model performance, both studies utilized RMSE and bias. In addition to these, Nash criterion and relative error were applied by (El-Alem et al., 2021), while normalized root mean square error (NMSE) and mean absolute percentage error (MAPE) were applied by (Cillero Castro et al., 2020). Both studies found the performance of their models satisfactory, but it is necessary to have a large, diverse data set for adequate model training. Also, model performance was lower when estimating higher chl-a values. In addition, turbid waters make chl-a estimation difficult. Future research should be on developing algorithms calibrated with a higher, broader range of chl-a values. These methods provide tools to accurately estimate and predict chl-a in water bodies at local and regional scales. This could allow public health resources to be dispersed to afflicted locations in a timelier manner.

5.1.2 Studies Focused on Phycocyanin

Although PC is more indicative of cyanobacterial presence, less studies focused on PC estimation (Almuhtaram et al., 2021). This is because most sensors do not have the spectral resolution necessary for estimating PC concentrations. Sensors that have this capability are usually hyperspectral, resulting in an increase in cost and UAV carrying capacity requirements. All studies estimating PC also estimated chl-a concentrations (Aguirre-Gómez et al., 2017, Kwon et al., 2020, Hong et al., 2021). In addition to PC and chl-a, one study evaluated other pigment concentrations such as lutein, fucoxanthin, and zeaxanthin (Pyo et al., 2022). One study utilized an UAV equipped with an RGB sensor for PC concentration estimation. Briefly, this

process utilized the PC absorption peak at 619 nm in combination with in-situ hyperspectral radiometer measurements and cyanobacterial lab analysis. Mean value maps were produced with the inverse distance weighting method for the PC absorption peak. This method views non-sampled locations as a function of values gathered from sampled locations within a designated radius (Aguirre-Gómez et al., 2017). The results indicated that UAVs combined with in-situ can be a powerful tool for detecting and predicting HABs in water reservoirs. These methods could be applied to generate predictive spatial maps of HABs, allowing for proactive decisions to be made by public health officials. In addition, this method uses an RGB sensor, which is a cheaper option than a multispectral or hyperspectral sensor.

Three studies used hyperspectral sensors for PC estimation. (Kwon et al., 2020) explored how diel vertical migration of cyanobacteria may affect UAV derived PC estimations. To do this, a vertical pigment concentration profile was created for surface and three subsurface depths utilizing a portable Rrs sensor and UAV surface reflectance. Then bio-optical algorithms were developed and compared. The best performing bio-optical algorithm was used to determine spatial and temporal distribution of PC. A two-band ratio algorithm using the 709 and 620 nm band was used to estimate PC pigment concentration. A PC distribution map was generated using a linear-regression-based bio-optical algorithm from UAV surface-reflectance data, portable Rrs sensor PC concentrations, and cumulative PC concentration. Both (Pyo et al., 2022) and (Hong et al., 2021) applied deep learning models to UAV hyperspectral data for estimating PC concentrations. Similar to (Kwon et al., 2020), (Hong et al., 2021) was interested in monitoring the vertical distribution of PC using UAV data. To do this, four different deep neural network models were applied to estimate the vertical distribution of PC. These models used

UAV and meteorological data as input datasets and provided vertical water quality profile data as the output dataset. After hyperparameter optimization, the trained models were applied to UAV imagery to map PC spatial distribution. (Pyo et al., 2022) applied a one-dimensional convolutional neural network to estimate PC concentrations, along with chl-a, lutein, fucoxanthin, and zeaxanthin. After training, the model was applied to UAV reflectance maps to generate an absorption coefficient map. Then, drone input maps with pixels containing reflectance and absorption spectra were applied to the trained deep learning model to produce spatial distribution maps for the pigments of interest. Both studies implementing deep learning models utilized R^2 and RMSE to assess model performance. (Hong et al., 2021) used MAPE, MAE, and Wilmote Agreement Index (WAI) additionally. All three studies state that UAVs equipped with hyperspectral sensors are useful for analyzing algal phenomenon both quantitively and qualitatively.

5.1.3 Studies with Other Applications

The remaining 16 studies applied UAVs for HAB monitoring by focusing on parameters other than chl-a and PC, although some studies chose to assess these as well. These can be divided into 5 broad categories being microcystin evaluation, HAB sampling, HAB detection, algal biomass/concentration estimation, and evaluation of different water constituents. A single paper attempted predicting microcystin concentration distributions using a UAV equipped with a multispectral sensor. To do this, in situ and remote sensed values were analyzed and correlations drawn between chl-a content and microcystin concentrations for seven vulnerable Iowa lakes. The results suggested that the relationship between chl-a and microcystin vary significantly between lakes, with microcystin concentrations predicted within 33%. The researchers concluded

that although possible, multispectral imagery is presently insufficient for predicting microcystin concentrations due to inadequate spectral resolution (Douglas Greene et al., 2021).

Although the majority of research utilized UAVs for remote sensing purposes, three studies utilized them for HAB sample collection. (Kimura et al., 2019) developed an early detection system for HABs using two UAVs. The first UAV was used to detect the HAB, while the second UAV was equipped with a custom sampling device for collecting seawater samples. This device was able to collect seawater samples at 1M, 3M, and 5M in depth during one flight. (Hanlon et al., 2022) utilized a custom 3-D printed DrOne Water Sampling SystEm (DOWSE) to collect 180 water surface samples from 3 different water bodies. In addition, the UAV was able to photograph water quality conditions and collect GPS locations of samples simultaneously with sample collection. The UAV greatly improved water sampling efficiency, taking approximately 12 minutes to collect 10 samples. (Bilyeu et al., 2022) developed and deployed an Airborne DROne Particle-monitoring System (AirDROPS) to monitor, collect, and characterize airborne particles over HABs. Particle counts acquired by the AirDROPS were robust and consistent with those simultaneously acquired by a commercially available particle counter. All three studies concluded that UAVs can be outfitted with custom attachments to aid water resource managers and public health professionals by providing critical and timely information for regulatory decisions.

Four studies focused on detecting cyanobacterial blooms with UAVs. Both (Stoyneva-Gärtner et al., 2020) and (Son et al., 2020) flew UAVs to visually identify the presence of a HAB. (Stoyneva-Gärtner et al., 2020) conducted aerial observations to help choose water sampling locations. (Son et al., 2020) were interested in forecasting HAB prone regions using

data collected by an acoustic Doppler current profiler (ADCP). Before the development of a HAB, an ADCP mounted to a boat was used to collect data along the river, then airborne monitoring was conducted using an UAV to visually verify the previously derived HAB prone regions. A third study focused on developing a framework for HAB detection by understanding flight parameters influencing UAV performance and image quality. Results provide guidance for successful UAV design and flight parameter choices (Lyu et al., 2017). A real-time HAB detection technique was designed and implemented by (Kim et al., 2019). HABs were detected near desalination plants using UAV imagery and The HSV Color Detection Image Processing Algorithm. Once detected, the velocity and direction of HABs were determined. HAB extraction from the UAV imagery was over 80%, but minor improvements need to be made for the velocity and directional analysis. Once completed, this research could provide an early warning tool for desalination plant managers, preventing HABs from entering the plants.

Algal biomass and concentration were evaluated in four studies, with two focusing on algal biomass and the other two focusing on concentration. (Xu et al., 2018) identified green algae using UAV equipped with RGB camera, then a biomass estimation model was proposed based on S2A imagery. Red algae biomass estimation was conducted by (Che et al., 2021) using an UAV equipped with multispectral sensor. Four vegetation indices were calculated from the multispectral imagery and regressed to estimate biomass. Both (Silvarrey Barruffa et al., 2021) and (Becker et al., 2019) looked to estimate CC using UAVs equipped with a multispectral sensor and spectroradiometer respectively. (Silvarrey Barruffa et al., 2021) implemented a novel image processing workflow and established regression models to find the optimal correlations between band or band ratios and water quality parameters. The result of this research suggests it

is possible to identify cyanobacteria among other photosynthetic organisms using a 4-band multispectral camera. Two custom built UAVs equipped with spectroradiometers were deployed by (Becker et al., 2019) for CC estimation. After imagery processing, four algorithms were applied to the imagery, and CI products derived. High agreement between ground-based surface reflectance values and UAV reflectance values was observed, indicating that UAVs could soon be a common tool in water resource managers toolbox.

Although the four remaining studies evaluated chl-a, apart from (Luo et al., 2021), other water quality parameters were also assessed. (Windle & Silsbe, 2021) sought to evaluate the efficacy of methods that remove surface reflected light (LSR) in UAV hyperspectral imagery to improve the accuracy of remotely sensed water constituents, specifically chl-a and TSS. Results demonstrated that the blue, red, rededge, and NIR bands were most important for estimating TSS concentrations. In addition to the water quality parameters discussed above, (Arango & Nairn, 2019) evaluated TP, TN, and SD. Models were developed using single and multiple variable linear regressions and validated. (McEliece et al., 2020) was interested in estimating the spatial distribution of chl-a and turbidity in a marine environment using a UAV equipped with a multispectral sensor. Calibration functions were formulated and variability in parameter estimates were used to evaluate this methodology. Then, this methodology was implemented on an independent dataset. (Luo et al., 2021) evaluated the spatiotemporal distribution and causes of eutrophication in a desert lake. CDOM was estimated using a UAV equipped with RGB camera. The CDOM absorption coefficient was used as an indicator for CDOM concentration. Blue and green band ratios were most successful for CDOM estimation. For all the studies mentioned in this section, once optimal band ratios were discovered and the developed algorithms were

validated, spatial distribution maps of the desired parameters were generated. All studies concluded that UAVs have the ability to fill current HAB monitoring gaps and should be combined with in situ monitoring and laboratory analysis to verify UAV collected data.

5.2 Hardware and Software

5.2.1 Types of UAV

UAVs (unmanned aerial vehicle less than 55lbs (Small Unmanned Aircraft Systems (UAS) Regulations (Part 107) | Federal Aviation Administration, n.d.)) come in many different forms. Each unique design has benefits and shortcomings, so the nature of the research should match the choice of UAV (Gaffey & Bhardwaj, 2020). The three broad categories of commercially available UAVs are fixed wing aircraft, rotorcraft, and vertical takeoff/landing system (VTOL) (Mohsan et al., 2022). It is important to note, “blimp” systems are also available, but these are much less common. Here, blimps are categorized as rotorcrafts since the system was tethered and is capable of hovering. Only one study included utilized a blimp system (Kim et al., 2019). Fixed wing aircrafts can cover large distances in a single flight due to longer battery life. Rotorcrafts have a shorter battery life but are more agile and easily deployed than fixed wing systems (Bernard et al., 2017, Boon et al., 2017). For example, if there is a need to deploy the UAV from a smaller area (i.e from a boat or small opening in a canopy) then a rotorcraft would be the better solution of these two. VTOLs are hybrids between rotorcrafts and fixed wing aircrafts. They are capable of vertical takeoff but have a fixed wing design to increase flight times. Once a VTOL aircraft reaches the desired flight elevation, the aircraft will turn, making its belly parallel to the ground. It will then rely on its fixed wing design to increase flight duration. The disadvantages to this type of UAV are that they are generally expensive, not as controllable as other models, and

the transition between vertical to horizontal flight requires the UAV to reach a certain altitude (Zhang et al., 2019). Payload size should also be considered before choosing a UAV. Larger payloads reduce battery life, and subsequently flight time. Flight capabilities are specified by UAV manufacturers and should be reviewed before selection. Regardless of UAV type, aircraft performance is heavily dependent upon environmental conditions. Flight time is a function of battery life, which is greatly affected by air temperature, flight elevation, humidity, and wind speeds. Table 1.3 summarizes advantages and disadvantages between these three systems.

Table 1.3 Summary of the advantages and disadvantages between the three main UAV designs: fixed wing aircraft, rotorcraft, and VTOL.

	FIXED WING	**ROTORCRAFT**	**VTOL**
ADVANTAGES:	Longer flight times	Perform closer analysis	Vertical take-off and landing
	Survey larger areas	Vertical take-off and landing	Longer flight times
	Carry heavier payloads	Higher spatial resolution	Survey larger areas
		More stable in high winds	
		Can be automated	
DISADVANTAGES:	Difficult takeoff and landing	Shorter flight times.	Expensive
	Low maneuverability		User control limited
	Inability to hover		Altitude requirement for transition to occur

Figure 1.7 shows the different types of UAVs selected for the studies. It should be noted, rotorcraft has been divided into three subcategories: quadcopter, hexacopter, and octocopter. These categories denote how many rotors the UAV possesses, these being 4,6, and 8 respectively. Of the studies selected, 93% utilized rotorcrafts and 7% fixed wings. For the rotorcraft subcategories, 66% utilized quadcopters, 17% hexacopters, and 10% octocopters (Figure 1.7). Rotorcrafts were the most popular UAV choice, with quadcopters being the most popular rotorcraft selected. Some reasons for this could be that rotorcrafts are generally less expensive than fixed wing vehicles, and quadcopters are the cheapest rotorcraft option (Gaffey & Bhardwaj, 2020). Also, many studies were conducted from boats so there may not have been adequate room for a fixed wing to take off and land. In addition, some studies flew at low altitudes and hovered in single positions, which fixed wings are unable to do. No VTOL was used in any of the studies selected. Reasons for this could be that they are more expensive than both rotorcraft and fixed wing systems, there are less VTOL products commercially available, and less flight software is available for VTOLs. However, with advancements in technology these systems could become more prevalent in future research.

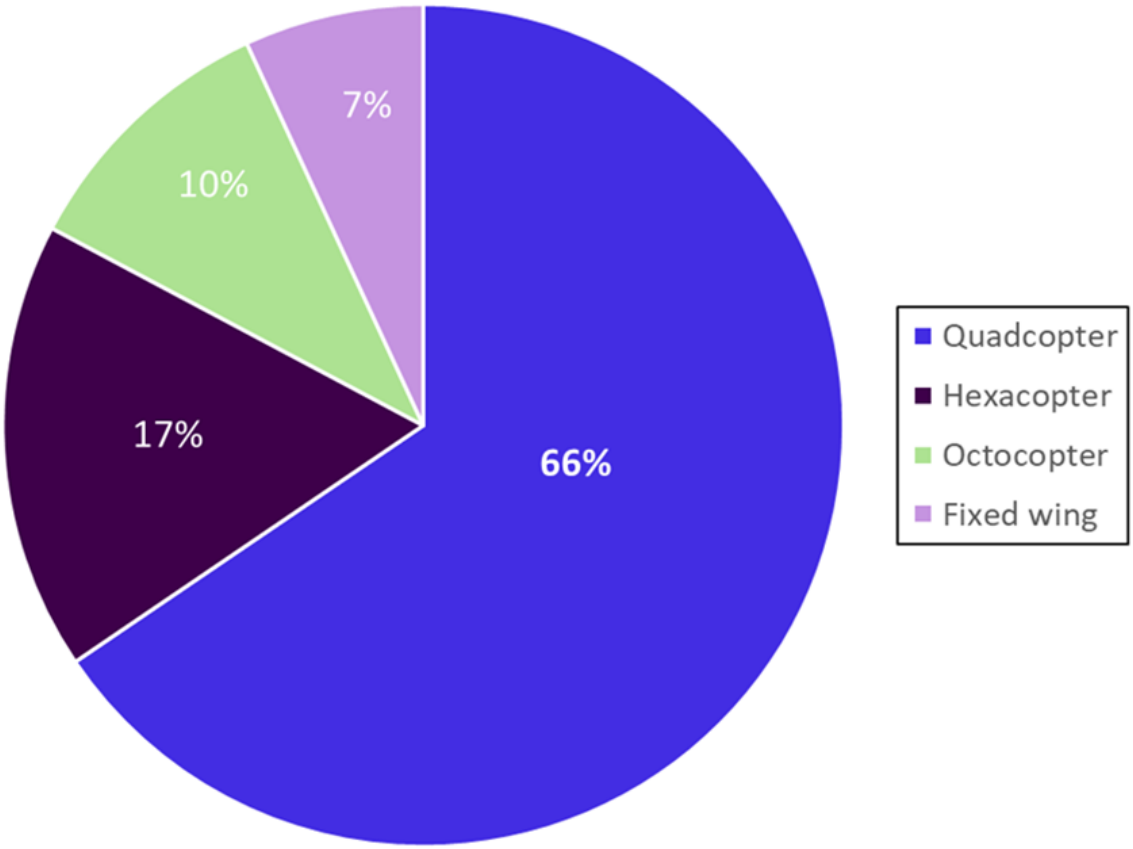

Figure 1.7 The UAV types used by the studies. Percentages represent the frequency of use in the studies. If a study utilized multiple UAV platforms, all were included.

To tailor UAV systems for specific tasks, some researchers customized UAVs that were commercially available or built custom UAVs. (Windle & Silsbe, 2021) 3-D printed custom camera mounts for their UAV systems, allowing both researchers to equip their UAVs with multispectral sensors. Additionally, (Tóth et al., 2021) printed landing gear extensions to prevent the newly equipped sensor from hitting the ground upon landing. (Becker et al., 2019) built a completely custom UAV. This system was waterproof and relatively inexpensive, costing under $2000 to build (not including a sensor). The UAV was controlled by a Pixhawk PX4 flight

controller and equipped with a hyperspectral camera. A drone particle monitoring system was developed by (Bilyeu et al., 2022). The system consisted of an impinger, an optical particle counter, and an environmental sensor. It was mounted on top of the UAV frame to limit the effects of downwash from the UAV propellers. The impinger was based on a design previously developed by (Powers et al., 2018) and was powered using a lithium-ion battery. The optical particle counter recorded six particle size bins and the environmental sensor measured ambient temperature, relative humidity, and barometric pressure.

Both (Hanlon et al., 2022, Kimura et al., 2019) customized UAVs to collect water samples. (Hanlon et al., 2022) retrofitted a commercially available quadcopter to collect surface water samples in three large freshwater lakes. This sampling device, referred to as DOWSE, consisted of a 3-D printed sampling apparatus and a 4.6 m tether line. The sampler was lowered to the water's surface until the tube filled with water, and an image was taken of the sampling location simultaneously. This provided an opportunity to visually inspect the sampling sites and collect GPS locations for all samples. The UAV would then transport the sample back to the researchers, where a new sterile tube was inserted into the sampling device. (Kimura et al., 2019) created a custom UAV with a custom water sampling device. The UAV developed was a quadcopter using a DJI (DJI - Official Website, n.d.) flight controller. The water sampling device consisted of a pulley attached to the frame of the drone by a wire. The sampling device could be lowered and raised remotely. It consisted of three bottles with valves that automatically open at a certain water pressure. This allows water samples to be collected at predetermined depths by adjusting the length of a spring using a bolt in advance. The device could sample at three depths (1, 3, and 5 m). Ultimately microscopic images of the samples were taken, HAB densities

quantified, and real time alert notifications sent to relevant people. This provided public health officials and water resource managers with a real-time notification system.

Although rotorcrafts were the most popular UAV of choice in these studies, that does not mean it is the better platform. In fact, for general monitoring of algal blooms (Kislik et al., 2018) reports that systems were used equally. In some instances, the goal and requirements of the research will determine which platform is the best fit. In situations where both platforms are appropriate, multiple factors can be considered, such as cost and ease of deployment. Currently, no study has directly compared products derived from fixed wings, rotorcrafts, and VTOLs, making it difficult to select the best overall performing platform (Harder et al., 2016).

5.2.2 Types of Attachments

UAVs, especially rotorcrafts, can be equipped with many different attachments. The two types of attachments equipped to UAVs in these studies were sampling devices and sensors. Sampling devices consisted of water samplers and aerosol samplers. Sensors used included RGB, thermal, multispectral, and hyperspectral sensors. Since the previous section highlighted different UAV sampling attachments, this section will focus on the different sensors used throughout the studies. The most popular sensor used throughout the studies was RGB (41%), followed by multispectral (35%), hyperspectral (21%), and thermal (3%) (Figure 1.8). RGB cameras were the most popular sensor used. Some reasons for this could be that almost all commercial UAVs come pre-assembled with an RGB camera and this is the cheapest sensor option.

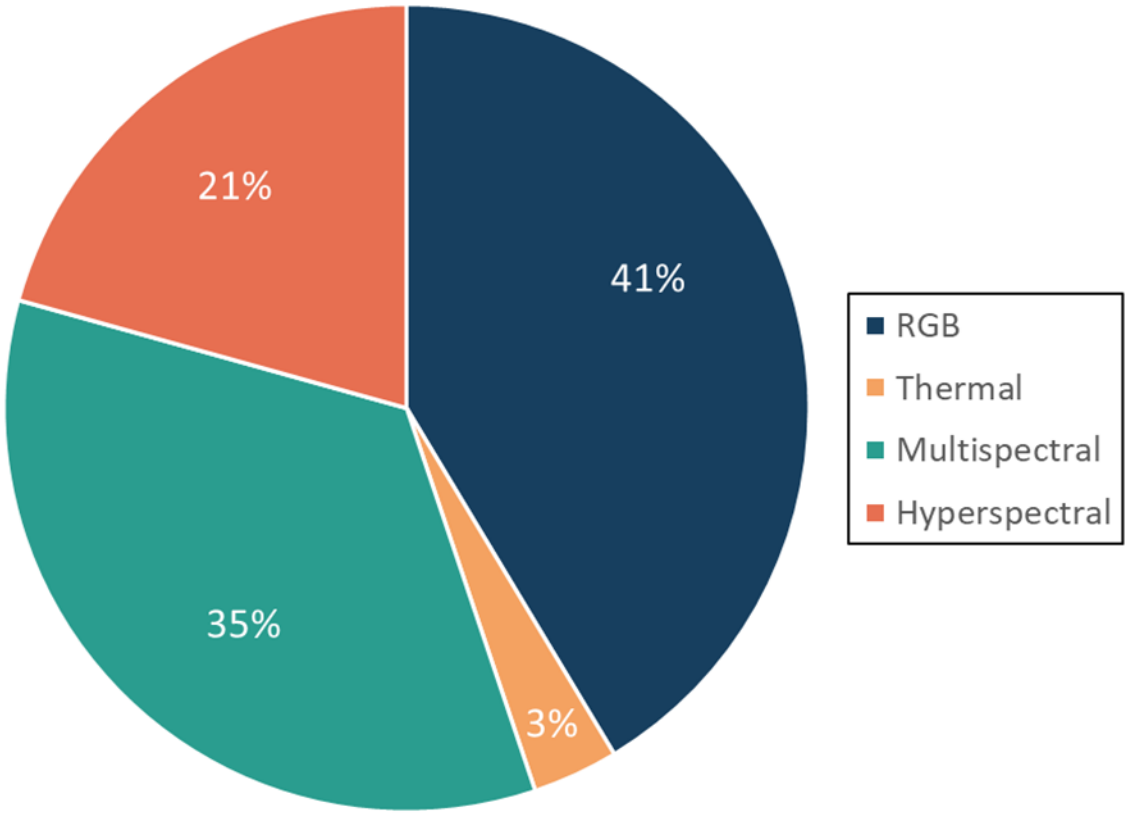

Figure 1.8 The different types of sensors used by the studies. Percentages represent the frequency of use in the studies. If a study utilized multiple sensors, all were included.

Each sensor type has strengths and weaknesses. Although inexpensive, RGB cameras are limited in the type of data that can be collected. These cameras only include three bands (i.e red, green, and blue) limiting the type of analysis that can be conducted. A thermal camera was utilized in a single study (Tóth et al., 2021) and coupled with a multispectral sensor. The advantage of these cameras is that they allow algal warming events to be analyzed (Song et al., 2022). Multispectral sensors are more expensive than RGB cameras but allow data to be collected outside the visible

light spectrum. These sensors utilize imaging technology and spectral technology to obtain data from images using several or dozens of spectral bands. Using photoelectric detection technology, electromagnetic waves are divided into narrower spectral sections. Then information from different bands can be acquired for a desired target. Targets can then be extracted using the spectral differences between target and other features within the imagery (Wang et al., 2019). For example, (Silvarrey Barruffa et al., 2021) research indicates that it is possible to identify cyanobacteria among other photosynthetic organisms when using a multispectral camera. The benefits of this type of sensor are that it provides more spectral data than RGB cameras, at a lower price point than a hyperspectral sensor. Although still quite expensive, an advantage of hyperspectral sensors is that many products can be derived from the data. This is because these sensors can use hundreds of bands. In addition, satellite algorithms can be tested using hyperspectral data by resampling the data, and simulating satellite bands (Becker et al., 2019). Disadvantages to these sensors are that they are expensive and larger than other sensors, which reduces the UAV's flight time.

As with UAV platform selection, many times the goals of the research will determine what type of attachment is needed. If sampling is the goal, custom attachments will most likely need to be developed, as commercially available options are limited. If passively monitoring HABs with sensors, determining what information needs to be extracted will aid in sensor choice. If looking to visually monitor HABs or locate optimal sampling locations, RGB cameras would be the best choice. If looking to quantify HABs using chl-a or PC, multispectral solutions would be an adequate and cost-effective solution. When greater precision is needed, such as

examining genus compositions of HABs, hyperspectral sensors would be the best choice (Kislik et al., 2018).

5.2.3 Software and Programming Languages for Imagery Processing

General steps for processing UAV imagery include reflectance calibration, photo alignment, radiometric calibration, atmospheric correction, and post processing (Eskandari et al., 2020). It is important to note that UAV imagery processing has not been standardized, so many different methodologies can be found in the literature. To aid in deriving meaningful products from UAV imagery, certain software or programming languages can be utilized. Different options are available depending on the sensor type used. In general, software that processes multispectral imagery can also process RGB and thermal images. Hyperspectral data requires different processing techniques, as there is a larger amount of data, and it is formatted differently. For hyperspectral processing, SpectralView Software was the only software used throughout the studies. For RGB, thermal, and multispectral image processing there was more variation in software and programming language choices. Figure 1.9 shows the frequency of different software and programming languages used from all studies. Of the studies selected, 46% utilized Pix4D, 13% Agisoft, 13% Python, and 7% for all four-remaining software.

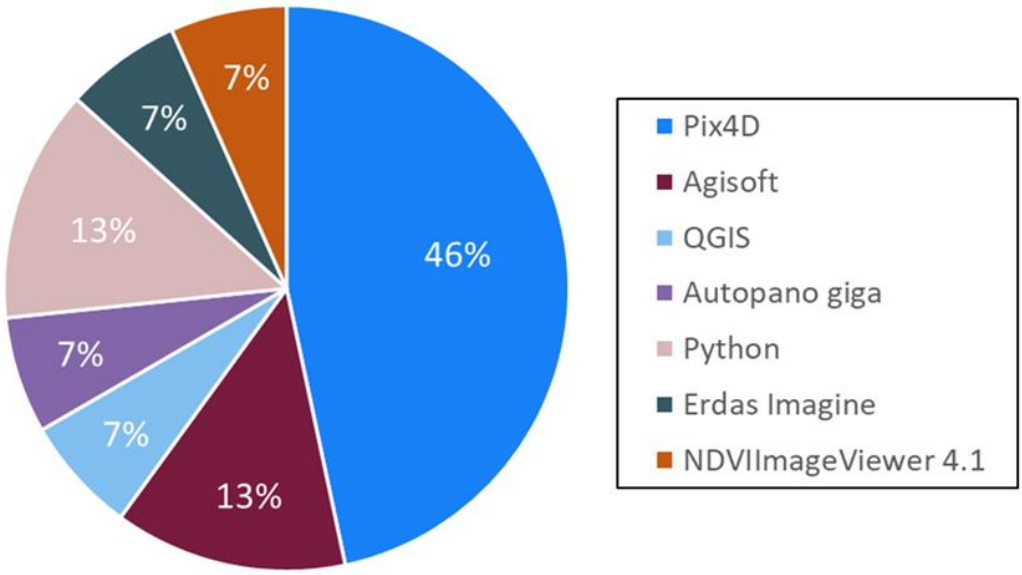

Note: If a study utilized multiple software's all were included. If the study did not generate spatial products or did not specify the software used it was not included.

Figure 1.9 The different software and programming languages used by the studies. Percentages represent the frequency of use in the studies.

Software and programming languages can be used together to create desired spatial products. For example, (Douglas Greene et al., 2021) utilized python code to geo-reference, rotate, and convert images to reflectance. Then the Erdas Imagine Software was used to mosaic and apply band math algorithms to the imagery. Although no studies directly compared products derived from different software, others have. (Isacsson, n.d.) used Agisoft and Pix4D to generate orthomosaics from raw images. Agisoft aligned 142 images, while Pix4D successfully aligned 108 images out of a total of 203. When error reports were compared it showed Agisoft had higher error in the x and y position, while Pix4D had a higher error in the z position. A review on image-based

surface reconstruction workflows conducted by (Eltner et al., 2016) showed that Agisoft was the most popular software choice by far. To our knowledge, no studies monitoring HABs for protecting public health have directly compared products derived from different image processing software. Mapping HABs poses unique difficulties due to the homogenous nature and movement of water. It is possible that one software could better handle these issues, generating higher quality UAV imagery products.

5.3 Quantitative Analysis of Cyanobacteria Related Parameters

5.3.1 Indices Used for Cyanobacteria Quantification

Many different spectral band combinations were utilized for HAB detection and monitoring. Spectral band combinations are either an index, a band ratio, or an algorithm (Cillero Castro et al., 2020). A full list of indices used, and the associated band math can be viewed in Table 1.4. If a study did not apply or mention indices used it was excluded from the table. In addition, studies who did not use pre-defined indices, but generated their own, utilizing band ratios or algorithms, were not included in the table. Studies not included in the table will be discussed in more detail in section 5.3.3.

Table 1.4 Spectral indices used for distinguishing HAB from all studies reviewed. Only pre-defined indices were included in this table. If multiple researchers used the same index, all were cited under "reference".

Index	Formula	Reference
Normalized Difference Vegetation Index (NDVI)	(NIR − Red)/(NIR + Red)	Choo et al. (2018), Silvarrey Barruffa et al. (2021), Che et al. (2021), Douglas Greene et al. (2021), Cillero Castro et al. (2020)
Normalized Green Red Difference Index (NGRDI)	(Green − Red)/(Green + Red)	Xu et al. (2018)
Normalized Green Blue Difference Index (NGBDI)	(Green − Blue)/(Green + Blue)	Xu et al. (2018)
Green Leaf Index (GLI)	(2 * Green – Red − Blue)/(2 * Green + Red + Blue)	Xu et al. (2018)
Excess Green (EXG)	2 * Green − Red − Blue	Xu et al. (2018)
Cyanobacteria Index (CI)	CI = −SS (681)	Becker et al. (2019)
The Colour Producing Algorithm (CPA-A)	Bio-optical inversion model	Becker et al. (2019)
Surface Scum Index (SSI)	SSI = ((NIR)-(VIS)/(NIR)+(VIS))	Becker et al. (2019)
Kab 1	1.67–3.94 ∗ ln(Blue) + 3.78 ∗ ln(Green)	Cillero Castro et al. (2020), Douglas Greene et al. (2021)
Surface Algal Index (SABI)	(NIR − Red) / (Blue + Green)	Cillero Castro et al. (2020), Douglas Greene et al. (2021)
KIVU	(Blue − Red) / Green	Cillero Castro et al. (2020), Douglas Greene et al. (2021)
Normalized Difference Chlorophyll Index (NDCI)	(RE−Red)/(RE + Red)	Cillero Castro et al. (2020)
2BDA_1 (2 band algorithm)	NIR/Red	Cillero Castro et al. (2020)
2BDA_2 (2 band algorithm)	RE/Red	Cillero Castro et al. (2020)

Continued

Table 1.4 continued

3BDA_1 (3 band algorithm)	$(Red^{-1} - RE^{-1})*NIR$	Cillero Castro et al. (2020)
3BDA_MOD (3 band algorithm modified)	$Red^{-1} - RE^{-1}$	Cillero Castro et al. (2020)
B3B1 (normalized index)	(Green − Blue)/(Green + Blue)	Cillero Castro et al. (2020)
GB1 (Simple ratio)	Green/Blue	Cillero Castro et al. (2020)
GR (Simple ratio)	Green/Red	Cillero Castro et al. (2020)
Normalized Difference of Red Edge(NDRE)	(NIR − RE)/(NIR + RE)	Che et al. (2021), Douglas Greene et al. (2021)
Difference Vegetation Index (DVI)	NIR − Red	Che et al. (2021)
Ratio Vegetation Index (RVI)	NIR/Red	Che et al. (2021)
Blue Normalized Difference Vegetation Index (BNDVI)	(NIR − Blue) / (NIR + Blue)	Douglas Greene et al. (2021)
Fluorescence Line Height (FLH Blue)	Green − (Red + (Blue − Red))	Douglas Greene et al. (2021)
SHI Index	$(e^{Red} - e^{NIR})/(e^{Red} + e^{NIR})$	Douglas Greene et al. (2021)

Five of the seven studies utilizing pre-defined indices applied multiple, allowing the optimal index to be determined. (Silvarrey Barruffa et al., 2021) only applied NDVI but used the index as an initial image correction step to distinguish between water pixels, emergent plants, and submerged vegetation. (Choo et al., 2018) also applied NDVI and found reasonable agreement between the index and measured chl-a values (R^2=0.7031). Out of the 16 indices analyzed by (Cillero Castro et al., 2020) the best performing models for retrieving chl-a were B3B1, GB1, and G/R. Out of these, B3B1 produced the highest Pearson correlation coefficient (r=0.9907), highest R^2 (0.98), and highest significance level (****). These results suggest that the

combination of blue-green bands is best for discriminating between very different chl-a concentrations. (Xu et al., 2018) found that NGRDI had the highest accuracy out of the four vegetation indices tested. In addition, NGBDI was able to distinguish blue nylon ropes from algae, but incorrectly classified some shadows and water as algae. With this information, both indices were combined to identify algae. All four of the indices examined by (Che et al., 2021) exhibited strong positive correlations with algal biomass, indicating that DVI, RVI, NDVI, and NDRE are all promising indicators of biomass estimation. (Douglas Greene et al., 2021) found that all eight of the indices tested resulted in poor relationships with measured chl-a values. The SHI index produced the highest R^2 value at 0.18. These low values were attributed to poor weather conditions during UAV imagery acquisition. This study highlights the need for ideal conditions (i.e clear weather, wide range of HAB concentrations) when calibrating and testing a new model.

5.3.2 Validation Techniques

All studies employed some form of validation. This is because UAV imagery processing has yet to be standardized and is still a relatively new technology, so results should be compared to traditional quantification methods (Silvarrey Barruffa et al., 2021). Most studies collected water samples directly before or after the UAV flights. GPS locations were taken for all sampling locations as well. Samples were taken for lab analysis of chl-a using either a spectrophotometer or fluorometer. Some studies used microscopy to identify specific algal species. In addition to chl-a validation, some studies used handheld spectroradiometers to collect "at surface" reflectance values. These values can then be compared to post-processed UAV imagery reflectance values to evaluate how effective the implemented imagery processing

workflow was. In summary, when conducting UAV research for HABs, some form of validation should be used.

5.3.3 Modelling Approaches

Since advancements in UAV platforms and sensors, many HAB detection algorithms have been developed. These fall into three categories: empirical, semi-empirical (ratio-based), and more sophisticated statistical algorithms, such as those utilizing spectral derivatives (El-Alem et al., 2021, Sawtell et al., 2019). Several developed algorithms have been shown to perform well for chl-a estimation. For example, both (Kim et al., 2019) and (Shang et al., 2017) implemented previously developed algorithms with success. (Kim et al., 2019) utilized an HSV-based color detection algorithm to extract HABs from UAV imagery with over 80% efficiency. The perk of using this algorithm is it allows for the same color to be tracked in imagery, even if its position and brightness changes. (Shang et al., 2017) generated an empirical algorithm for chl-a estimation based on previously developed wavelength-shift (Gitelson, 1992) and a fluorescence line height algorithm (Letelier, 1996). Results suggested that UAVs were a good option to meet urgent needs during HAB outbreaks. Out of the studies selected, most utilized empirical or semi-empirical methods to estimate HAB indicators. A few utilized more sophisticated statistical methods such as Ensemble-based systems or deep learning models. Studies were categorized as using three main approaches for quantitative assessment of UAV gathered data: linear regression, multiple linear regression, and machine learning models.

Linear regression was the most popular method, most likely due to its ease of implementation. (Luo et al., 2021) extracted CDOM absorption coefficients from UAV imagery as a proxy for lake eutrophication during three stages of crop growth. The CDOM absorption

coefficient was modelled using the B/G band ratio. To evaluate the accuracy of the estimated CDOM absorption coefficients, fluorescent dissolved organic matter (fDOM) values taken using a YSI water quality probe were used. Regressions showed a strong correlation during all three crop growth stages between the two (r=0.85, 0.86, 0.71 respectively). This suggested that the B/G band ratio was best for estimating CDOM at this location. Similarly, (Tóth et al., 2021) found that B/G band ratio using light level data (rather than irradiance or reflectance) was a better input than NIR/R band ratios when estimating chl-a concentrations, producing a r=0.96. Using 450 surface chl-a measurements, (Cheng et al., 2020) developed a chl-a concentration model using linear, power, and exponential regressions. It was found that R/B was the best input for the chl-a estimation model at this site when utilizing a UAV with RGB camera. This linear model produced a R^2=0.84 and a RMSE of 3.17 µg/L. (Cheng et al., 2020) notes that the model's prediction accuracy is less adequate for chl-a concentrations greater than 20 µg/L. Using a hyperspectral sensor and in situ vertical pigment concentrations, a semi-empirical algorithm was developed by (Kwon et al., 2020) for PC and chl-a. For PC, the 709 and 620 nm bands were used, while 709 and 665 nm were utilized for chl-a. Coefficients for algorithms were obtained using linear regressions between band ratios and measured pigment concentrations. The best performing bio-optical algorithm produced an R^2=0.82. Orthogonal regression was utilized by (McEliece et al., 2020) to calibrate their chl-a estimation algorithm. Best model fits were achieved when utilizing wavelength bands centered around 448 and 550 nm. The percentage of variance explained by the fitted function was 78%.

(Silvarrey Barruffa et al., 2021) utilized multiple linear regression models to find optimal correlations between band ratios and water quality parameters. All band ratios were evaluated as

limnological properties can influence remotely estimated chl-a values (Zhao et al., 2011). For linear regression the best model utilized G, RE, G/RE, R/NIR, RE/NIR, R/NIR^2, R^2, RE/NIR^2 band ratios and resulted in R^2 equal to 0.79 for chl-a and 0.77 for CC. Single and multiple linear regression models were utilized by (Arango & Nairn, 2019) for TSS, chl-a, SDD, TP, and TN estimation. The highest performing model for chl-a estimation (R^2=0.846) was a multiple linear regression model using green and red bands. (Baek et al., 2019) took a similar approach for chl-a estimation utilizing blue, green, and red wavelengths. In addition, red edge was used for distinguishing suspended matters and NIR utilized for sun glint corrections. The best performing model produced an R^2=0.942 for UAV derived chl-a and in situ chl-a measurements. A multiple linear regression model developed by (Windle & Silsbe, 2021) for chl-a produced an R^2=0.43 and RRMSE=37%. These results were compared to other studies (Gons, 2002, Sawtell et al., 2019, Gitelson et al., 2007) whose results were standard error of 9.2 µg/L, relative root mean square error (RRMSE) 37%, and RRMSE=51.9% respectively.

More advanced statistical methods used for estimations included the application of ensemble-based system and deep learning models. (El-Alem et al., 2021) developed a chl-a estimation model based on UAV imagery data utilizing an EBS. This model was applied to both UAV imagery, and satellite imagery, providing local and regional estimations. To improve accuracy, specific models were made for three different trophic levels of waterbodies: oligotrophic, mesotrophic, and eutrophic. (Tóth et al., 2021) took a similar approach for linear regression model development, dividing measurements into five unique water level categories. This approach suggests that categorizing measurements and developing models specific to each could enhance the quality of estimates. The EBS developed by (El-Alem et al., 2021) performed

well at a local scale and regional scales, producing R^2= Nash = 0.94 and RMSE = 5.6 μg/L and R^2 = 0.85, RMSE= 2.4 μg/L, and Nash = 0.79 respectively. It is worth noting, the model failed to correctly estimate chl-a in highly turbid waters. Both (Pyo et al., 2022) and (Hong et al., 2021) applied deep learning models for estimations. (Pyo et al., 2022) utilized a one-dimensional convolutional neural network (CNN) to generate spatial maps and estimate concentrations of chl-a, PC, lutein, fucoxanthin, and zeaxanthin. Bio optical algorithms were also applied to the data, and results of all models were compared. The CNN utilized UAV gathered absorption and reflectance data as inputs. The network performed well in estimating concentration for all pigments, showcasing the highest R^2 when estimating chl-a (R^2=0.87). Comparatively, the bio-optical algorithms showed relatively low performance when estimating chl-a (R^2=0.66). (Hong et al., 2021) monitored the vertical distribution of HABs using four different CNN structures (ResNet-18, ResNet-101, GoogleNet, and inception v3). To do this, chl-a, PC, and turbidity were estimated by the CNN using hyperspectral drone imagery as the input. The ResNet-18 model performed the best with R^2=0.7. Although not applied to UAV imagery, (Kimura et al., 2019) utilized a CNN to classify five different classes of plankton found in water samples collected by a UAV. After the model was trained, classification accuracy of plankton was 99.5%. This allowed hazardous species to be detected and quantified.

5.4 Discussion and Recommendations

5.4.1 Issues Encountered in Using UAVs for CyanoHAB Monitoring

The main issues encountered by researchers were adverse weather conditions affecting UAV flights, the inability to stitch images over water, and removing external influences from spectral data (Douglas Greene et al., 2021) performed UAV flights during cloudy days, with

intensifying winds and light rain. It was noted, these weather conditions negatively affected model development, and highlights the need for optimal environmental conditions when developing models based on UAV data. High winds, rain, and changing lights conditions can negatively affect UAV gathered data by adding additional noise or altering reflectance values (Stoyneva-Gärtner et al., 2020, Wierzbicki et al., 2015). In addition, lag between UAV collected data and in situ data should be minimized (Becker et al., 2019). This is because solar illumination can greatly affect many properties of water, resulting in different reflectance values (Sekrecka et al., 2020), Choo et al., 2018). In addition, solar illumination can cause sunglint (specular reflection), which makes reflectance values in this area higher, leading to inaccurate estimations. Solar illumination can also cause shadows to be present in the imagery, resulting in inaccurate reflectance values. To avoid this, (Silvarrey Barruffa et al., 2021) suggested conducting flights mid-morning or mid-afternoon.

To overcome the issue of stitching images over water, (Douglas Greene et al., 2021) developed a novel geometry-based image stitching framework for overwater images and implemented it successfully. Briefly, images were georeferenced by generating words files for each image containing dimension of pixels in x-direction, rotation in x-direction, x-coordinate of the upper left pixel, dimension of pixels in y-direction, rotation in y-direction, and y-coordinate of the upper left pixel. Once created, these were read by Erdas Imagine Software to facilitate imagery stitching. (Douglas Greene et al., 2021) published the python code for this framework, making it publicly available, potentially removing a substantial obstacle for others by providing an effective method for overwater image stitching. Other options for improving overwater image stitching include flying at higher elevations and including other forms of terrain in each image.

Doing this allows for more features to be in a single image, providing higher chances for key points to be detected (Elhadary et al., 2022).

Removing undesired influences from spectral data was the most common issue faced in the studies. Aguirre-Gómez et al., 2017 found that absorption and reflectance peaks can be slightly shifted by external factors. In this case, small islands and a waterfront restaurant were presumably responsible for shifts. (McEliece et al., 2020) highlights major limitation in measuring water quality with UAVs in complex, shallower waters, which is the issue of bottom reflectance. Bottom reflectance can cause deviations in reflectance data between shallow and deepwater locations. In addition, aquatic vegetation can influence UAV derived data in shallow waters, causing overestimation of HAB indicators such as chl-a (Zeng et al., 2017). Currently, there is no simple solution for removing the influence of bottom reflectance in optically complex, shallow waters. Water quality parameters can also influence UAV data quality. (El-Alem et al., 2021) found that the EBS failed to accurately estimate chl-a concentrations in highly turbid waters. However, it was discovered that highly turbid waters reflect strongly in the red portion of the spectrum, instead of green. With this information, it is possible to identify highly turbid waters and exclude these before chl-a modelling. In future research of turbid waters, researchers may benefit from sensor packages that utilize longer wavelengths (e.g. shortwave infrared, SWIR) (Windle & Silsbe, 2021).

5.4.2 Regulations

The Federal Aviation Administration (FAA) is a United States government agency that regulates all aspects of aviation in the country, including in scientific research. The FAA categorizes UAV usage as either “recreational” or “commercial”. Scientific research is usually

categorized as “commercial” usage, subjecting it to Part 107 regulations. These require the researcher to become Part 107 certified by passing an aeronautical knowledge test (Small Unmanned Aircraft Systems (UAS) Regulations (Part 107) | Federal Aviation Administration, n.d.). Following Part 107 guidelines ensures safety for researchers, and other pilots who may be in the area. For individuals engaged in international collaborations, it is important to note that UAV regulations differ internationally (Gaffey & Bhardwaj, 2020). Nations may have different regulations regarding operational requirements and limits (Cracknell, 2017). Understanding these and meeting these is essential for avoiding legal consequences and ensuring desired outcomes are met. In addition, international UAV regulations may be concerned with privacy and data collection, especially in protected or restricted locations. For example, the FAA restricts any UAV be flown in National Parks without pre-approval. Also, certain UAV models are completely restricted from flying in certain locations. Researchers should be aware of these restrictions, and coordinate with local governing entities to meet requirements (Duffy et al., 2018). Staying up to date with current regulations is also important for individuals engaging in UAV research, as laws are constantly being adapted. For example, as of September 16, 2023, the FAA requires all UAVs be equipped with remote ID (UAS Remote Identification | Federal Aviation Administration, n.d.). Remote ID provides information on UAVs in flight, such as identity, location, altitude, and take-off location. In addition, authorized individuals from public safety organizations may request UAV information from the FAA. In summary, the FAA has provided a general framework for safe UAV usage within the United States. Researchers engaging in global collaborations should recognize that regulations can vary drastically internationally, impacting research feasibility and objectives. Proactively addressing these

regulations will lead to the best outcomes, ensuring that UAV based research is conducted safely and legally across borders (Cracknell, 2017).

5.4.3 Considerations Before an UAV Mission

Several factors should be considered before conducting a UAV flight to ensure safe and effective research. Key factors for consideration include type of UAV and attachments, sensor type, flight location characteristics, altitude of flight, weather conditions, and ground control station requirements (Mohsan et al., 2022, Duffy et al., 2018, Gaffey & Bhardwaj, 2020). Selecting the appropriate UAV is crucial for HAB quantification. Depending on the objectives of the research, one type of UAV may be a better fit. Factors to consider include flight stability, payload capacity, GPS capabilities, and the ability to integrate custom attachments or sensors. Refer to section 3.1 for in-depth discussion of UAV types. Payload capacity is an important factor to consider. Understanding a UAVs' payload capacity will result in longer and safer flights (Mohsan et al., 2022). Having GPS capabilities aboard the drone is optimal. This will provide geolocation data for all images or samples collected by the UAV, aiding in data analysis and map generation (Hanlon et al., 2022). If special modifications or attachments are necessary, these should be evaluated and tested before research is conducted. After-market modifications can affect flight times and aerodynamics of the system, so UAV manufacturers or experts should be consulted before modifications are made. In addition, if commercial sensors are being purchased, understanding the limitations of the sensor is important. Refer to section 3.2 for discussion of the different sensor types, and ideal applications of each. Ensuring that the sensor is compatible with the UAV is crucial. Most UAV and sensor manufacturers can provide necessary information on this.

In addition to UAV parameters, flight location characteristics such as size and volume of air traffic should be evaluated and understood thoroughly. The size of the study site will influence flight planning and flight time requirements, such as appropriate flight paths, data collection strategy, and battery requirements. To avoid gaps in data collection, flight paths should extend over the entire area of interest and beyond, as data collected on the edges of the flight area tend to be lower quality (Eskandari et al., 2020). Also, waypoints can be strategically placed within flight planning software to better fit the shape of the study site minimizing unnecessary overlap or gaps in data acquisition (Duffy et al., 2018). This helps reduce data processing time and results in higher quality UAV products. In addition, choosing the correct "overlap" is necessary for generating maps from UAV data. "Overlap" is a term used to describe how much forward and side overlap there is between each image. In general, a front and side overlap between 60-80% is adequate for generating high quality UAV map products, but sensor guidelines should be reviewed for guidance (Eskandari et al., 2020). Increasing overlap requires longer flights to take place and more images to be taken, while smaller overlap values will result in faster flights with fewer images (Elhadary et al., 2022). A final characteristic to consider about study location is the volume of air traffic in that area. The UAV pilot is responsible for knowing what other aerial vehicles are in the area and avoiding them. Flights should be scheduled to minimize conflicts with manned aerial vehicles (Duffy et al., 2018). Many tools are available to help with this such as airspace maps and mobile applications. In addition, it is the pilot's responsibility to ensure compliance with local regulations and avoid restricted flight zones unless a permit has been acquired. Discussing these with aviation authorities, environmental agencies,

and local authorities will help ensure all requirements are met and prevent any legal consequences.

UAV flight altitude is also an important factor to consider when planning a UAV mission (Elhadary et al., 2022). Higher flight altitudes will negatively impact battery life resulting in short flight durations. Conversely, higher flight altitudes allow for larger areas to be covered by the UAV in a shorter amount of time. Flight altitude directly impacts GSD as well (Eskandari et al., 2020). GSD refers to the distance between pixel centers measured on the ground, usually in units of cm/pixel. Of the studies selected, GSD varied from 3 cm to 20 cm, with most studies utilizing a GSD below 10 cm. The selected GSD will affect resolution of the imagery and is usually smaller than the effective resolution due to image blur and changes in lighting conditions (Lyu et al., 2017). Higher GSD values allow for faster data acquisition but result in lower resolution, while lower GSD values provide higher resolution at the cost of longer flight times and increased data processing requirements (Choo et al., 2018). GSD should be determined based on research objectives and hardware limitations. Conducting test flights prior to data collection can help determine the optimal flight altitude that balances data quality, flight durations, and required GSD.

Briefly mentioned previously, weather conditions such as wind speed, precipitation, visibility, and temperature will affect UAV capabilities (Duffy et al., 2018). UAVs should not be flown in adverse weather conditions that could affect UAV stability or data quality. Doing so could endanger individuals in the area or result in the destruction of the UAV and accompanying equipment. If wind speeds are relatively high, but still within UAV flight capabilities, consider flying perpendicular or at an angle to the wind direction (Coombes et al., 2020). This will help

minimize power consumption and prolong battery life. Currently, many commercially available UAVs are waterproof to an extent, so it is possible to fly during light precipitation events. Although this is the case, it is not recommended as it will reduce data quality (Douglas Greene et al., 2021). Also, extreme temperature conditions can impact UAV performance (Silvarrey Barruffa et al., 2021). Cold temperatures can reduce battery capacity, while high temperatures can increase the chances of equipment overheating. Consider using some form of temperature regulation if operating UAVs in extreme temperatures. Monitoring weather forecasts and selecting flight times with suitable weather conditions is crucial for the safety and effectiveness of UAV data collection.

A final factor to consider when planning a UAV flight is ground control station requirements (GCS). A reliable GCS provides researchers with the ability to monitor UAV status, control flight parameters, and oversee data collection. In addition, ground control points (GCPs) in conjunction with global navigation satellite systems (GNSS) can be utilized to aid in post processing of UAV imagery. Ground control points are distinct markers that can be located within the imagery. These can be unique features naturally in the image or manually placed in open canopy locations by the researcher. GCPs can improve imagery stitching and improve the accuracy of georeferenced data (Awasthi et al., 2020). For some study sites, such as flights over open water, placing GCPs may be unrealistic, as GCPs should not move during flights, or they are useless. (Gaffey & Bhardwaj, 2020) notes four different methods to aid in georeferencing when using GCPs. No matter the method selected, it is important to ensure that the GCS selected is compatible with both the UAV and sensor being used.

5.4.4 Future Opportunities

The most common recommendation for future studies is the standardization of UAV imagery processing. Both (Kimura et al., 2019) and (Shang et al., 2017) state that obtaining accurate surface reflectance values can be challenging, so data processing protocols should be standardized, and new techniques developed. Improvements could be made to prevent interferences on surface reflectance so that true surface reflectance values can be determined accurately. Also, as mentioned previously, the influence of the seabed on reflection values should be corrected for, but no simple solution exists for this yet, so future research could provide a solution to this problem (McEliece et al., 2020). (Baek et al., 2019) mentions that future work could be done to evaluate the effects of atmospheric interference on UAV imagery and create methods for correcting these effects. Other future areas of research include validating current models with more data and UAV hardware improvements. Both (Xu et al., 2018) and (Son et al., 2020) state that more data must be collected to improve and validate the models developed. A way to do this, proposed by (Luo et al., 2021), is combine more lab analysis data with UAV data. (Cheng et al., 2020) states that future research should explore the effects of suspended solids and algal species on models developed, while (Cillero Castro et al., 2020) mentions a need for more data to be collected on waterbodies with different eutrophication levels. Similarly, (Pyo et al., 2022) mentions a need for the model developed to be applied to different waterbodies, assessing the model's performance at other locations. Furthermore, future research should consider weather data with UAV data, as (Hong et al., 2021) showed that weather factors affected water quality parameters at both surface and subsurface levels in the water. (Douglas Greene et al., 2021, Che et al., 2021, Lyu et al., 2017) all state that future

research could be conducted on improving UAV and sensor performance. If lightweight hyperspectral sensors become more common, spectral libraries could be developed, aiding HAB monitoring using UAVs.

6. Major Objectives of the Thesis

As increases in frequency, duration, intensity, and geographical location of harmful algal blooms (HABs) have been observed, more timely monitoring and targeted treatment of HABs and their cyanotoxins are crucial for freshwater bodies that are used for drinking water, recreation, and food production sources. To combat this, new management practices with tools that can handle the spatial and temporal variability of HABs are needed (Shi et al., 2019) for water treatment plants and other sectors to ensure human health and ecosystem health. As reviewed, UAVs are emerging as a low cost and efficient tool for monitoring HABs, but UAVs alone are not adequate as they cannot provide insight on cyanobacterial genera present or cyanotoxin concentrations in water. In addition, the seasonal dynamics and microbial roles filled by cyanobacteria should be evaluated, as seasonal succession could affect UAV derived cyanobacteria levels. Therefore, there is a need for a multi-scale and multi-modal (multiple methods, each with different spatial extents) approach for detection and monitoring of cyanoHABs in PWS. To my knowledge, this is the first attempt at detecting and monitoring cyanobacteria using both microbial and geospatial techniques. Molecular and sequencing techniques employed here go beyond standardized lab testing (ELISA, LCS/MS, etc.), and instead analyze the whole microbial community, not just cyanobacteria and associated toxins.

In chapter 1, major relevant topics are summarized related to cyanoHABs, public health, and UAV systems. This provides a holistic view of current knowledge, methods, and limitations

in cyanoHAB monitoring and detection. In chapter 2, microbial techniques are used to explore the microbiome within an urban, hypereutrophic lake. The objectives of chapter 2 are to 1) analyze the seasonal dynamics of water quality, cyanobacteria, and microbial community, 2) determine the microbial community composition, with a focus on the cyanobacterial community, using 16S and 18S rRNA sequencing data, and 3) analyze cyanobacterial interactions within the microbial community to provide insight on the seasonal variation within cyanobacterial communities, and how cyanobacteria taxa interact and impact other microorganisms within a hypereutrophic waterbody. In chapter 3, the feasibility and accuracy of using an UAV system for monitoring a hypereutrophic, urban water body was assessed. The objectives of this chapter are to 1) propose a UAV system and imagery processing framework that can be used by non-geospatial experts, 2) evaluate the relationship between ground sampled fluorometer values and remotely sensed values, and 3) determine best algorithms and buffer sizes for cyanobacteria quantification.

Chapter 2. Seasonal Dynamics and Relationships of Water Quality, Microbial Community, and Cyanobacteria in a Hypereutrophic Urban Lake

1. Abstract

The occurrence of cyanobacterial harmful algal blooms (cyanoHABs) in urban water bodies is relatively under studied. Most studies are focused on large bodies of water such as Lake Erie and Grand Lake St. Mary's in Ohio, United States, and the same trend has been shown in other countries. However, small urban waterbodies are intensively used by relatively dense populations and are in close proximity to nearby residents. Thus, they can pose a risk to public health. This study aimed to get a wholistic view of potential cyanoHAB drivers and cyanobacterial interactions within microbial communities in a small urban lake located in Columbus, Ohio. For this, bi-weekly samples were collected from the beginning of April to the end of September 2022. The temporal dynamics of the microbial community were analyzed using 16S and 18S rRNA gene sequencing data, with a focus on the cyanobacterial community. Additionally, variations in environmental variables were analyzed and correlated with microbial diversity indices. Our results showed that seasonal variations affected diversity indices. *Planktothrix* NIVA-CYA 15 was the dominant cyanobacteria genus throughout the entire sampling period. Digital droplet polymerase chain reaction (ddPCR) assay results showed the presence of toxic cyanobacteria that possess microcystin-, anatoxin- and saxitoxin-producing genes. Analyses indicated that seasonal shifts were caused by multiple environmental variables, with the most apparent one being increasing water temperature. Our study observed seasonal

dynamics of cyanobacteria and confirmed the association between temperature and average relative abundances of cyanobacteria genera. Although cyanotoxins (microcystin, anatoxin, and saxitoxin) were under recreational water advisory levels, certain environmental parameters could trigger the production and release of these toxins, posing a risk for public health. Thus, continuous monitoring is recommended during the warm season.

Keywords: microcystin, microbiome, anatoxin, saxitoxin, microbial diversity, recreational water

2. Introduction

Microorganisms are the most abundant organisms on Earth and play crucial roles within freshwater ecosystems (Konopka, 2009). Microorganisms rarely exist in isolation, but instead form complex, interconnected communities. Recently, anthropogenic impacts have negatively impacted microbial communities, specifically by decreasing biodiversity (Ghoul & Mitri, 2016, Amorim & Moura, 2021). For example, non-pervious surfaces have led to over nutrification of water systems, resulting in more frequent and intense cyanoHABs. These can negatively impact biodiversity within aquatic ecosystems (Toporowska & Pawlik-Skowrońska, 2014). This loss in biodiversity diminishes the efficiency of microbial ecosystem services, including those beneficial for human health (Amorim & Moura, 2021). Therefore, to protect microbial diversity and subsequently human health, regular monitoring of cyanoHABs is necessary. Methods for monitoring cyanoHABs in the environment include molecular methods, amplicon sequencing, and fluorescence techniques (Chorus, 2021). A current molecular method used is ddPCR. This method is targeted, quantifying a specific DNA sequence. This method indicates the potential for cyanotoxin production but does not provide information about actual toxin concentrations in the water body (Chorus, 2021). Nevertheless, this method can be implemented as an early warning

tool, indicating the potential for toxin production of a developing cyanoHAB. In addition, ddPCR can be used for microbial source tracking (MST), which helps identify sources of fecal pollution (Hart et al., 2023). Excess amounts of fecal pollution can lead to over nutrification, aiding in cyanoHAB formation (Ballesté et al., 2021). Identifying sources of fecal input is necessary for mitigating cyanoHAB formation and the protection of human health.

Amplicon sequencing approaches include, but are not limited to, 16S and 18S rRNA gene sequencing. The 16S rRNA region provides information on all bacteria present, not just cyanobacteria. This allows for analysis of the microbial community as a whole and provides insight into what portion is comprised of cyanobacteria (Casero et al., 2019). Additionally, different genera of cyanobacteria can be distinguished, providing information on dominant cyanobacteria taxa. Furthermore, sampling throughout the development of cyanoHABs can provide insight into cyanoHAB dynamics, and how the formation of these alters the microbial community. 18S rRNA gene sequencing provides information on eukaryotic microbes present in a waterbody. This provides information on non-toxic algae taxa and potential cyanobacteria grazers (Santhakumaran et al., 2019). Amplicon sequencing techniques are widely used due to its convenience in taxonomic classification and ability to derive information on microbial diversity (Escobar-Zepeda et al., 2015). It is well known that aquatic ecosystem health is affected by microbial diversity. Thus, understanding the role cyanobacteria play in altering microbial diversity is necessary to develop proper management strategies. Disadvantages of amplicon sequencing methods include low taxonomic resolution at the species level and difficulties in amplification of the desired gene when samples have a low abundance of genomic sequences (Bodilis et al., 2012, Nalbantoglu et al., 2014).

Multiple methods for quantifying cyanoHABs based on fluorescent characteristics are available. These include the use of handheld fluorometers, on-site monitoring network, and remote sensing applications (Almuhtaram et al., 2021). These methods measure the fluorescence of specific pigments such as chlorophyll-a (chl-a) and phycocyanin (PC). Chl-a is a pigment present in all phytoplankton, making it useful for estimating phytoplankton biomass and the eutrophication status of a waterbody (Gupana et al., 2021). PC is more specific to cyanobacteria, making it useful for determining cyanobacterial biomass (Chorus, 2021). Many commercially available handheld fluorometers are capable of measuring both pigments, providing an efficient method for monitoring eutrophication and cyanobacterial biomass in aquatic systems (Thomson-Laing et al., 2020). Disadvantages to this method are that it only provides point data and requires field personnel for sample collection. To overcome these, on-site monitoring networks can be utilized. These systems are suited for online real-time monitoring, eliminating the need for concurrent field sampling (Almuhtaram et al., 2021). These can be placed at areas of importance, such as water intakes, for constant monitoring as well as automated alerts if chl-a or PC thresholds are exceeded. Although these systems provide high frequency monitoring, they are unable to address the spatial extent of cyanoHABs, as they are inconsistent in space and time (Chorus, 2021). Remote sensing applications are a solution to this. Remote sensing applications include satellite remote sensing, manned aerial surveys, and unmanned aerial vehicles. For more information on the advantages and disadvantages of each of these, refer to chapter 1 section 4.1.2. As highlighted, each method mentioned has advantages and disadvantages, so it is necessary to use a combination of these for adequate monitoring and quantification of cyanoHABs.

Based on this information, a hypereutrophic urban lake located in Columbus, Ohio was selected as the research site for the implementation of a multi-method monitoring framework for cyanoHABs. In addition, environmental, meteorological, and water quality parameters were examined for their influence on the cyanobacterial community, as it is well known seasonality affects cyanoHAB development (Yang et al., 2020). The main objectives for this study were to 1) evaluate which parameters showed the strongest correlation with cyanobacterial presence, 2) determine microbial community composition, with a focus on the cyanobacterial community, and 3) assess cyanobacteria taxa's interactions within the microbial community. The hypotheses for each of these objectives are that 1) water temperature and microbial evenness will be strongly correlated with parameters indicative of cyanobacterial presence 2) that the cyanobacteria community will be dominated by *Microcystis* (one of the most common cyanobacteria genera in Ohio), and 3) a genus of cyanobacteria will be a keystone species within the water body. This is because cyanobacteria are primary producers, which fulfill critical roles within the microbial community. To our knowledge, no prior research has been conducted at this site, heightening the need to examine the cyanobacterial community using multiple methods. Analyzing the body of water over an extended period is necessary for implementing effective monitoring strategies. Additionally, it is possible that seasonal shifts in microbial diversity could affect unmanned aerial vehicle (UAV) acquired data, so better defining these shifts, and associated microbial community compositions could be beneficial for UAV data interpretation in Chapter 3.

3. Materials and Methods

3.1 Study Site, Water Quality Measurements, and Meteorological Data Acquisition

This study was conducted in Schiller Park which is in Columbus, Ohio United States. In the park there is a one-acre freshwater lake with a max depth of approximately 1.8 meters (Figure 2.1). Its water level is maintained by a well running several hours a day. Additionally, if the water level gets too high, there is an overflow system to drain excess water. This results in the lake maintaining a constant water level year-round. Furthermore, according to The City of Columbus Recreation and Parks Department, fertilizer applications are not applied near the lake, indicating other sources of nutrient input. This site was chosen to study for a few reasons, these being 1) the lake is hypereutrophic, possibly due to an overabundance of cyanobacteria 2) the lake is too small for other remote sensing applications such as satellites (chapter 3), 3) there is an island located in the middle of the body of water which aids in imagery processing (chapter 3), and 4) the lake is located in the middle of a public park frequently visited by individuals and companion animals, so there is a public health concern.

Figure 2.1 Satellite image of the lake located in Schiller Park, Columbus, Ohio United States (Google Earth Pro V 7.3.6.9345 (64-bit), Schiller Park, Columbus, Ohio United States Lat: 39.941317°, Long: -82.993250° Eye alt: 410ft [August 31, 2022]).

A total of 12 field sampling campaigns were conducted bi-weekly from April to September in 2022. During each field visit, four locations were sampled. Each of these locations were equally separated from one another and located in the four cardinal directions. To match sample numbers for ddPCR data, these values were averaged and used as representative for the entire water body. Duplicate water surface samples were collected in 50ml amber glass vials for toxin analysis. Directly after collection, these samples were wrapped in aluminum foil, placed on ice, and kept out of direct sunlight. Physical water quality parameters were measured at each

location using a YSI 650 MDS with a 600XL sensor (Yellow Springs, OH, USA). Water quality parameters measured included pH, water temperature, secchi disc depth, and conductivity. Furthermore, chl-a and PC fluorescence were measured at each location in duplicate using the Aquafluor handheld fluorometer (Turner Designs, San Jose, CA, USA). Additionally, within three days of the initial sampling date, a 1-liter composite surface water sample was collected in a plastic Nalgene bottle. These were immediately placed on ice and transported to the lab for analysis. Meteorological data was downloaded from the National Oceanic and Atmosphere Administrations' (NOAA) Climate Data Online (CDO) website (*Climate Data Online (CDO) - National Climatic Data Center (NCDC)*, n.d.). Weather parameters downloaded included average daily wind speed, fastest 5-second wind speed, 3-day cumulative rainfall, average, maximum, and minimum daily temperatures. The weather station collecting this data is located at the John Glenn International Airport in Columbus, Ohio (Lat: 39.99068, Long: -82.87703). This station was chosen because it was the closest weather station to the study site.

3.2 Cyanotoxin Analysis

Cyanotoxin analysis was conducted for three different toxin classes: microcystin, anatoxin-a, and saxitoxin (separately). Before analysis, all samples underwent three freeze thaw cycles (Rushford et al., 2022). This process lyses all cells within the sample, allowing quantification of both extra and intra-cellular toxins. Cyanotoxins were quantified using the enzyme-linked immunosorbent assay (ELISA) (Abraxis Microcystins/Nodularins, Abraxis Anatoxin-a, and Abraxis Saxitoxin (PSP) ELISA kits, Gold Standard Diagnostics, Davis, CA, USA) in a BioTek EL808 Microplate Reader (Agilent Technologies, Santa Clara, CA, USA) within 15 minutes after the addition of the "stop" solution. Absorbance was read at 450 nm.

Instructions included in each kit were followed during analysis (These methods have been widely adopted for cyanotoxin quantification in water samples (Zhang et al., 2022, Rushford et al., 2022). The detection limits for the microcystin, anatoxin-a, and saxitoxin ELISA test kits are 0.1 µg/L, 0.1 µg/L, and 0.015 µg/L respectively.

3.3 DNA Extraction and ddPCR Analyses

Microbial DNA was extracted from the 12 composite water samples with the DNEasy PowerSoil Kit (Qiagen, Valencia, CA, USA). Before extraction, 150 mL and 50 mL of water from each sample were concentrated through a sterile, Isopore^{TM} 0.2 µm pore-sized filter (Merck KGaA, Darmstadt, Germany). DNA was extracted from the filters immediately. Differences in volumes filtered were accounted for later in data analysis. DNA concentration and quality were measured using the NanoDrop™ 2000 Spectrophotometer (ThermoFisher Scientific, Waltham, Massachusetts). Samples with DNA concentrations above 5 ng/µL were used for gene quantification. For gene sequencing, the maximum threshold for DNA concentration was 100 ng/µL, so samples exceeding this concentration were diluted to 100 ng/µL with sterile PCR-grade water.

To determine the concentrations of cyanotoxin-producing cyanobacteria and quantifying the major sources of fecal pollution in water samples, several cyanobacteria, cyanotoxin producing cyanobacteria genes, and MST gene markers were quantified using a ddPCR system (Bio-Rad, Hercules, CA, USA). Microcystin producing *Planktothrix* and microcystin producing *Microcystis* were determined by targeting the *mcy*E gene which encodes microcystin production (Lee et al., 2021, Ai et al., 2020). Total *Microcystis* concentrations were determined by targeting the phycocyanin intergenic spacer (PC-IGS) (Ai et al., 2020). In addition, anatoxin and saxitoxin

producing cyanobacteria concentrations were quantified by targeting anatoxin-a synthetase C (*ana*C) gene and saxitoxin-biosynthesis (*sxt*A) gene respectively (Kelly et al., 2019, Kim et al., 2022). All ddPCR amplifications were performed using 20 μL reaction mixtures. For measuring concentrations of the mcyE of *Microcystis*, mcyE of *Planktothrix*, and PC-IGS, mixtures contained ddPCR mastermix for probes (Bio-Rad, Hercules, CA, USA), sterile PCR grade water, Bio-Rad primer-probe mix (Bio-Rad, Hercules, CA, USA), and DNA templates. For quantification of anaC and sxtA, amplification reaction mixtures contained ddPCR mastermix for Evagreen (Bio-Rad, Hercules, CA, USA), sterile PCR grade water, respective primer-probes, and DNA templates (Nshimyimana et al., 2019, Ai et al., 2020). MST assays included GFD (goose), BacCan (dog), and HF183 (human) (Rytkönen et al., 2021). For GFD, one sample was diluted using sterile PCR water at 1:25 ratio. No dilutions were made for BacCan or HF183 as it was not necessary. GFD reaction mixture consisted of ddPCR mastermix for Evagreen (Bio-Rad, Hercules, CA, USA), sterile PCR grade water, Biorad primer-probe mix (Bio-Rad, Hercules, CA, USA), and DNA template. BacCan and HF183 reaction mixtures were the same as GFD, except mastermix for probes was utilized in place of Evagreen mastermix. Droplets were generated with the QX200 Droplet Generator (Bio-Rad, Hercules, CA, USA). Then target genes were amplified using a Bio-Rad C1000 PCR thermal cycler (See Table A.3 and A.4) (Bio-Rad, Hercules, CA, USA). After amplification, target gene concentrations were obtained using a QX200 droplet reader (Bio-Rad, Hercules, CA, USA) and QuantaSoft version 1.7 (Bio-Rad, Hercules, CA, USA).

3.4 DNA sequencing and Bioinformatics

The V4-V5 region of the 16S rRNA gene and 18s rRNA gene were sequenced at the Molecular and Cellular Imaging Center at the Ohio State University (Wooster, OH) on an Illumina MiSeq platform (Illumina Inc., San Diego, CA). The primers used for the 16S rRNA gene were 515F (5′-GAGTGCCAGCMGCCGCGGTAA-3′) and 806R (5′-ACGGACTACHVGGGTWTCTAAT-3′). For the 18S rRNA gene, the V3-V4 protozoal region was targeted. Primers P-SSU-316F (5'-GCTTTCGWTGGTAGTGTATT-3') and GIC758R (5'-CAACTGTCTCTATKAAYCG-3') were used (see Figure A.5). Raw reads for both were analyzed using the QIIME2 pipeline (Bolyen et al., 2019). DADA2 was used for quality control, by removing lower quality portions of reads (Callahan et al., 2016). The base cutoff for forward reads for 16s rRNA reads was 246 and the cutoff for reverse reads was 247. For 18S rRNA reads the cutoff for forward and reverse reads were 248. To normalize for alpha diversity analysis, the rarifying threshold for 16s rRNA reads was set at a depth of 19,496, which was the lowest library size in the samples. For 18s rRNA reads this threshold was set at 8201. Sequences were clustered using 99% identity and taxonomic classification referenced against the SILVA high quality rRNA database (Quast et al., 2013). A total of 49 non-prokaryotic taxa were removed before diversity calculations. Although not targeted, these taxa were present due to chloroplast and mitochondrial DNA being sequenced. Alpha diversity was measured via Shannon's diversity index, richness, and Pielou Evenness in QIIME2 (Bolyen et al., 2019). Significant differences were assessed using the Kruskal Wallis tests ($p < 0.05$). Taxonomy for both 16s and 18s rRNA genes were classified using the 99% SILVA database (Bolyen et al., 2018, Amin et al., 2023).

3.5 Statistical Analysis

Statistical analysis and figures were generated using the R software (version 4.2.1). Diversity outputs from QIIME2 were tested for normality using the Shapiro-test function in the "stat" R package (version 4.0.3). Additionally, normality was examined visually using the "hist" function, which is part of base R. To test if data was homoscedastic, the "nvcTest" function in the "car" R package (version 3.1.2) was used. Spearman's correlation coefficient was used to explore correlations between diversity indices, water quality, ddPCR, cyanotoxin, and meteorological data. The t.test function in base R (version 4.2.1) was used to conduct unpaired two-sample t-test to test significant differences by season for all data. Seasons were defined using the solar calendar to have statistically comparable groups. Each season, spring and summer, had six sampling campaigns. Additionally, principal component analysis (PCA) was conducted to further explore the statistical significance between seasons. To do this, all data was scaled, and principal components obtained using the "prcomp" function in the "stats" (version 4.0.3) R package. To investigate taxa contributing to the differences in the microbial communities between seasons, linear discriminant analysis effect size (LEfSe) was performed using the tool hosted online (Segata et al., 2011) (hosted on Galaxy huttenhower.sph.harvard.edu/galaxy). Analysis was conducted at a phylum and genus level with a threshold of 2 for the logarithmic LDA score, and an alpha value for the pairwise Wilcoxon test of 0.05 (Mills et al., 2022).

3.6 Microbial Network Analysis

For analyzing the microbial networks, microbial taxa (OTUs) less than 1% of the largest OTU count in each sample were removed. These taxa are considered rare and can negatively

affect network analysis methods (Beiko et al., 2018). Additionally, taxa not classified to a phyla level were removed. The network analysis was run at the family level using the sparse neighborhood algorithm. Model selection was conducted using the Stability Approach to Regularization Selection (StARS) method with 50 repetitions (Kurtz et al., 2015). The estimation method used was neighborhood selection (Meinshausen & Bühlmann, 2006). All network analyses were conducted using the "SpiecEasi" and "igraph" (version 1.4.3) R packages (Kurtz et al., 2015). Clusters within the network were detected "multilevel.community" functions. With this method, communities are not merged, but instead nodes are moved between communities so that each node maximizes its contribution to the modularity score (Blondel et al., 2008). To test the strength of these clusters, the "modularity" function was used. Link-analysis methods "page_rank" and "hub_score" were used to determine keystone species within the network. The number of nodes and edges within the network were examined using functions "num.nodes" and "num.edges" respectively. The average nearest neighbor degree (ANND) of a given node (or a set of nodes) can be calculated using the "knn" function. ANND is a measure of the dependencies between degrees of neighbor nodes (Beiko et al., 2018). This was done for the cyanobacteria within the network. To find nodes directly or indirectly reachable by nodes of interest, the "subcomponent" function was utilized. To assess whether the network consisted of multiple disconnected parts, the "components" function was employed. The degree of nodes and distribution of degrees amongst all nodes was analyzed and visualized using the "degree" and "plot" function respectively. Visualization of the network was achieved using "plot_network" function.

4. Results

4.1 Seasonal Dynamics in the Hypereutrophic Urban Lake

4.1.1 Environmental Variations

Both ambient and water temperature exhibited a typical seasonal pattern with the lowest values being observed in the early spring (April) and highest values being in the middle of the summer season (late June/ early July). The largest temperature variation observed in a single day was 18.6 °C. Towards the end of the summer season (end of July- early August), temperatures began to decrease, but never reach values as low as those measured in April. Secchi disc depth showed a similar trend, with the highest values in April, and slowly decreasing until mid-July. After, secchi disc values gradually increased, but never reached those observed in April. Secchi disc depth showed the greatest range of values among all variables sampled. Conductivity showed low values observed at the beginning of the sampling period (starting in April) and decreasing into the middle of the summer (early July). Towards the end of the sampling period conductivity began increasing. pH showed the smallest range of values, ranging between 8.56 and 9.26, indicating that the lake is a basic freshwater system year-round. Average wind speeds and fastest 5 second wind gusts did not show strong trends throughout the sampling season. Only secchi disc depth showed a significant difference between seasons ($p < 0.1$). A summary of all environmental parameters is shown in Table 2.1.

Table 2.1 Summary statistics for all environmental parameters gathered during the sampling period. All variables are in metric values. Wind speed and all air temperature measurements are daily averages.

Variable	Mean	Standard Deviation	Median	Minimum	Maximum	Range
Precipitation (3 previous days) (mm)	8.60	16.6	3.80	0.00	59.9	59.9
Average Wind Speed (m/s)	2.61	0.80	2.45	1.70	4.00	2.30
Fastest 5 second Wind Speed (m/s)	9.47	3.09	8.90	6.30	17.9	11.6
Average Ambient Temperature (°C)	18.4	7.25	21.2	3.20	25.7	22.5
Max Ambient Temperature (°C)	24.3	7.43	26.4	10.0	33.3	23.3
Minimum Ambient Temperature (°C)	12.7	7.70	15.3	-3.80	20.0	23.8
Water Temperature (°C)	23.8	5.62	25.2	10.3	30.3	20.0
Secchi Disc Depth (m)	0.29	0.14	0.26	0.13	0.65	0.52
Conductivity (µS)	503.06	67.58	505.6	414.8	617.8	203.0
pH	8.91	0.220	8.85	8.56	9.26	0.680

4.1.2 Cyanotoxins, Cyanobacteria, and Microbial Source Tracking

Microcystin concentrations were above the detection limit in all 12 samples. Additionally, saxitoxin and anatoxin-a were above the detection limit in 10 and 9 of the samples, respectively (Figure 2.2).

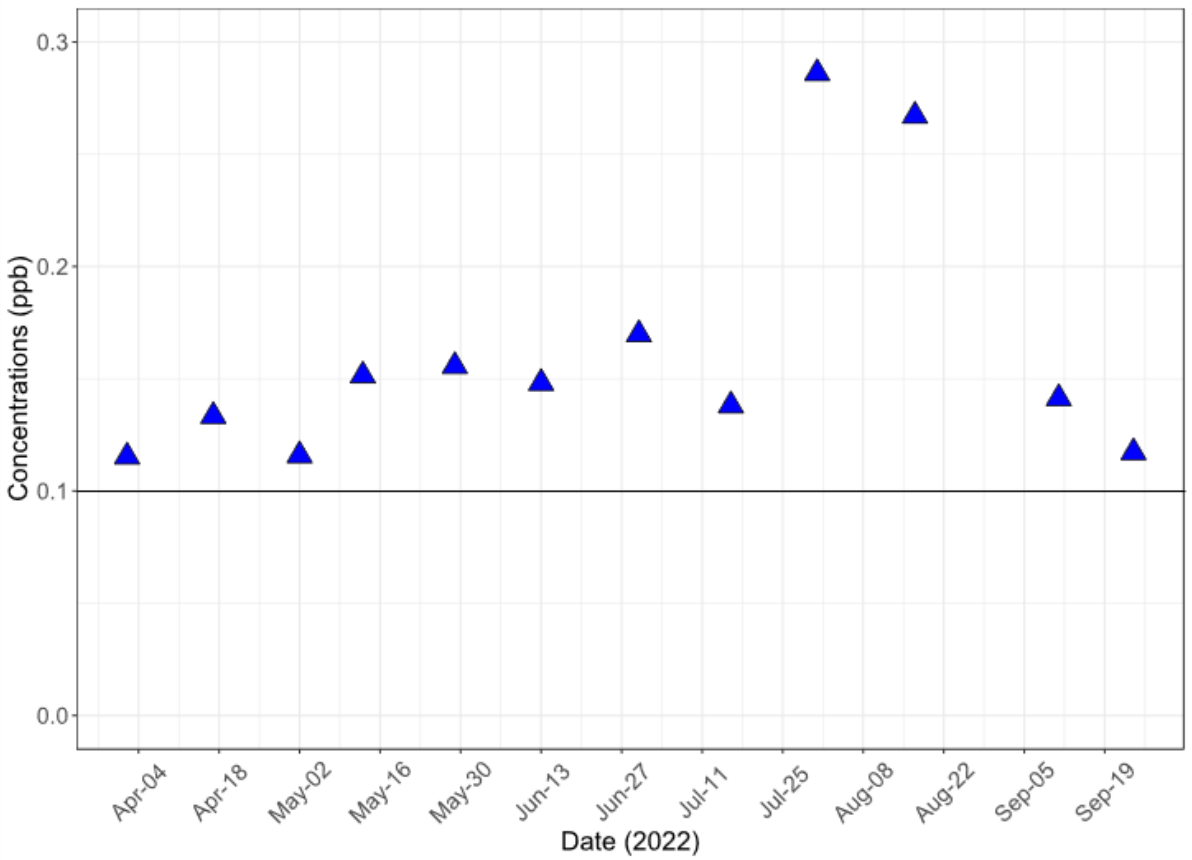

A continued

Figure 2.2 Cyanotoxin concentrations detected throughout the sampling period by date. A) microcystin concentrations, B) saxitoxin concentrations, and C) anatoxin-a concentrations. Solid line on figures represents the detection limit of ELISA kit used.

Figure 2.2 continued

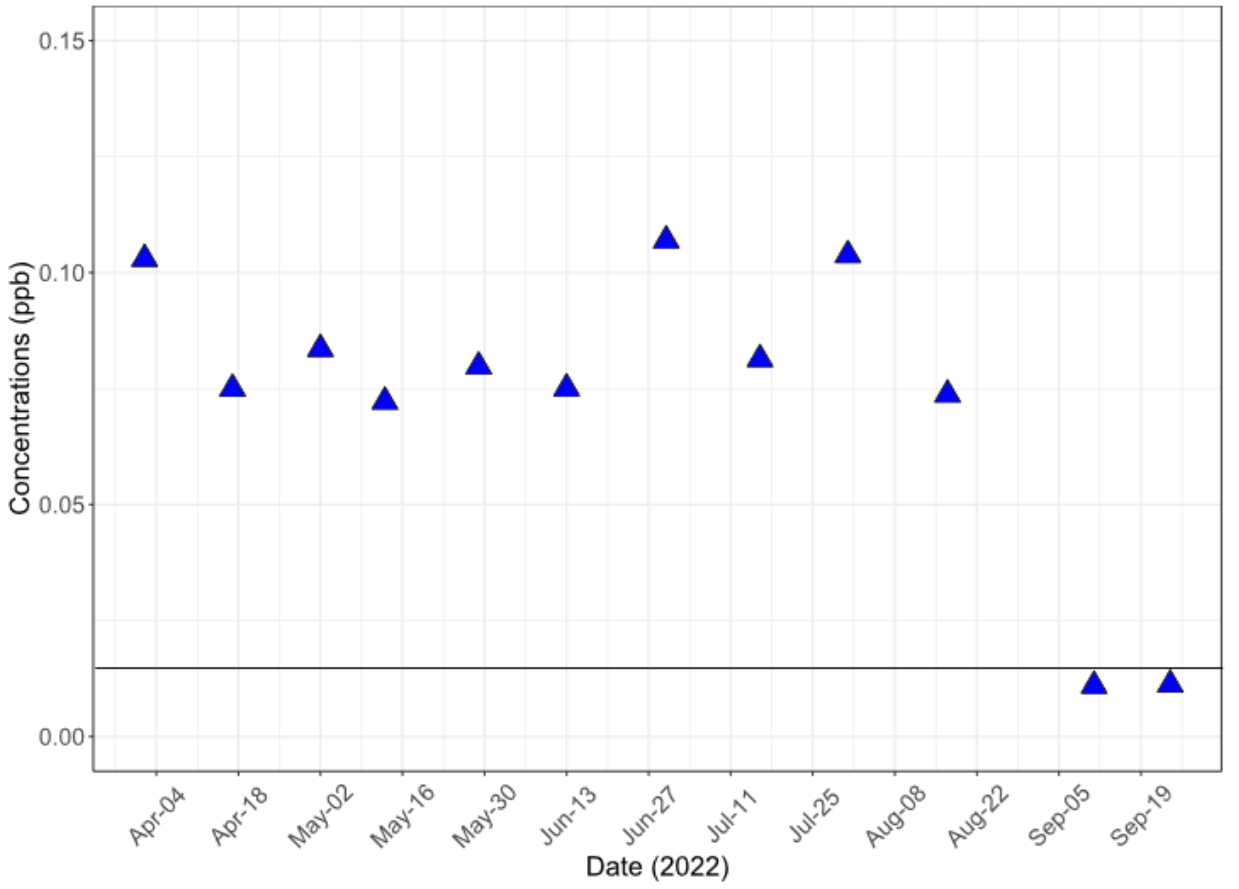

B continued

Figure 2.2 continued

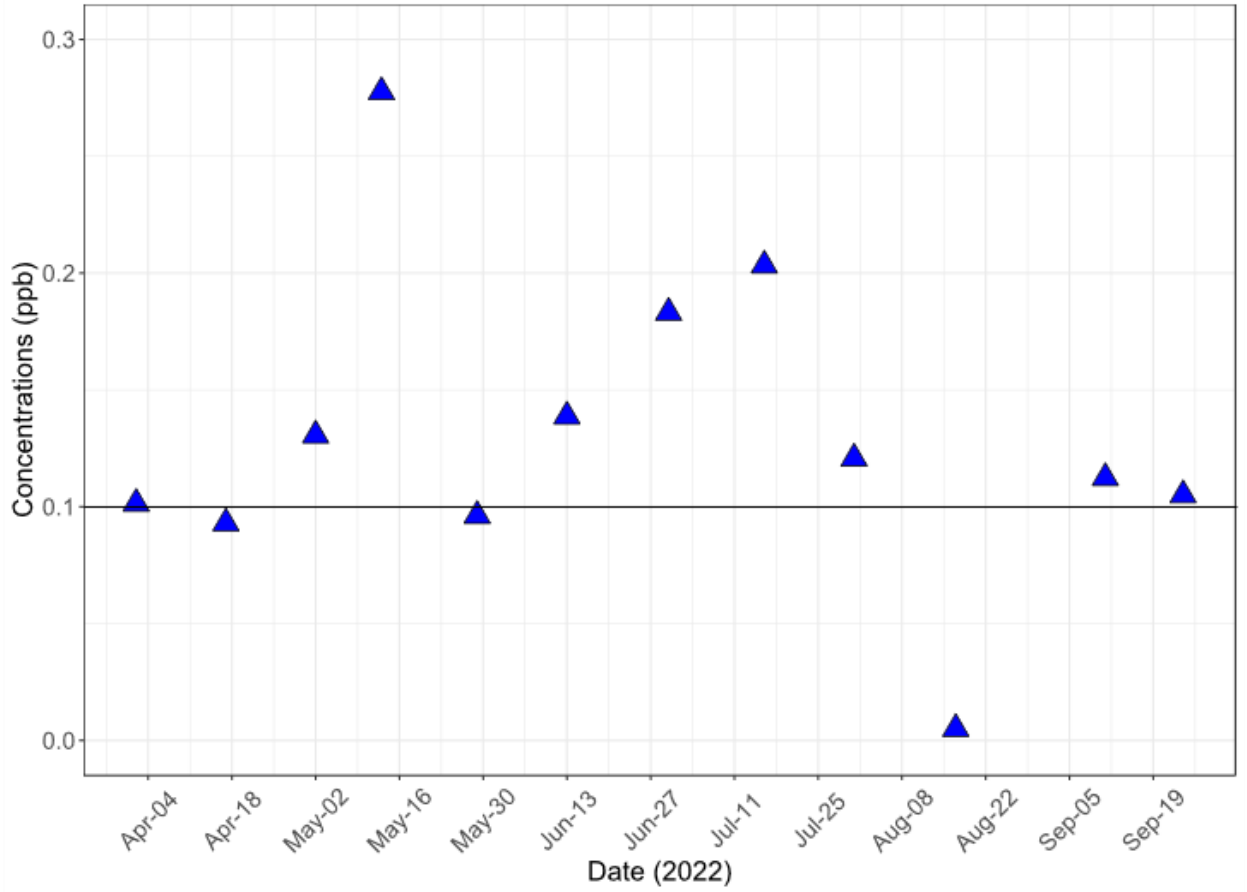

C

No concentrations were observed above the recreational limit set by EPA (US EPA, 2019). Spearman correlations were used to analyze monotonic relationships between cyanotoxin concentrations and environmental parameters. Saxitoxin concentrations were not significantly correlated with any environmental parameters except conductivity (r_s=-0.52, p-value = 0.05). Both microcystin and anatoxin-a showed strong statistically significant correlations with temperature parameters. Microcystin showed the strongest correlations with water temperature and max daily temperature (r_s=0.88, p-value < 0.001 & r_s=0.84, p-value < 0.001) respectively.

Anatoxin-a showed the strongest correlations with water temperature and average daily temperature (r_s=0.73, p-value < 0.05 & r_s=0.85, p-value < 0.001) respectively. Additionally, microcystin showed strong statistically significant negative associations with secchi disc depth and average daily wind speeds (r_s=-0.83, p-value < 0.001 & r_s=-0.97, p-value < 0.001), respectively. Anatoxin showed similar correlations with conductivity secchi disc depth (r_s=-0.61, p-value < 0.05), cumulative rain from three previous days (r_s=-0.71, p-value < 0.05), and conductivity (r_s=-0.61, p-value < 0.05). No cyanotoxin concentrations showed statistically significant differences between seasons.

Cyanobacteria and toxic cyanobacteria analyzed include PC-IGS, microcystin producing *Microcystis*, microcystin producing *Planktothrix*, anaC, sxtA. Additionally, MST measured include GFD, BacCan, and HF183. Out of the cyanotoxin producing genes, microcystin producing *Microcystis* was the most prevalent overall. Out of the MST results, BacCan was the most prevalent followed closely by GFD, which means dog-associated and goose-associate fecal contamination was frequent in the water. Both microcystin producing *Microcystis* and sxtA were significantly different between seasons ($p < 0.05$). Higher values of sxtA were observed during the summer, while microcystin producing *Microcystis* showed higher concentrations in the spring. No fecal indicators were significantly different between seasons. Trends for both cyanobacteria genes and fecal indicators can be seen in Figure 2.3.

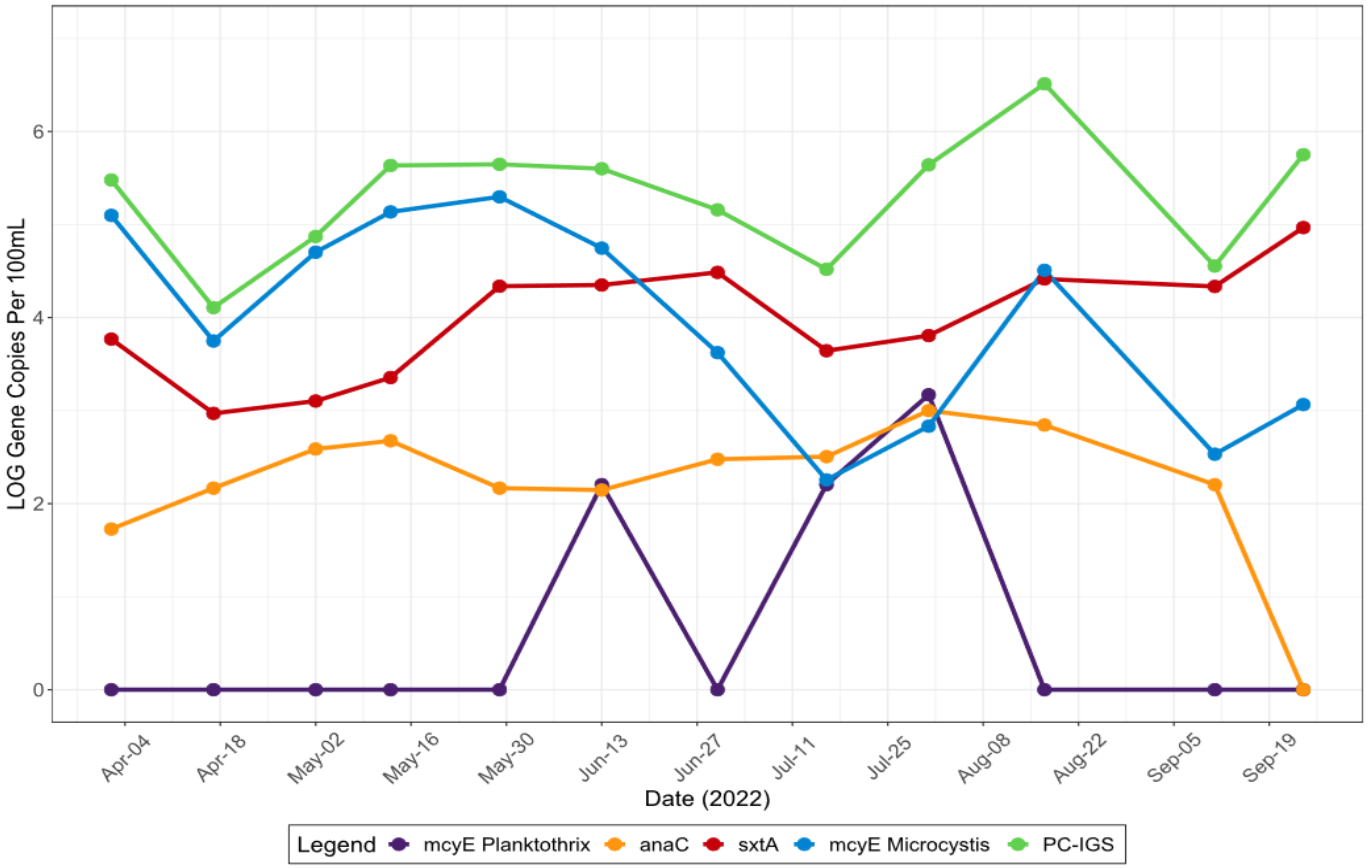

A continued

Figure 2.3 Trends for A) cyanobacteria and toxic cyanobacteria concentrations, and B) MST result for the entire sampling period. Values are in $\log_{10}$ gene copies per 100 mL.

Figure 2.3 continued

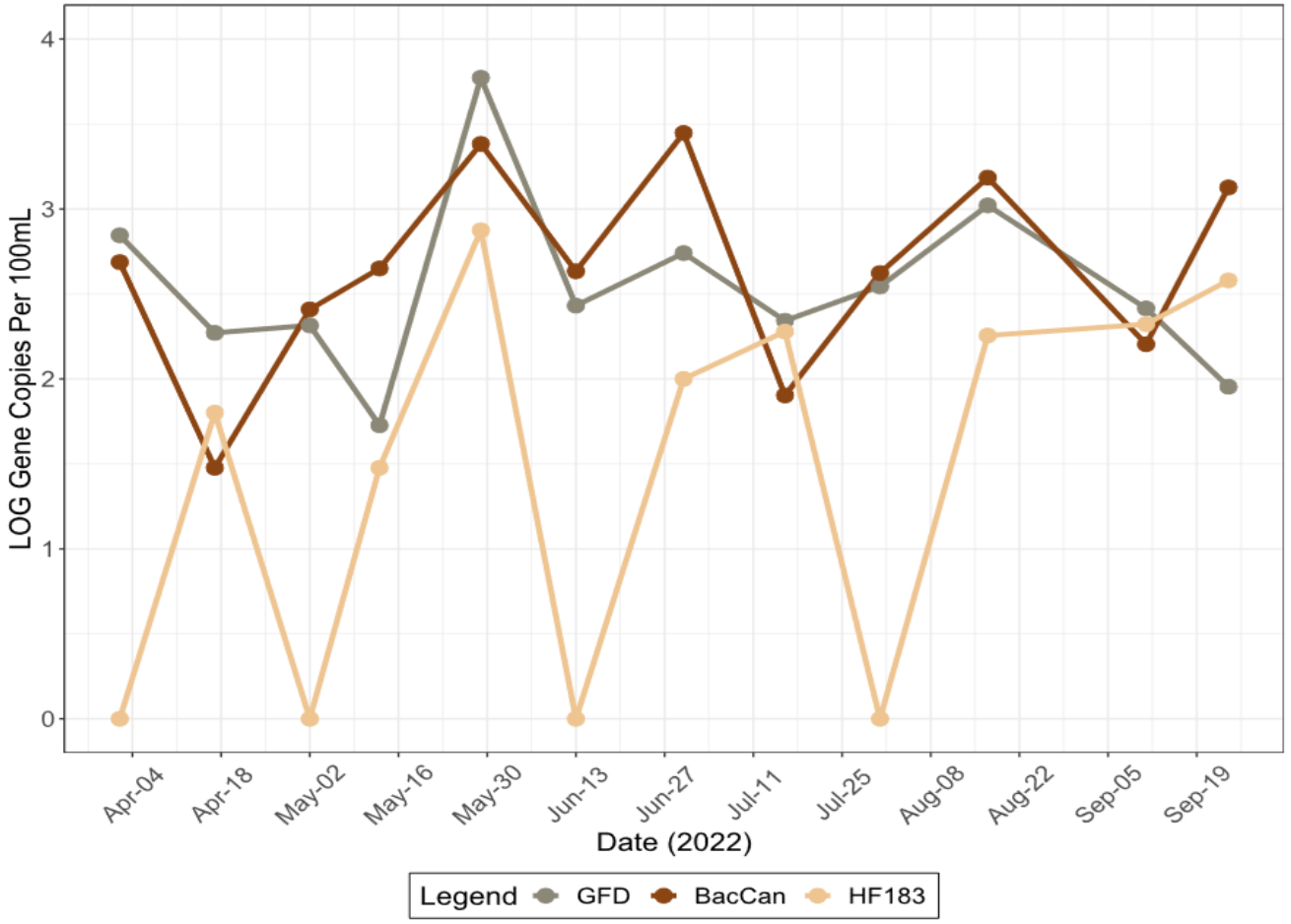

B

Additionally, correlations between MST and cyanobacteria genes were examined as fecal input may contribute some nutrients into the body of water (Lee et al., 2016). Microcystin producing *Microcystis,* PC-IGS, and sxtA showed the strongest correlations with fecal indicator BacCan. Additionally, these showed strong positive correlations with one another. Microcystin producing *Planktothrix* had strong negative correlations with microcystin producing *Microcystis.* Furthermore, sxtA showed strong positive and statistically significant correlations with all fecal indicators and PC-IGS. Associated correlation coefficients and p-values for these can be viewed in Figure 2.4.

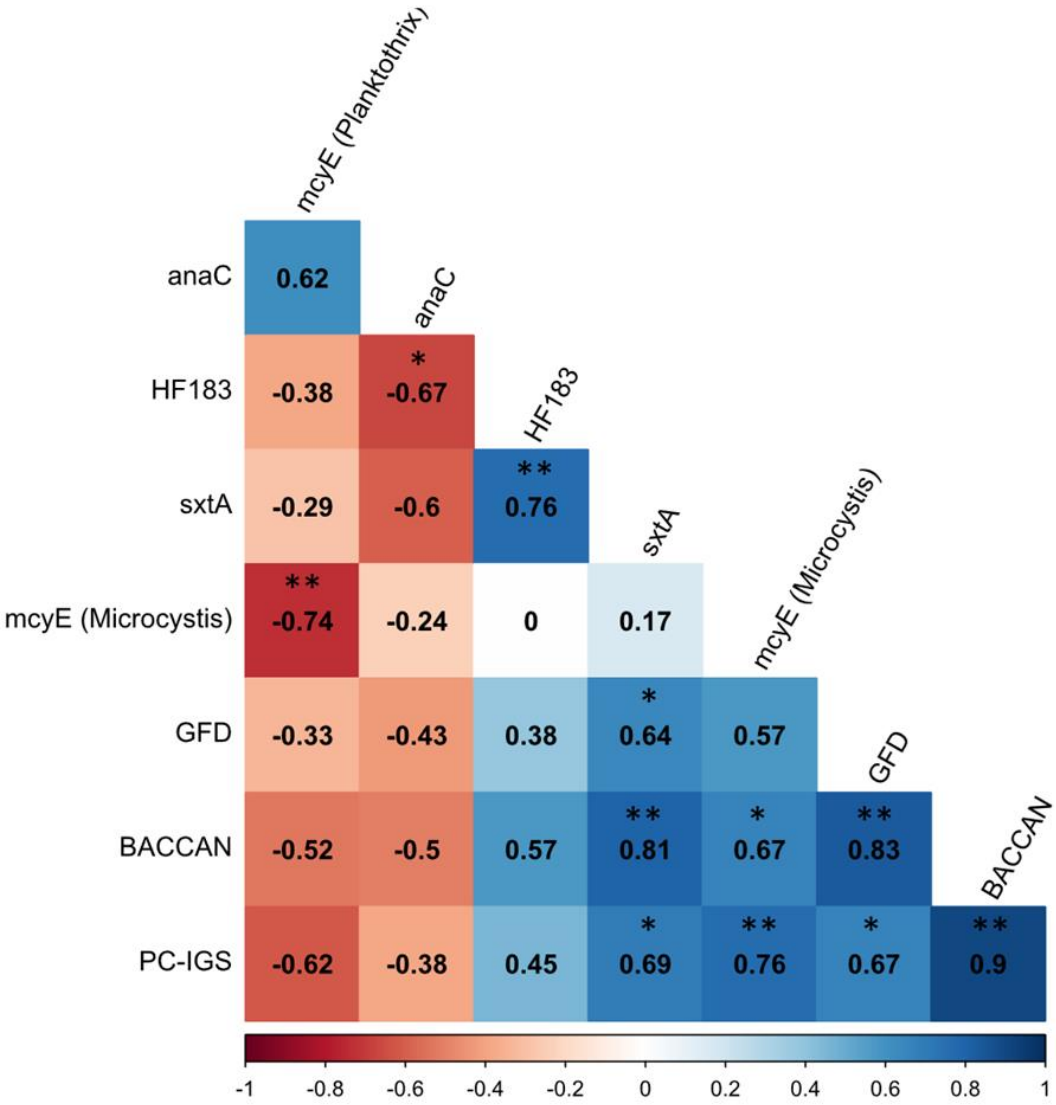

Figure 2.4 Spearman's correlation heatmap between cyanobacteria related genes and fecal indicators. * and ** represent p-values of 0.1 and 0.05, respectively.

4.2 Microbial Community Structure

A total of 657 and 19 unique taxa were identified after pre-processing of 16S and 18S rRNA gene sequencing data using the QIIME2 pipeline, respectively (Bolyen et al., 2019). Initially, to examine relationships between 16S and 18S communities Spearman's correlations

for alpha diversity values between the two were examined. Results showed that evenness for 16S and 18S rRNA gene sequencing showed strong negative and statistically significant correlations. Additionally, 18S rRNA gene sequencing richness and evenness showed strong negative and statistically significant associations. Measures for evenness of 16S rRNA gene sequencing were strongly positive and statistically significant with 18S rRNA gene sequencing richness. 0.05) respectively. Furthermore, Shannon diversity and richness for 16S rRNA gene sequencing showed strong positive and statistically significant correlations. Associated correlation coefficients and p-values can be seen for these in Figure 2.5.

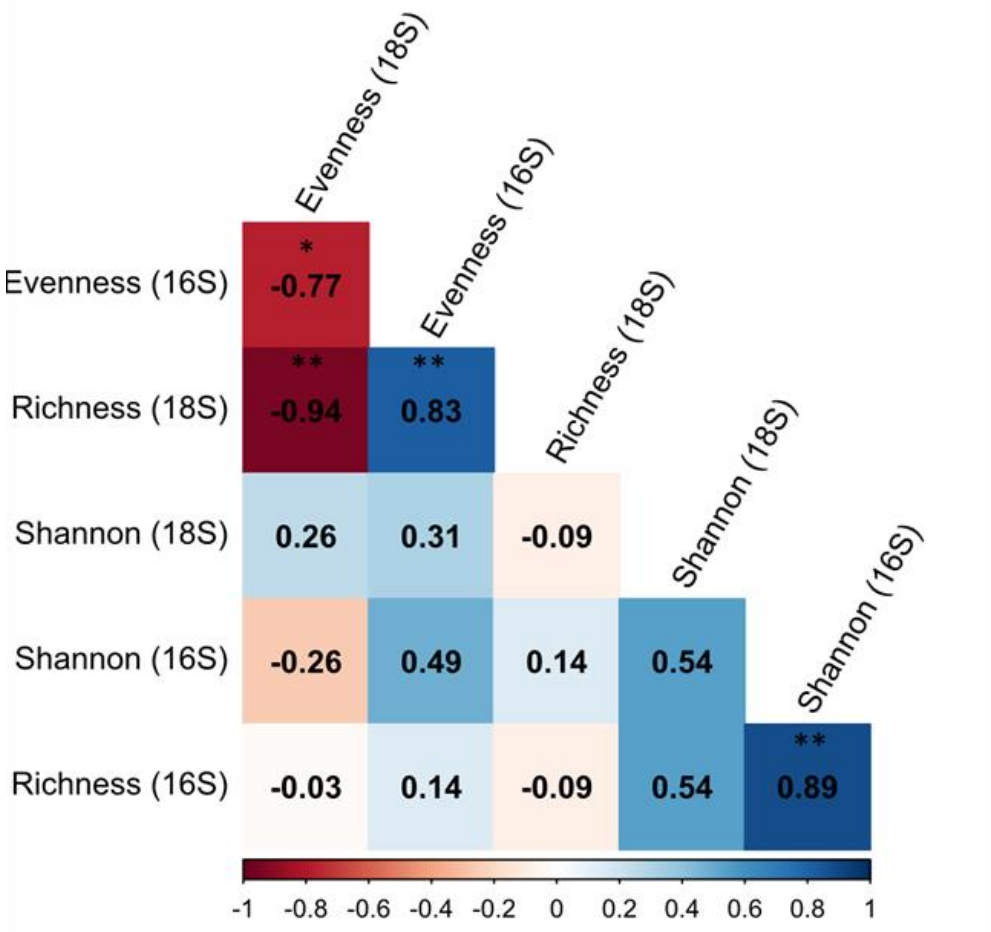

Figure 2.5 Spearman's heatmap for 16S and 18S rRNA gene sequencing data. Symbols * and ** represent p-values of 0.1 and 0.05, respectively.

After examining correlations for alpha diversity between the two communities, the microbial community was examined further. The most significant factor in describing the microbial communities analyzed via 16S rRNA gene sequencing was season. Shannon index (p-value < 0.05), richness (p-value < 0.001), and Pielou evenness (p-value < 0.05), all measures of alpha diversity, were significantly different by season, measured via unpaired t-test (Figure 2.6). For

all alpha diversity indices, values were higher during the summer, revealing that the microbial community within the water is more diverse during the summer months.

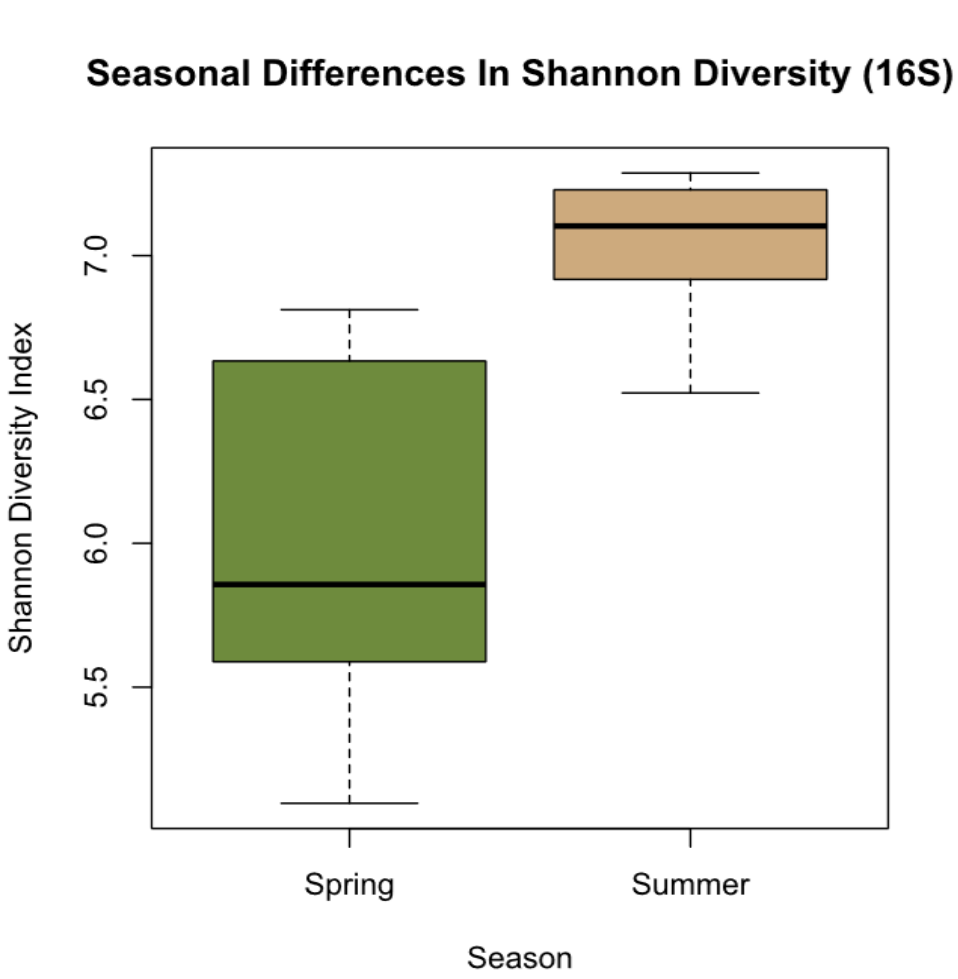

A continued
Figure 2.6 Summary of microbial community alpha diversity analysis by season using A) Shannon Diversity B) richness, and C) Pielou Evenness.

Figure 2.6 continued

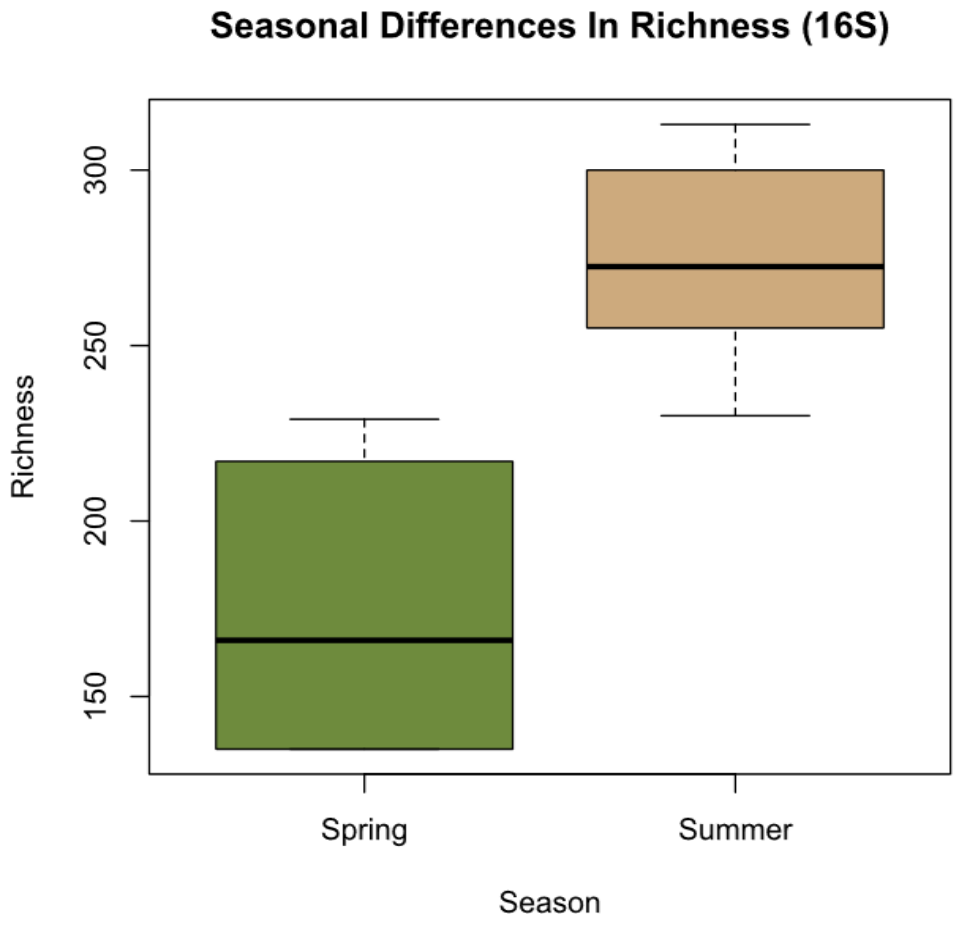

B continued

Figure 2.6 continued

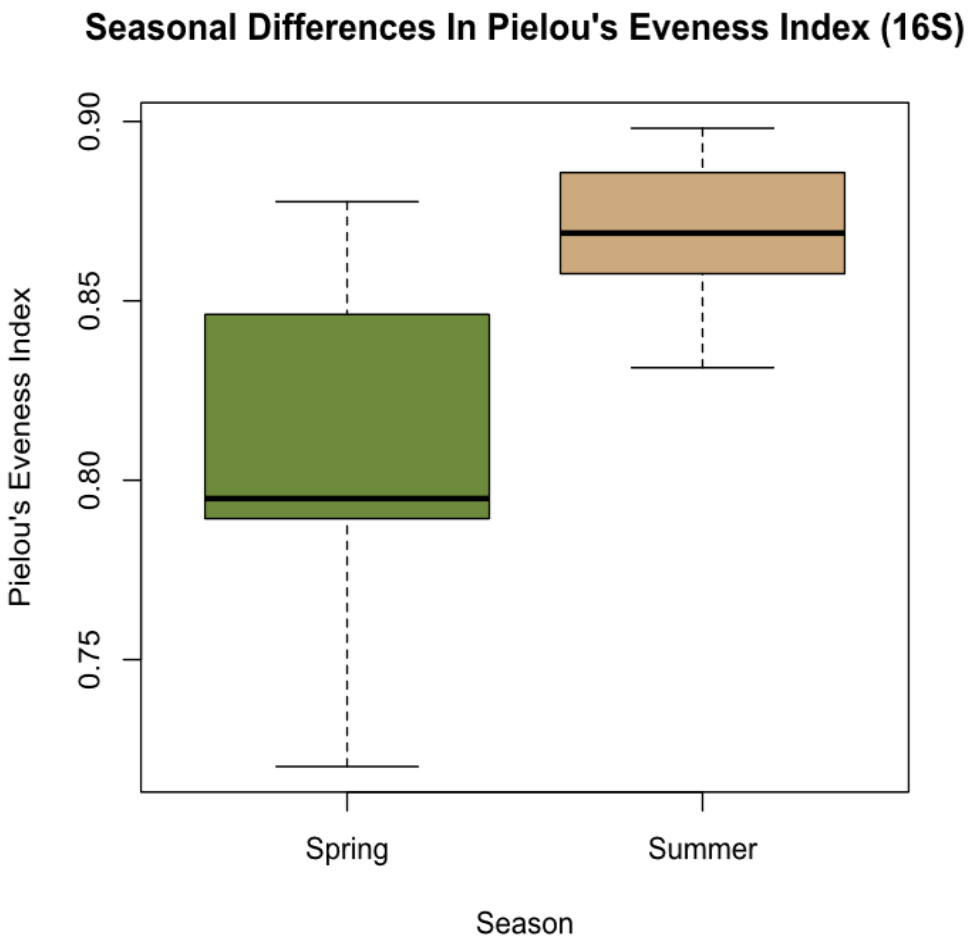

C

The composition of the microbial community was also analyzed. To start, the relative abundance of different phyla was analyzed for all 12 samples. Results showed that the top five phyla present in the water included Proteobacteria, Actinobacteria, Bacteroidetes, Cyanobacteria, and Planctomycetes. The relative abundances for each of these were 41%, 26%, 13%, 7%, and 4% respectively. Additionally, the relative abundances for all 12 samples were analyzed at the

genus level. The analysis showed that the top five genera present included unknown genera, *hgcl clade, Planktothrix* NIVA-CYA 15, *Sphaerotilus*, and *Mycobacterium*. The relative abundances for each of these were 35%, 6%, 5%, 5%, and 4%, respectively. Visualization of these results can be seen in Figure 2.7. Unknown genera occur due to low phylogenetic power of 16S rRNA sequencing data at lower taxonomic levels (16S rRNA Gene Sequencing for Bacterial Identification in the Diagnostic Laboratory, n.d.).

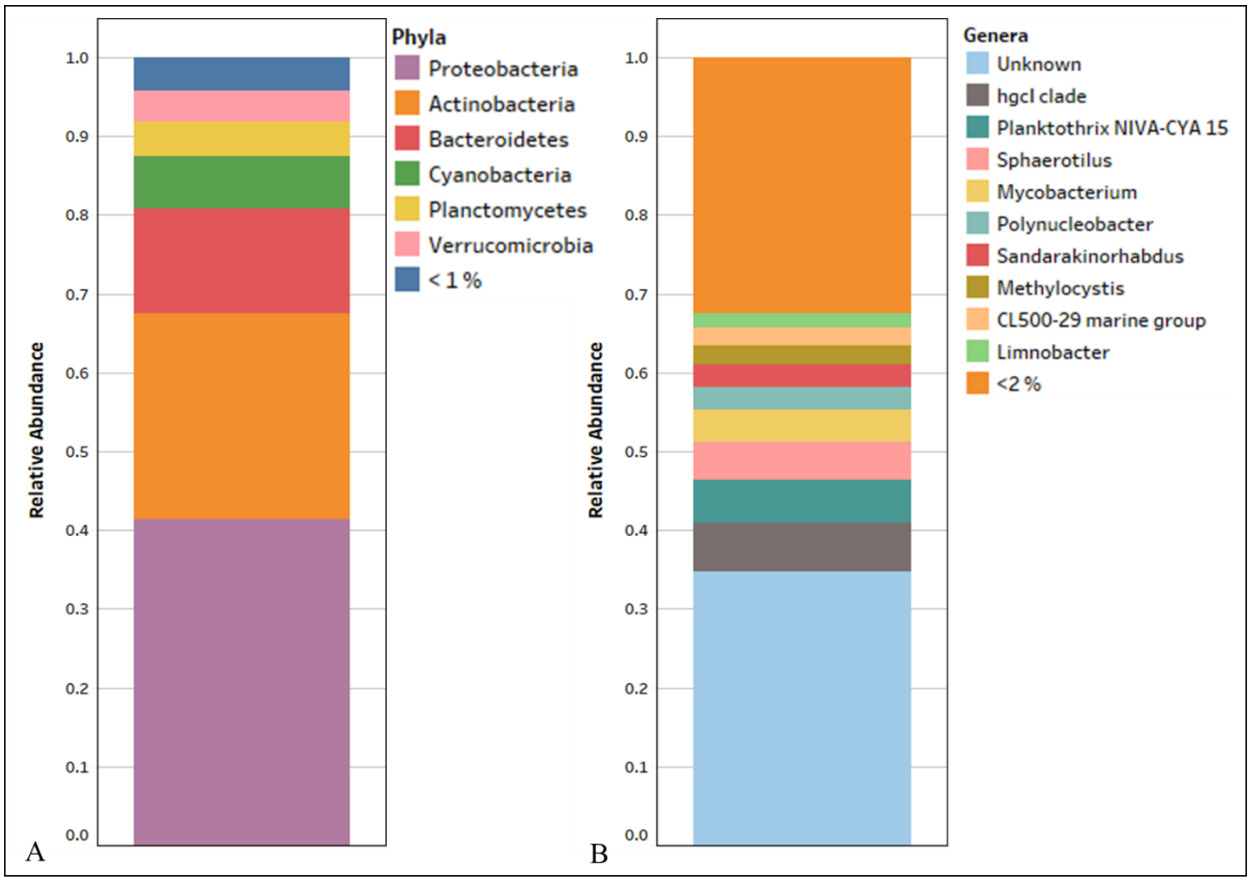

Figure 2.7 Averaged relative abundances for taxa in all 12 samples at the A) phyla and B) genus level.

Since the cyanobacteria phylum was of interest, further analysis was conducted on this phylum specifically. To begin, the average relative abundances in all 12 samples of cyanobacteria genera was examined. Results showed that the top 5 cyanobacteria genera present were *Planktothrix* NIVA-CYA-15, *Cyanobium* PCC-6307, *Tychonema* CCAP 1459-11B, *Microcystis* PCC-7914, and *Gleocapsa*. The average relative abundance of each of these were 82%, 8%, 6%, 3%, and 1%, respectively (Figure 2.8A). Next, the differences in cyanobacteria genera by season were examined. Results showed that *Planktothrix* NIVA-CYA 15 showed the highest average relative abundances in both seasons. Although, during the spring, other cyanobacteria genera average relative abundances increased (Figure 2.8B). During the spring, the average relative abundance for *Planktothrix* NIVA-CYA 15 was 83%, while in the summer it decreased to 59%. During the spring, the average relative abundances for other top cyanobacteria genera were *Cyanobium* PCC-6307 (7%), *Tychonema* CCAP 1459-11B (6%), and *Microcystis* PCC-7914 (2%). While in the summer, top cyanobacteria genera average relative abundances, besides *Planktothrix* NIVA-CYA 15, were *Microcystis* PCC-7914 (18%), *Cyanobium* PCC-6307 (13%), and *Gleocapsa* (7%). Since *Planktothrix* NIVA-CYA 15 represents a large portion of both the entire microbial community, and the cyanobacteria community, LEfSE was used to determine whether this taxon had significant differences in abundance between the spring and summer groups. Additionally, the entire cyanobacteria phyla were tested for the same purpose. Results showed that both cyanobacteria, and *Planktothrix* NIVA-CYA 15 contributed to differences in the microbial community for seasons (Figure 2.9).

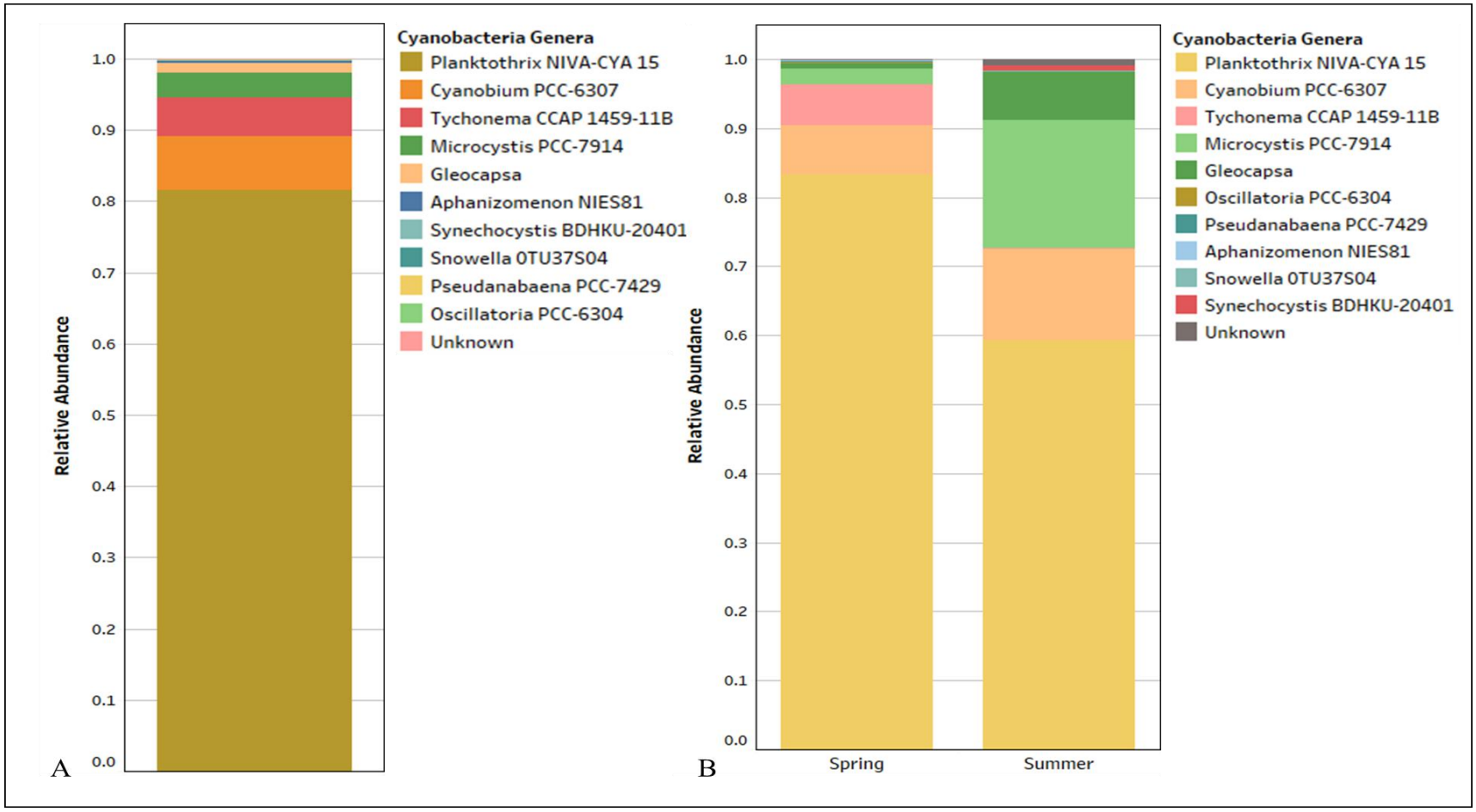

Figure 2.8 Average relative abundances of cyanobacteria for A) all 12 samples and B) season.

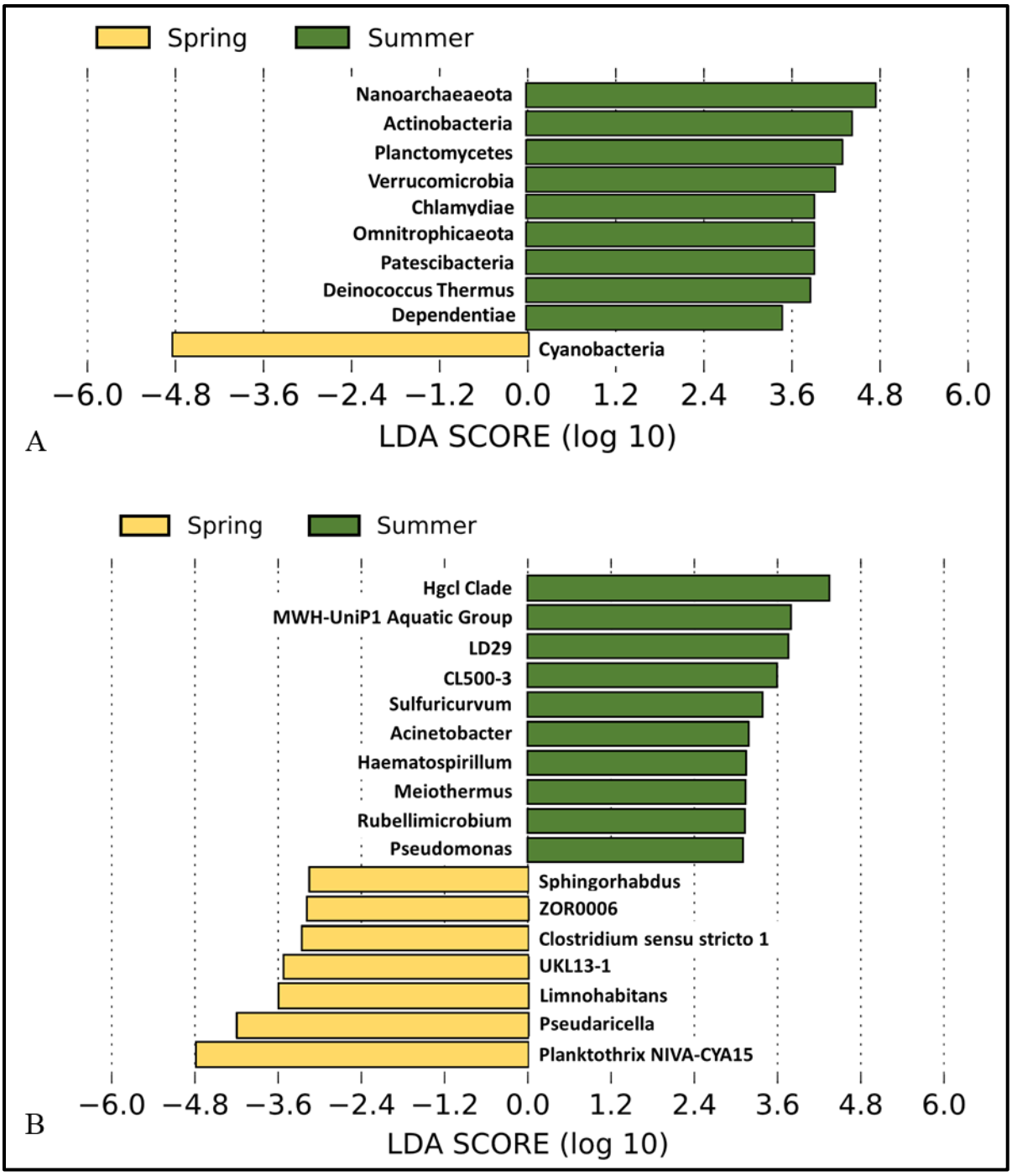

Figure 2.9 Pairwise statistical comparisons of microbial community composition via LEfSE (LDA > 2.0, $p < 0.05$) for A) all bacterial phyla and B) all genera.

4.3 Eukaryotic Microbial Community Structure

To further analyze the microbial community in the water, 18S rRNA gene sequencing data was utilized. As mentioned previously, 19 unique taxa were identified after pre-processing utilizing the QIIME2 pipeline (Bolyen et al., 2019). To begin, alpha diversity indices were examined using unpaired t-tests to see if there were significant differences between seasons. Out of the three diversity indices utilized, only the Shannon diversity index showed a statistically significant difference (p-value < 0.05) (Figure 2.10). The Shannon diversity index results showed similar trends to those seen in the microbial community analysis (16S rRNA gene sequencing data). Lower diversity values were observed during the spring season, while diversity increased during the summer.

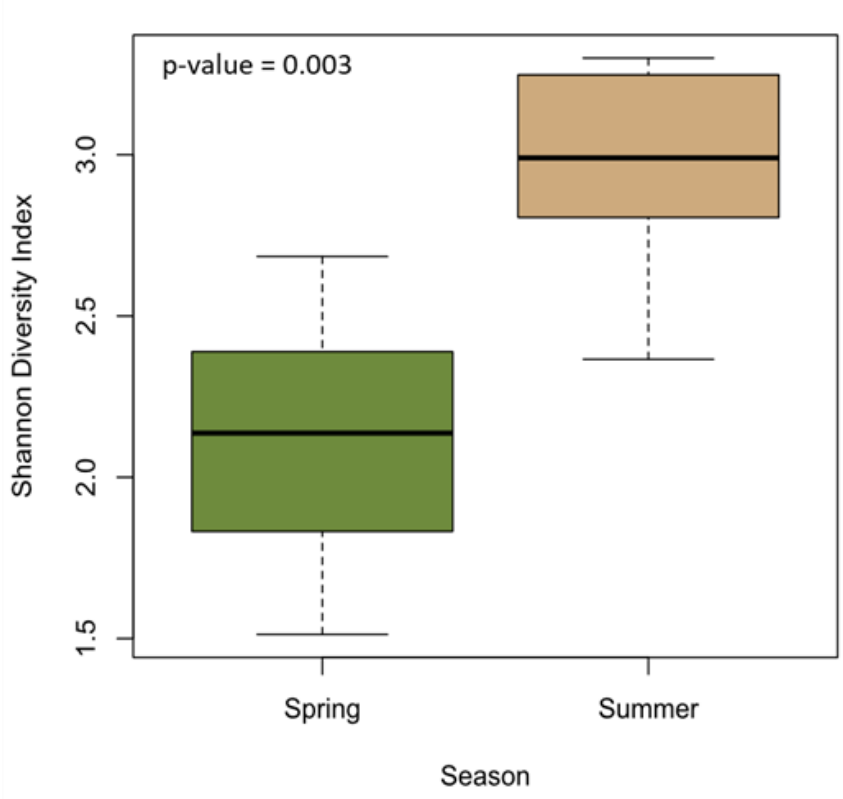

Figure 2.10 Differences in eukaryotic microbial community diversity by season using the Shannon diversity index.

Additionally, the community composition was analyzed. It should be noted, in lower taxonomic levels, there were high percentages of "unknown" reads, meaning that the sequenced DNA could not be classified at lower taxonomic levels. This is common for 18S rRNA gene sequencing data, and one of the limitations of this method. This is due to 18S rRNA gene sequencing libraries not being as complete as those for 16S rRNA gene sequencing, making it difficult to classify at lower taxonomic levels (Meyer et al., 2010). Nevertheless, the 18S rRNA data provided useful information about the eukaryotic microbial community dynamics, and taxa present within samples. At a phyla level, the community was completely dominated by the Stramenopiles,

Alveolates, and Rhizarians (SAR) supergroup (99%). This is a large and diverse group of microorganisms including photoautotrophs, mixotrophs, and chemoheterotrophs (Gad et al., 2022). Analysis at the family level shows that Haptoria dominated, with an average relative abundance of 91%. At the genera level, 45% of the community was classified as “unknown”. Identified taxa with significant average relative abundances included *Arcuospathidium* (23%), *Didinium* (19%), and *Teuthophyrs* (1%) (Figure 2.11).

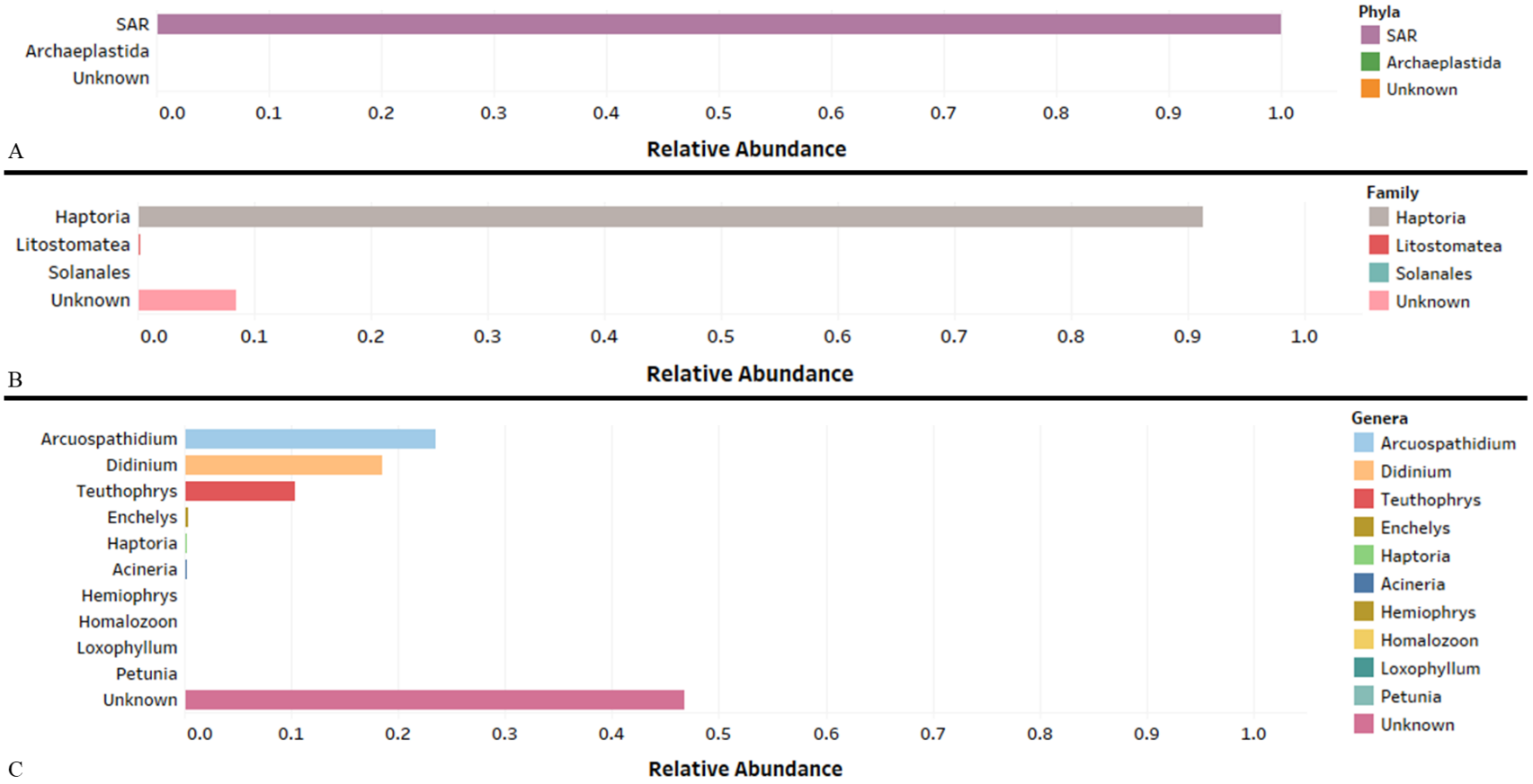

Figure 2.11 Average relative abundances of taxa for all 12 samples at the A) phyla B) family, and C) genus level.

In addition, differences in average relative abundances by season were explored at the genus level (Figure 2.12). Results showed that *Arcuospathidium* had lower average relative abundance in the spring (4%) than in the summer (35%), while *Didinium* showed a higher average relative abundance in the spring (24%) than in the summer (15%). Additionally, *Teuthophyrs* were nearly undetectable in the spring samples (1%) but had a large increase in average relative abundance during the summer (16%). For both the spring and summer samples “unknown” genera composed much of the community with average relative abundances of 71% and 32% respectively.

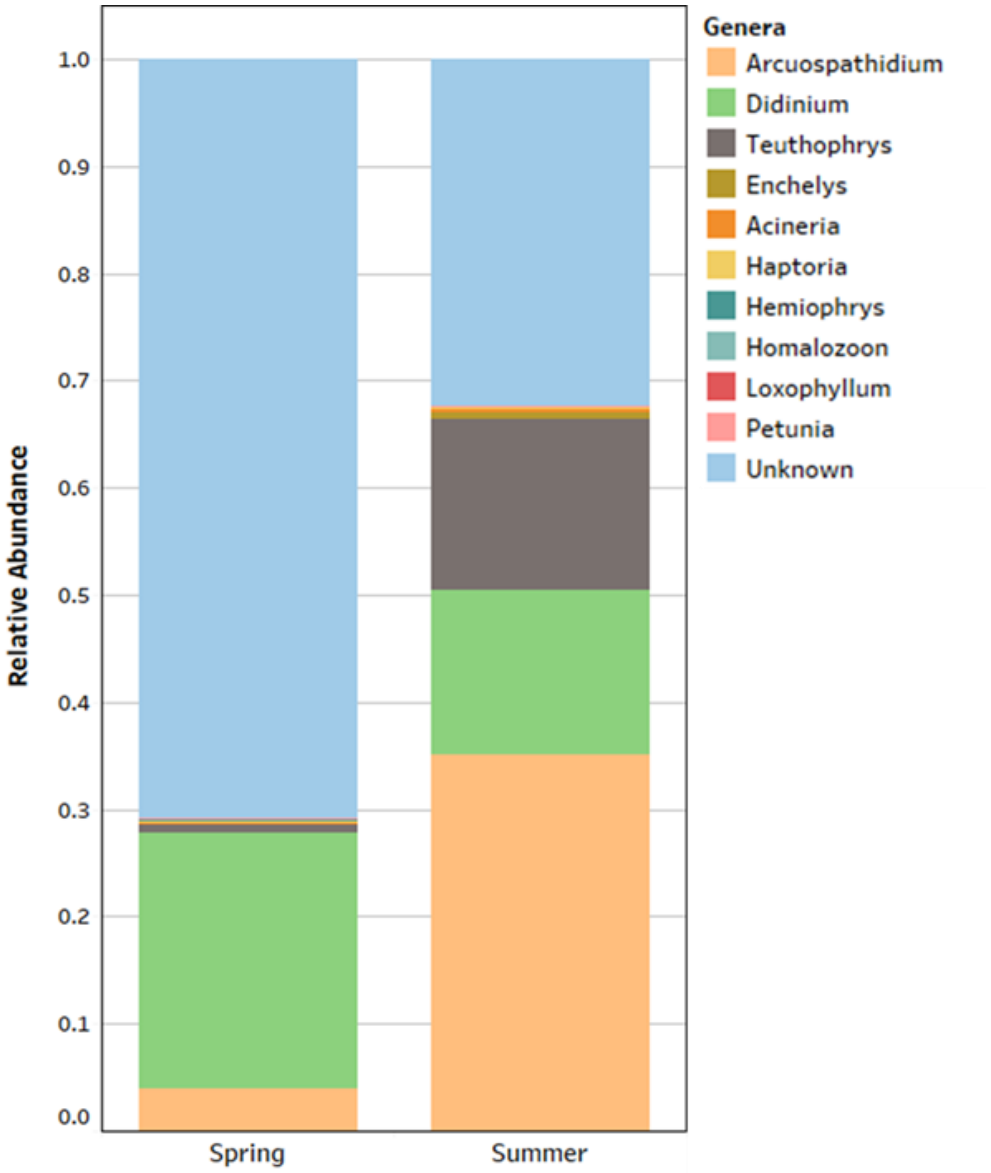

Figure 2.12 Average relative abundances for different genera based on 18S rRNA gene sequencing data by season.

The overall differences between seasons were high, therefore principal component analysis (PCA) was used to help understand data variability. All data was used for PCA analysis including water quality, meteorological, cyanobacteria genes, fecal indicators, and diversity data.

A total of 12 principal components were required to explain all the variance in the data set. The first two principal components (PC1 and PC2) together only explained 50% of the data variability; together with PC3 and PC4, the explained variance is 75%. Other PCs explain less than 10% of the variance (Figure A.6). PC1 is negatively correlated with 16S rRNA gene sequencing diversity indices and water temperature, while positively correlated with secchi disc depth. PC2 is negatively correlated with cumulative precipitation, pH, and fecal indicators. Variables impacting PC2 and showing positive associations include 18S rRNA gene richness and conductivity. Samples for each season have clear separation from one another, with spring samples showing larger spread across the PCA plot (Figure 2.13).

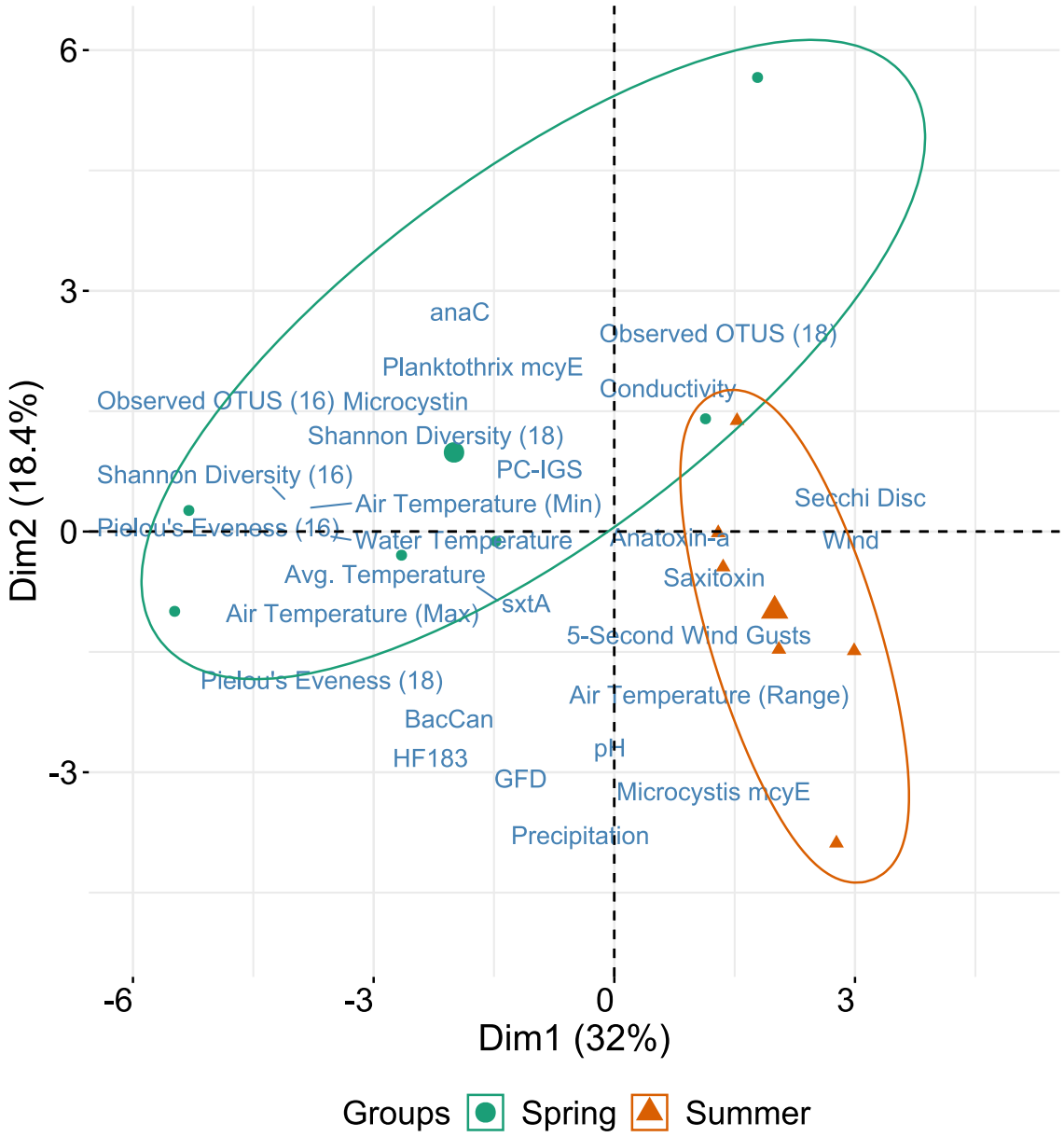

Figure 2.13 2-D PCA plot showing variables effects for PC1 and PC2. Large points in the middle of each ellipse represent the centroid, while smaller points contained within the ellipse represent individual samples.

4.4 Network Analysis of the Microbial Population

A microbial network analysis was conducted to understand the overall microbial matrix using 16S rRNA gene sequencing data. Overall, the network showed that the microbial community in the water is very diverse and composed of many interactions between different taxa. A total of 137 nodes and 130 edges were detected within the network. These represent individual taxa and interactions between taxa respectively. Using the multi-level community algorithm 31 clusters were detected. Clusters represent communities within the network that interact within that community, but do not necessarily interact with other communities in the network. Modularity represents how readily a network can be divided into subnetworks. The modularity score for the clusters detected was 0.79. Next, centrality vectors were sorted to identify keystone species within the network. Four unique taxa were identified as having a probability over 70% of being keystone species. Ordered from highest probability to lowest, these at a family level (with phyla in parenthesis) were Erysipelotrichaceae (Firmicute), Phormidiaceae (Cyanobacteria), Burkholderiaceae (Proteobacteria), and Sporichthyaceae (Actinobacteria). Since Cyanobacteria was of interest, the genus for this keystone species was derived, showing it was *Planktothrix* NIVA-CYA 15. The number of connections, both direct and indirect, for *Planktothrix* NIVA-CYA 15 was examined. This showed that this taxon was connected to 92 other taxa either directly or indirectly. In some cases, a network consists of multiple disconnected components. The microbial network in the lake consisted of 7 disconnected subcomponents, with two of these including most taxa. One subcomponent consisted of 92 taxa, while the next largest consisted of 17. The degree of a node in a network represents how many direct connections it has to other nodes. The degree distribution represents

the probability of these connections throughout the whole network. Results of the degree distribution show that taxa have high probability of two direct connections (~90%), but there is a sharp decrease in the probability of three direct connections, and an even larger decrease in the probability for four direction connections (Figure 2.14).

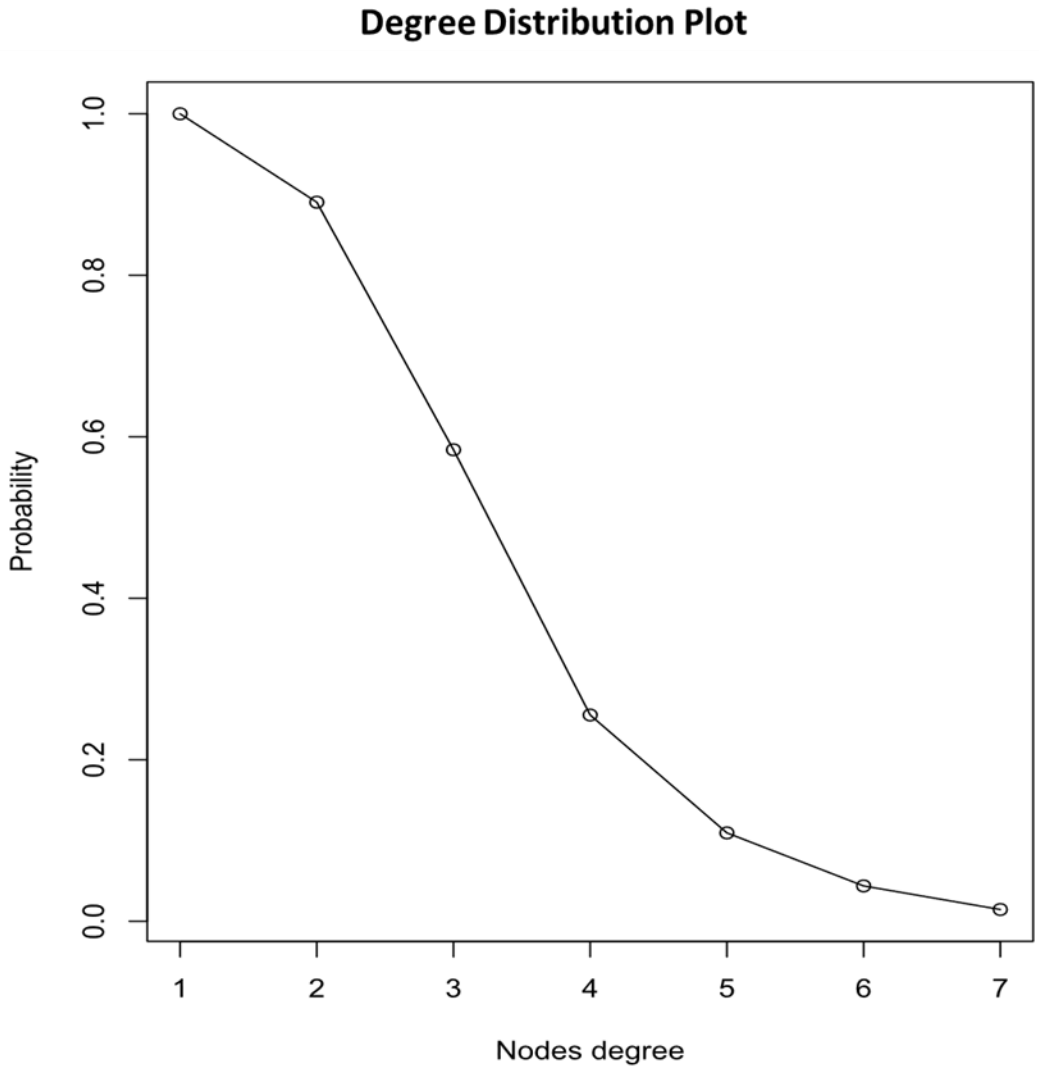

Figure 2.14 Degree distribution plot showing the degree probability distribution over the entire microbial network.

ANND, which is a measure of dependencies between degrees of neighbor nodes, was calculated for all cyanobacteria within the network. Results showed that values for the five cyanobacteria within the network ranged from 1-4. A visualization of the network can be viewed in Figure 2.15.

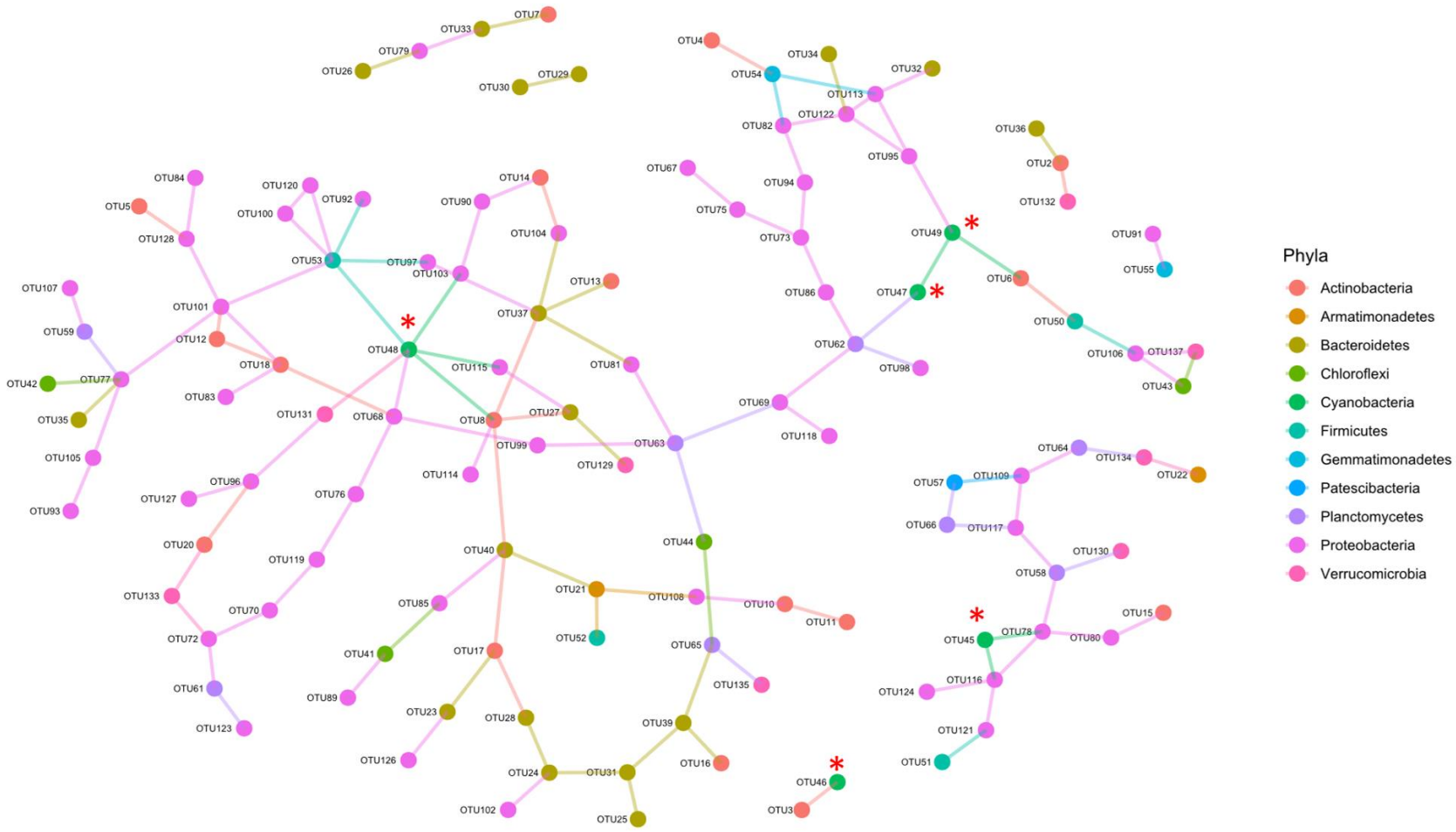

Figure 2.15 Visual representation of the microbial network. Colors indicate unique phyla. Nodes or individual taxa are represented by points. Lines between nodes represent direct interactions between taxa. Cyanobacteria taxa are marked using a *.

5. Discussion

Collecting water quality, meteorological, molecular, and sequencing data allowed us to determine significant factors affecting both prokaryotic and eukaryotic microbial communities, with a focus on the cyanobacterial community, within the urban lake (Rousso et al., 2020). Environmental variables were assessed initially, as previous research has not been conducted on at this study site. It was necessary to observe changes in water quality parameters as it is well known these can affect microbial communities, and result in cyanoHAB eutrophication events (Xu et al., 2022). Secci disc was the only environmental parameter showing statistically significant differences between seasons. This parameter is associated with eutrophication, indicating eutrophication was heightened during the summer (Ding et al., 2023). Although not significantly different by season, water temperature, MST genetic markers, pH, and cumulative precipitation from the three previous days were important water quality parameters contributing to seasonal differences within both communities according to PCA results and Spearman correlations. High pH, favors non-nitrogen fixing cyanobacteria such as *Microcystis* PCC-7914 and *Planktothrix* NIVA-CYA 15 as they are bicarbonate adapted (Visser et al., 2016). At pH levels higher than 8.8 dissolved inorganic carbon is only present as bicarbonate, causing photosynthesis to cease for other aquatic photosynthetic microorganisms. Due to their adaptations, *Microcystis* PCC-7914 and *Planktothrix* NIVA-CYA 15 continue to photosynthesize, further increasing pH levels, negatively affecting water chemistry and other microorganisms (Gibbs et al., 2022). This could be one reason these genera dominate the cyanobacterial community in this lake. It is well known that nutrients, specifically nitrogen and phosphorus, are necessary for cyanoHAB formation. Both BacCan and GFD were positively and

significantly correlated with PC-IGS, which represents total *Microcystis*. This indicates that increases in BacCan and GFD concentrations are associated with an increase in PC-IGS. Furthermore, the first four principal components only explain 75% of the data variability, indicating that interactions in the aquatic system are complex, and many factors are involved. Cyanobacteria require high water temperatures, between 25°-35°C, for optimal growth rates (Smucker et al., 2021). Additionally, there is evidence supporting cyanobacteria species can adapt to high water temperatures faster than other environmental microorganisms (Barton et al., 2020). In the study site, the maximum temperature observed was 30.4°C, and median temperature of 25.2°C. As water temperature increased, the cyanobacteria community became more diverse according to the 16S rRNA gene sequencing data. In spring, when water temperatures were lower, *Planktothrix* NIVA-CYA 15 completely dominated the cyanobacterial community (83%), but as water temperatures began warming, the average relative abundance of *Microcystis* PCC-7914 increased from 3-18%. Additionally, Spearman's correlations revealed Microcystin showed the strongest correlation with water temperature (r_s=0.88, p-value < 0.001), and Microcystin producing *Microcystis* genes were significantly different between seasons (p-value < 0.05.) Furthermore, LEfSE analysis indicates a reduction in *Planktothrix* NIVA-CYA 15 contributes to the differences seen within the microbial community by season. These results indicate that *Microcystis* PCC-7914 is better adapted for higher water temperatures, and as the summer season continues, it will become more abundant in the water. Other research confirms this finding, as (Mowe et al., 2015) states *Microcystis* shows optimal growth rates between 28.8–30.5°C, while *Planktothrix's* optimal growth rates occur between 23–25°C. Nevertheless, *Planktothrix* NIVA-CYA 15 was the dominant cyanobacteria genera during the sampling period.

A possible explanation for this is due to the constant mixing in the water. The lake has five bottom diffusers, which continually mix the water column. Research has shown that *Planktothrix* often has high biomasses in bodies of water with constant mixing compared to other cyanobacteria (Chen et al., 2022). Although relatively high levels of cyanobacteria cyanotoxin producing genes were detected, cyanotoxin concentrations were low throughout the sampling season. No sample had cyanotoxin concentrations above the US EPA recreational limit (US EPA, 2019). Although high concentrations of toxins were not detected this is still of concern, as environmental parameters and pressures can induce toxin production.

Both the microbial communities represented by 16S and 18S rRNA gene sequencing data showed diversity increases from the spring to summer. Evenness for both microbial communities were negatively correlated when analyzed using Spearman's correlation, suggesting that as one increased the other decreased. Additionally, 16S rRNA evenness and 18S rRNA richness were positively correlated. Also, 18S rRNA evenness showed negative and statistically significant correlations with microcystin producing *Microcystis* genes. These results indicate that there could be some form of competition between the microbial communities defined by 16S rRNA and 18S rRNA gene sequencing. This competition results in shifts within these communities as environmental parameters change with the season. The 18S rRNA gene sequencing results show that much of the community is Haptoria (91%), which are free living predatory ciliates (Vďačný et al., 2014). These organisms would graze on cyanobacteria and other microorganisms. In addition, microorganisms within the microbial communities would be competing for necessary resources such as nutrients and sunlight. Further research would need to be conducted to validate

this statement. Overall, the transition from spring to summer resulted in increases in all diversity indices for both microbial communities.

Microbial network analysis was conducted to understand relationships between microbial taxa within the urban lake. Interestingly, the taxa with the second highest probability of being a keystone species was *Planktothrix* NIVA-CYA 15. This taxon was connected to 6 taxa directly, and 86 indirectly. This indicates that *Planktothrix* NIVA-CYA 15 has high interactions with other microbes. Furthermore, *Planktothrix* NIVA-CYA 15 was indirectly connected to two other cyanobacteria genera located in a different cluster, these being *Tychonema* CCAP 1459-11B and *Cyanobium* PCC-6307. *Planktothrix* NIVA-CYA 15 and *Tychonema* CCAP 1459-11B belong to the same family and are often present in the same water bodies (Millar et al., 2022, Shardlow, n.d.). Additionally, both can produce cyanotoxins. Since microcystin producing *Planktothrix* genes were not detected in almost all samples, it is possible these two genera are responsible for the anatoxin-a and saxitoxin levels detected in the lake. *Gleocapsa*, another genus of cyanoabcteria, was in a separate cluster comprised of mainly proteobacteria, with no connections to other cyanobacteria genera. *Microcystis* exhibited the least amount of interaction with other taxa, only being connected to one other. Overall, the network analysis indicated a complex, highly interconnected microbial community.

We acknowledge the following shortcomings in this experiment, as well as provide recommendations for future studies. The first is that the sampling period could have been longer, extending into the colder months and one more year. Additionally, seasons transition between one another and are not usually abrupt changes. Therefore, future studies should consider sampling for a longer period, and from unique locations, so a larger number of samples can be

acquired, and better comparisons made. Furthermore, this study utilized 16S and 18S rRNA gene sequencing data. For a more comprehensive understanding of the microbial community, other sequencing methods such as shotgun metagenomics and longread sequencing could be used. These enable genomic analysis of all microbes within a sample, allowing whole genome sequences, taxonomic composition, and metabolic potentials to be derived. More quantitative methods could be used in future research so stronger statistical analyses can be conducted. Nevertheless, this study provides a foundation for future research, indicating important environmental parameters, and highlighting unique relationships within aquatic communities that warrant future investigation.

6. Conclusion

Higher measures of diversity were observed in the summer for both microbial communities defined by 16S and 18S rRNA gene sequencing data. Our result suggests that seasonal variations in water temperatures, pH, MST, and cumulative rainfall contributed to microbial diversities. Interestingly, *Planktothrix* NIVA-CYA 15 was the dominant cyanobacteria genus throughout the entire sampling period. Furthermore, network analysis results show that *Planktothrix* NIVA-CYA 15 has a high probability of being a keystone species within the study site. Overall, this study indicates that microbial communities are affected by seasonal changes. Additionally, interactions within these aquatic ecosystems are complex. Although this is a baseline study of the prokaryotic and eukaryotic microbial communities, our study provides foundational microbiological and ecological information for hypereutrophic urban waterbodies.

Chapter 3. Evaluation of UAVs as an Emerging Tool for Cyanobacteria Detection and Monitoring

1. Abstract

Currently, traditional monitoring techniques may not be adequate for proper monitoring of cyanobacterial harmful algal blooms (cyanoHABs). This is because cyanoHABs' spatial distribution can change rapidly due to high winds, water currents, and microbial population dynamics. Therefore, new monitoring technologies are needed to supplement the monitoring techniques in place. Unmanned aerial vehicles (UAVs) are a possible solution, as they can be deployed rapidly, are relatively cost-effective, and can monitor large areas in a short amount of time. To evaluate the efficacy and accuracy of UAVs, this study used an UAV equipped with a 5-band multispectral camera for imagery acquisition over a five-month span. A small, hypereutrophic urban lake was selected for the study site, as it is too small for traditional remote sensing techniques. Five band algorithms, the Normalized Vegetation Difference Index (NDVI), Blue Normalized Vegetation Index (BNDVI), Surface Algal Bloom Index (SABI), Normalized Red-edge Difference Index (NDRE), and KIVU were evaluated for their accuracies in chlorophyll-a (chl-a) and phycocyanin (PC) quantification. These algorithms were selected because they each utilize different wavelengths, ensuring all bands were tested for accuracy. Linear regression analysis indicated that the SABI algorithm was the best performing for both chl-a and PC quantification. Additionally, results indicated that Ln transforming values substantially improves the accuracy of these algorithms. We concluded that UAVs equipped with multispectral cameras are a promising technology for cyanoHAB quantification and monitoring,

but more advanced imagery processing techniques are needed for accurate quantification. Additionally, multispectral sensors designed for water applications could greatly improve the accuracy of UAV data products. Nevertheless, with frequent flights over the same location, and the combination of traditional monitoring techniques, UAVs could be a beneficial tool for water resource managers.

Keywords: multispectral, UAV, cyanoHAB, phycocyanin, chlorophyll-a

2. Introduction

UAVs have emerged as a new technology with applications in various fields. UAVs are revolutionizing many industries such as agriculture, cinematography, law enforcement, emergency services, construction, surveying, mining, archaeology, delivery, and environmental conservation (Wu et al., 2019). This is occurring for many reasons, one being that UAVs are a cost-effective solution for increasing accessibility (Kislik et al., 2018). Traditionally, aerial data collection and monitoring required the use of manned aircraft or satellites, both of which are expensive and impractical for smaller-scale operations (Gaffey & Bhardwaj, 2020). UAVs, however, are relatively cost effective, enabling organizations to acquire aerial data without the need for expensive equipment or extensive planning. Furthermore, UAVs offer higher levels of flexibility and precision than other methods of aerial data collection (Kimura et al., 2019). This is because UAVs can be equipped with many different cameras, sensors, and niche attachments. This allows UAVs to be modified for specific use cases, providing the user with the ability to collect data at the desired resolution and in whatever manner is needed (Bilyeu et al. 2022, Hanlon et al. 2022). Also, the use of UAVs can enhance safety and reduce risks. For example, in industries such as law enforcement and disaster management, UAVs can enter hazardous

locations in search of individuals, provide aerial viewpoints to enhance situational awareness, and autonomously locate and follow individuals of interest. Moreover, some UAVs are equipped with audio devices, allowing emergency response professionals to provide instructions virtually, before arriving on scene (DJI Law Enforcement, n.d.). Additionally, UAVs offer significant time savings. Traditional methods for data collection and monitoring often require extensive field work and time-consuming laboratory analysis. With UAVs, these tasks can be completed much faster and autonomously (Kislik et al., 2018). This accelerated and routine analysis allows for informed and prompt decision making. Like other industries, the public health sector has been greatly impacted by the development of UAVs. Water resource managers and researchers are finding that UAVs are a cost-effective solution for efficiently and safely monitoring water resources globally (Sibanda et al., 2021). Currently, one of the many applications for UAVs within this sector is the detection and monitoring of cyanoHABs.

The main objectives for this study were to 1) propose a modified UAV system and simple imagery processing framework that could be used as a standard for non-geospatial experts (such as water resource managers), 2) evaluate five well known indices, these being NDVI, BNDVI, SABI, NDRE, and KIVU, all of which have been noted in prior literature for cyanobacteria quantification, and 3) analyze the effects of three different buffer sizes (2.5 m, 3.0 m, and 3.5 m) on cyanobacteria quantification when using UAV. For objectives 2 and 3, it is hypothesized that 2) the SABI index will show the best correlation with *in-situ* fluorometer values, and 3) that a buffer size of 3 m will produce the most accurate results. Overall, this study aims to assess the potential of UAVs as an efficient and practical monitoring tool for cyanoHABs.

3. Materials and Methods

3.1 Water Quality and Multispectral Imagery Data Collection

Refer to chapter 2, section 3.1 for additional information about the study site. In addition to the collection of water quality, meteorological, molecular, and amplicon sequencing data mentioned previously, in-situ fluorometer measurements were taken at four different locations around the lake. This resulted in a total of 48 *in-situ* fluorometer measurements. These were collected in duplicate using the Aquafluor handheld fluorometer (Turner Designs, San Jose, CA, USA). Fluorometer readings for both chl-a and PC were acquired. Additionally, GPS coordinates were collected for each sampling location using a Garmin GPSMAP 66S (Garmin & subsidiaries, Olathe, KS, USA). This device has a minimum error of 2.5 m, with one sampling location never providing a lower positional error than 3 m. Additionally, secchi disc measurements were taken at the deepest part of the lake. These values were used to determine the first optical depth and the 1% light level. Furthermore, 12 UAV flights were conducted directly before sampling (Table 3.1).

Table 3.1 Summary of all flights including date, start/stop time, number of images acquired, cloud cover percentage, and any notes about lighting changes during the flight.

Date	Flight Start	Flight Stop	Cloud Cover (%)	Lighting Changes	Number of Images
4/2/2022	15:04	15:19	76	No lighting changes	89
4/17/2022	16:36	16:57	0	Sunny clear skies	86
5/2/2022	15:19	15:41	25	No lighting changes	86
5/13/2022	11:32	12:15	0	No lighting changes	84
5/29/2022	13:53	14:19	76	No lighting changes	78

Continued

Table 3.1 continued

6/13/2022	**13:08**	**13:22**	**39**	**Slight lighting changes halfway through flight**	**80**
6/30/2022	15:02	15:24	0	No lighting changes	82
7/16/2022	17:16	17:30	81	No lighting changes	76
7/31/2022	14:33	14:52	76	Slight lighting changes, very slight	73
8/17/2022	13:13	13:30	49	Lighting changes for two flight lines in middle of lake	82
9/11/2022	14:38	14:57	89	Lighting changes throughout flight, panel pic taken in sun and shade	71
9/24/2022	13:18	13:30	76	No lighting changes	76

All flights were conducted following Micasense's guidelines for optimal data capture (*Best Practices*, 2023). Before each flight, four ground control points (GCPs) were dispersed evenly on the edges of the lake. This aids in pre-processing of the images. Also, a Trimble R8 Global Navigation Satellite System (GNSS) was used to measure the center of these (Trimble Inc, Westminister, CO). The center coordinates were then used during pre-processing to georectify all images using the NAD83 / Ohio South (ftUS) - EPSG:3735 coordinate system. All flights were at 91 m in elevation, using 75% forward and side overlap. This resulted in a ground sampling distance of 6.3 cm/pix. If weather conditions allowed, all flights were conducted within two hours of solar noon to reduce the effect of shadows and sun glint on the imagery. Additionally, flights were flown during constant lighting conditions. Partly cloudy days were avoided, or flights would be delayed until the cloud cover was gone. The best conditions to fly in were completely overcast days, as this reduced the effects of sunglint, while providing constant

lighting conditions. The UAV was controlled with a tablet, using DJI Ground Station Pro (DJI, Shenzhen, China). This is a flight planning software that makes the UAV autonomous. Within the software, a custom camera setting was used to match the parameters of the Micasense RedEdge-MX camera (Micasense, Seattle, Washington) (Table 3.2). Additionally, the "hover and capture mode" was used for imagery acquisition. This ensures that no image blur occurs due to the UAV moving too fast in comparison to the shutter speed.

Table 3.2 Custom camera parameter settings for Micasense RedEdge-MX multispectral sensor. These were retrieved from (Camera Parameters for Mission Planning Apps (DJI Pilot, GS Pro, Etc.), 2023).

Micasense RedEdge-MX	**Value**
Image Width (pix)	1280
Image Height (pix)	960
Sensor Width (mm)	4.8
Sensor Height (mm)	3.6
Focal Length (mm)	5.4
Min Shutter Interval (seconds)	1

All flights were conducted using a DJI Matrice 200 (DJI, Shenzhen, China). This UAV has a vertical positional accuracy of 0.5 m and a horizontal accuracy of 1.5m, with a max flight time of roughly 27 minutes. Additionally, the UAV has landing gear that prevents the camera from hitting the ground during landing. The UAV was equipped with a Micasense RedEdge-MX multispectral camera (Micasense, Seattle, Washington). This camera has five independent lenses,

each used to capture a different wavelength. The five wavelengths (λ) observed by the camera include: blue (475 nm), green (560 nm), red (668 nm), red edge (717 nm), and near-infrared (NIR= 840 nm) (Table 3.3).

Table 3.3 Indicates the center wavelength and bandwidth associated with each band. Information was retrieved from (What Is the Center Wavelength and Bandwidth of Each Filter for MicaSense Sensors?, 2023).

Band Name	Center Wavelength (nm)	Bandwidth (nm)
Blue	475	20
Green	560	20
Red	668	10
Red Edge	717	10
NIR	840	40

Furthermore, the camera has a GPS/IMU, which records the position and the posture of the camera at each image taken. Also, the camera produces its own wifi, which can be connected to using the tablet. This allows for manual control of the camera, and to be sure the camera has memory before flights are conducted. Additionally, the camera is connected to a DLS sensor. This DLS has small, circular sensors all around it. The DLS measures the irradiance associated with every image taken and stores this information in the image's metadata. This allows for corrections in light intensity during imagery processing. The DLS was mounted on top of the UAV to ensure it was not covered by any shadows. Additionally, to aid image reflectance calibration, a Micasense reflectance calibration panel was used (Micasense, Seattle, Washington). The reflectance panel is a Lambertian surface, meaning it reflects light equally in

all directions, no matter what angle the light enters at. Images were taken of this directly before and after every flight. Special care was taken to be sure images taken were not shadowed. If lighting conditions did change during the flight, an image of the calibration panel was taken during each lighting condition. In addition to the attachments and equipment mentioned previously, a DJI Skyport was installed on the drone (DJI, Shenzhen, China). This device is incredibly important as it keeps the camera facing the ground at a 90° angle (nadir) and allows the UAV to communicate with the camera. This allows for control of the camera through the flight planning software. An overview of the entire UAV system can be seen in Figure 3.1.

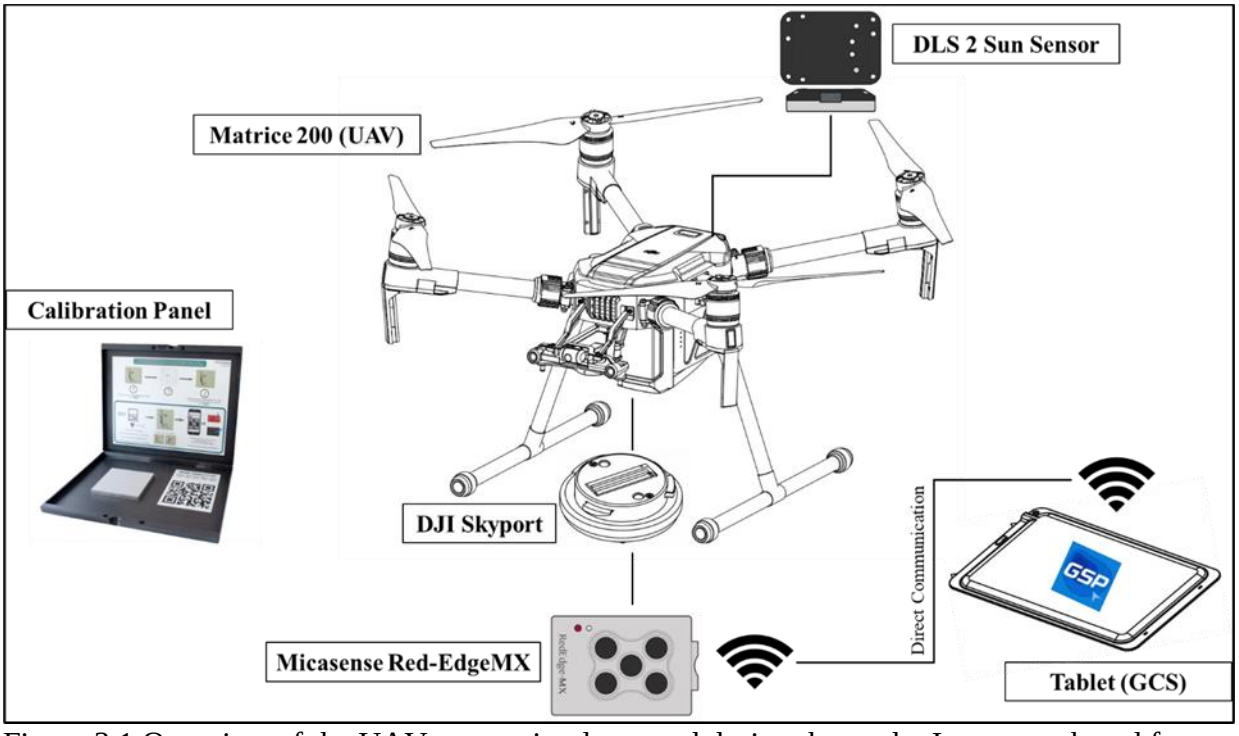

Figure 3.1 Overview of the UAV system implemented during the study. Images gathered from DJI and Micasense websites (Matrice 200 Series - Download Center - DJI, n.d., RedEdge-MX Integration Guide, 2022).

3.2 UAV Imagery Pre-processing

All imagery pre-processing was conducted in Agisoft Metashape Pro version 2.0.2 (Metashape, St. Petersburg, Russia). To begin, a radiometric calibration model provided by Micasense was utilized. The spectral radiance for each pixel value was computed using the following equation:

$$L = V(x,y) * \frac{a_1}{g} * \frac{P - P_{BL}}{t_e + a_2 y - a_3 t_e y}$$

This model compensates for sensor black level (P_{BL}), sensitivity and gain (g), exposure settings (t_e), and lens vignette effects ($V(x,y)$). Coefficients a_1, a_2, and a_3 are the radiometric calibration coefficients. Pixel column and row number are represented by x and y respectively. These parameters are stored within the metadata of each image. The lens vignette model ($V(x,y)$) used is a radial vignette model that corrects for fall off in light intensity for pixels farther from the center of the image. The radiometric calibration uses a normalized pixel value (p) in the range of 0 to 1. To compute this value, the raw digital number for each pixel is divided by 2^N. In this study N is equal to 65,536, as the sensor used produces 16-bit images. After radiometric calibration was performed, raw pixel values are in units of radiance. To convert these to reflectance values, images taken of the reflectance calibration panel before and after each flight are used. The average values of radiance for the calibration panel are acquired, then the transfer function for radiance to reflectance is calculated using the following equation:

$$F_i = \frac{\rho_i}{avg(L_i)}$$

Where F_i represents the reflectance calibration factor for the selected band, ρ_i is the average reflectance value acquired for the calibration panel for a specific band, and $avg(L_i)$ is the average value of the radiance for pixels in the calibration panel. Once this process was complete, images were aligned, and cameras optimized. Next, a high-quality point cloud was generated. This was then used to create a DEM. After DEM, creation, the DEM was flatted using a constant elevation for the water's surface. After, an orthomosaic was generated for the entire flight area.

3.3 UAV Imagery Post-processing

Once orthomosaics were obtained for all 12 flights, areas not representative of the waterbody were removed. Additionally, any areas including shadows or vegetation cover were removed. No atmospheric corrections were applied as there are no commercially available solutions designed for aquatic purposes or UAV imagery. Additionally, the purpose of this work is to deliver a simple imagery processing solution for non-geospatial experts. Furthermore, previous studies have shown that scattered irradiance from the atmosphere is negligible for UAV flights conducted at low altitudes. Therefore, the effect of the thin atmosphere between the sensor and water surface was neglected (Del Pozo et al., 2014; Zeng et al., 2017). Five algorithms were then applied to each image, these being the NDVI, BNDVI, SABI, NDRE, and KIVU. Multiple algorithms were selected to ensure that a range of band combinations were included. Algorithms using the red and NIR bands were selected, such as NDVI and NDRE. Other algorithms were selected using known features in the blue and green bands, as well as those in the NIR and red. Algorithms in this category include BNDVI, SABI, and KIVU. Additionally, these algorithms were selected because prior literature had shown success while implementing these for cyanoHAB quantification (Cillero Castro et al., 2020, Choo et al., 2018,

Brivio et al., 2001, Silvarrey Barruffa et al., 2021, Brivio et al., 2001). All algorithms were applied using Agisoft Metashape's "raster transform" function (Metashape, St. Petersburg, Russia). Once algorithms were applied, orthomosaics were loaded into ArcGIS Pro version 2.9 for further analysis (ESRI, Redlands, CA). To begin, sampling locations for each *in-situ* fluorometer measurement were imported. These locations were used as the center point, to create 2.5, 3, and 3.5 m circular buffers for the extraction of imagery information. These buffer sizes were selected to compensate for the error of the GPS unit being used, and for any drift that might have occurred between UAV flights and water sampling. The mean values within the circular radius were then exported for further analysis. All band algorithms and associated equations can be seen in Table 3.4.

Table 3.4 Band ratio algorithms implemented for all 12 orthomosaics.

Index	**Formula**
Normalized Difference Vegetation Index (NDVI)	(NIR − Red)/(NIR + Red)
Surface Algal Index (SABI)	(NIR − Red) /(Blue + Green)
KIVU	(Blue − Red) /Green
Normalized Difference of Red Edge (NDRE)	(NIR − RE)/(NIR + RE)
Blue Normalized Vegetation Index (BNDVI)	(NIR-B)/(NIR+B)

3.4 Statistical Analysis

Once imagery information was extracted, linear fits were applied to analyze the relationship between reflectance and values gathered at each of the *in-situ* fluorometer sampling

sites for both chl-a and PC. In addition, linear fits were assessed for Ln(chl-a) and Ln(PC) data. This approach is being tested by many other researchers to account for the non-normal distribution of chl-a and PC values (Boucher et al., 2018, Cillero Castro et al., 2020). After removal of shadows and vegetative overgrowth during post-processing, a total of 39 observations were used for regression analysis. Statistical analysis and figures were generated in Excel (version 2307).

4. Results

4.1 Water Quality and UAV System Performance

The study site is a hypereutrophic waterbody with reoccurring cyanoHABs according to the lake management companies who have overseen the site for some years. The research in chapter 2 showed that during 2021, *Planktothrix NIVA-CYA* was the most abundant cyanobacteria genera throughout the sampling period. In addition, *Microcystis PCC-7914* and *Tychonema CCAP 1459-11B* were also present. All these cyanobacteria genera are capable of producing multiple kinds of cyanotoxins, posing a risk to public health. During the sampling period chl-a and PC concentrations were rather high, with minimum values for chl-a and PC being 47.54 and 10.68 RFU, with maximums for these parameters being 3,893 and 355 RFU respectively. The general trend for both parameters were exponential increases starting at the beginning of June 2022, followed by an exponential decrease at the end of July 2022 (Figure 3.2).

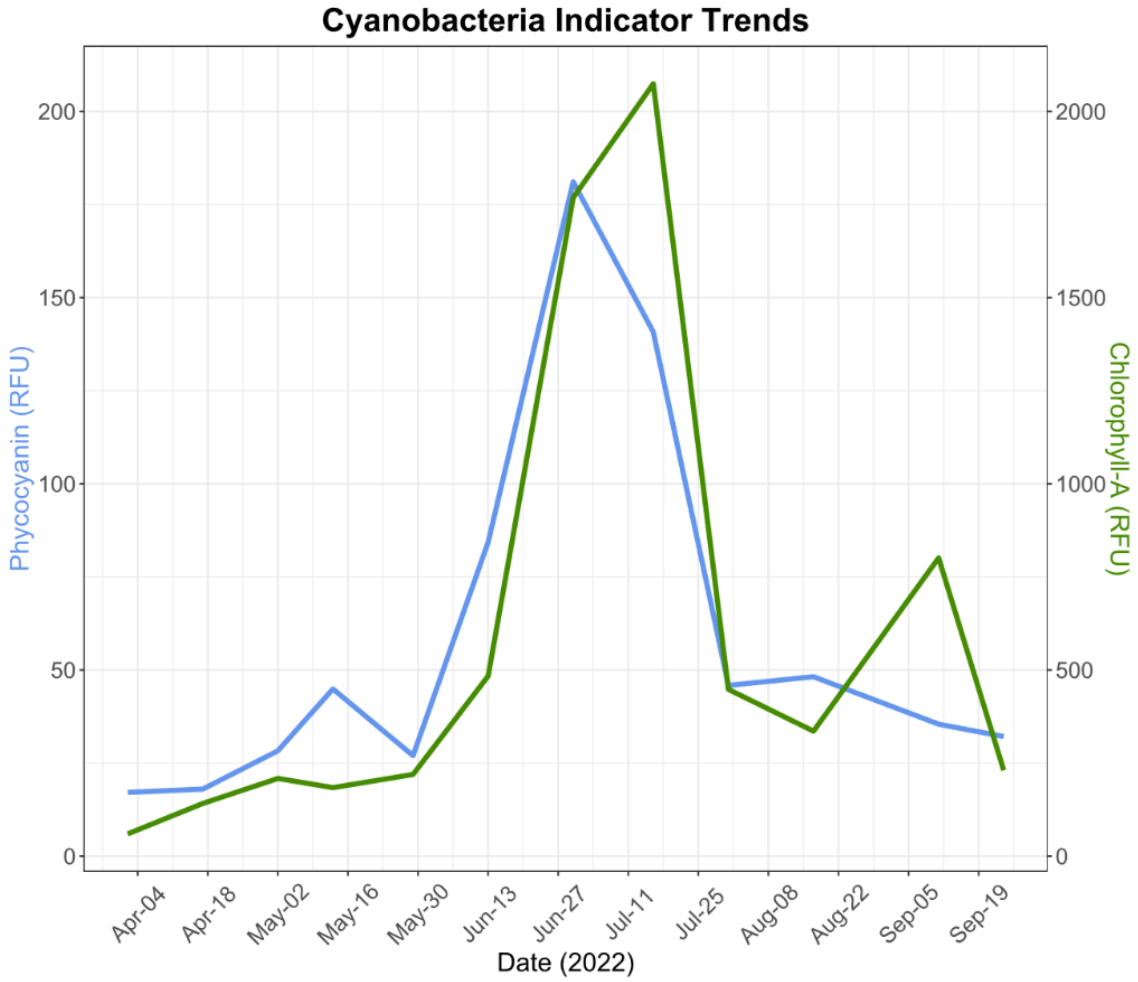

Note: Note, the left and right axis have different scales for better representation of the data. The scale on the left side is representative of PC concentrations, while the left scale is representative of chl-a values.

Figure 3.2 Line graph representing the temporal trends for PC and chl-a.

In addition to chl-a and PC measurements, secchi disc measurements were taken as well. These were taken at the deepest part of the lake during each sampling visit. The minimum and maximum secchi disc measurements taken during the sampling period were 0.13 and 0.65 mm

respectively. The average secchi disc measurement was 0.29 m, indicating that the lake suffered from eutrophication for much of the sampling period. Additionally, the first optical density and 1% light level were calculated using secchi disc measurements. The first optical density is equivalent to secchi disc depth, while the 1% light level can be calculated as 3*secchi disc depth (Roos & Pieterse, 1994). The mean first optical density for the study site was 0.18 m, with minimum and maximums of 0.076 and 0.39 m respectively. For the 1% light level, minimum and maximum values of 0.39 and 1.95 m respectively were observed. Table 3.5 summarizes these water quality parameter statistics and others.

Table 3.5 Summary statistics for UAV related water quality parameters measured during the sampling period. Secchi disc measurements are representative of the first optical depth.

	Mean	Standard Deviation	Median	Minimum	Maximum	Range
PC (RFU)	62.02	70.84	37.19	10.68	355.0	344.3
Chl-a (RFU)	652.6	936.9	281.9	47.54	3893	3845
Secchi Disc (m)	0.29	0.14	0.26	0.13	0.65	0.52
1% Light Level (m)	0.87	0.42	0.78	0.39	1.95	1.56

In addition, the performance of the UAV system and accompanying flight software implemented was assessed. Overall, the integrated UAV system performed well. To begin, the use of a tablet as a ground control station (GCS) made it possible to move around the site as the UAV was in flight to ensure safety and improve the visual line of sight. This is of importance as the FAA requires UAV pilots to maintain a constant line of sight with the UAV during flights. Additionally, the use of DJI Ground Station Pro allowed for flight planning and ensured that

during each site visit the same area was flown. Additionally, this software allowed for appropriate overlap, elevation, and flight speed to be maintained for the duration of the flight. Furthermore, using the "hover and capture mode" was beneficial, as no images exhibited image blur. These were checked at the end of every flight. Integrating the DLS sensor into the UAV allowed for measurements of irradiance to be associated with each image. This was confirmed by viewing the metadata associated with each image. Additionally, the use of the DJI Skyport substantially improved image acquisition. This device allowed the Micasense Red-EdgeMX camera and UAV to communicate with one another. This allowed for real time monitoring of image acquisition, camera memory, and automatic triggering of the camera. Also, this device always keeps the camera in a nadir position during flights. Without this device, the camera would have to be triggered manually. Furthermore, the user would have to manually place the camera in a nadir position, which could introduce error and result in difficulties during imagery pre-processing.

4.2 Regression Analysis and Statistics

Thirty-nine data points were used for linear regression analysis. In addition, three different buffer sizes were implemented to assess how this may affect data extraction from UAV imagery. In total, five different indices were utilized to compare UAV derived values to *in-situ* chl-a and PC fluorometer values. Linear fits were made with both non-transformed and Ln transformed *in-situ* data, with the latter providing substantially better results. For all buffer sizes and data types, SABI algorithm provided the best results. For non-transformed chl-a data, SABI showed the best fit based on all metrics (Table 3.6, Figure 3.3). Buffer size did not substantially impact the results. This algorithm was statistically significant with all three buffer sizes, with the

highest R^2 value (0.38) when using a buffer size of 3.5 m. Additionally, SABI had the strongest Pearson ($r > 0.6$). The second-best performing algorithm was BNDVI. Like SABI, this algorithm was statistically significant using all three buffer sizes, with the best results ($R^2 = 0.22$, $r = 0.47$, p-value=0.002) obtained when using a 3.5 m buffer. NDVI, NDRE, and KIVU all fit poorly, with $R^2 < 0.07$. KIVU produced slightly higher Pearson correlation values than NDVI and NDRE.

Table 3.6 Linear fit parameters for all algorithms tested for the retrieval of chl-a. These results are with non-transformed chl-a (N=39). (*) $p < 0.1$, (**) $p < 0.05$, (***) $p < 0.01$, (****) $p < 0.001$.

Algorithm	Buffer Size (m)	R^2	Pearson r	p-value	Significance Level
NDVI	2.5	0.020	0.16	0.34	
	3.0	0.020	0.15	0.35	
	3.5	0.020	0.15	0.36	
BNDVI	2.5	0.21	0.46	0.0040	***
	3.0	0.21	0.46	0.0030	***
	3.5	0.22	0.47	0.0020	***
KIVU	2.5	0.070	0.27	0.10	*
	3.0	0.070	0.26	0.16	
	3.5	0.070	0.27	0.10	*
SABI	2.5	0.36	0.60	0.000060	****
	3.0	0.37	0.60	0.000050	****
	3.5	0.38	0.62	0.000030	****
NDRE	2.5	0.030	-0.17	0.31	
	3.0	0.040	-0.19	0.24	
	3.5	0.040	-0.22	0.18	

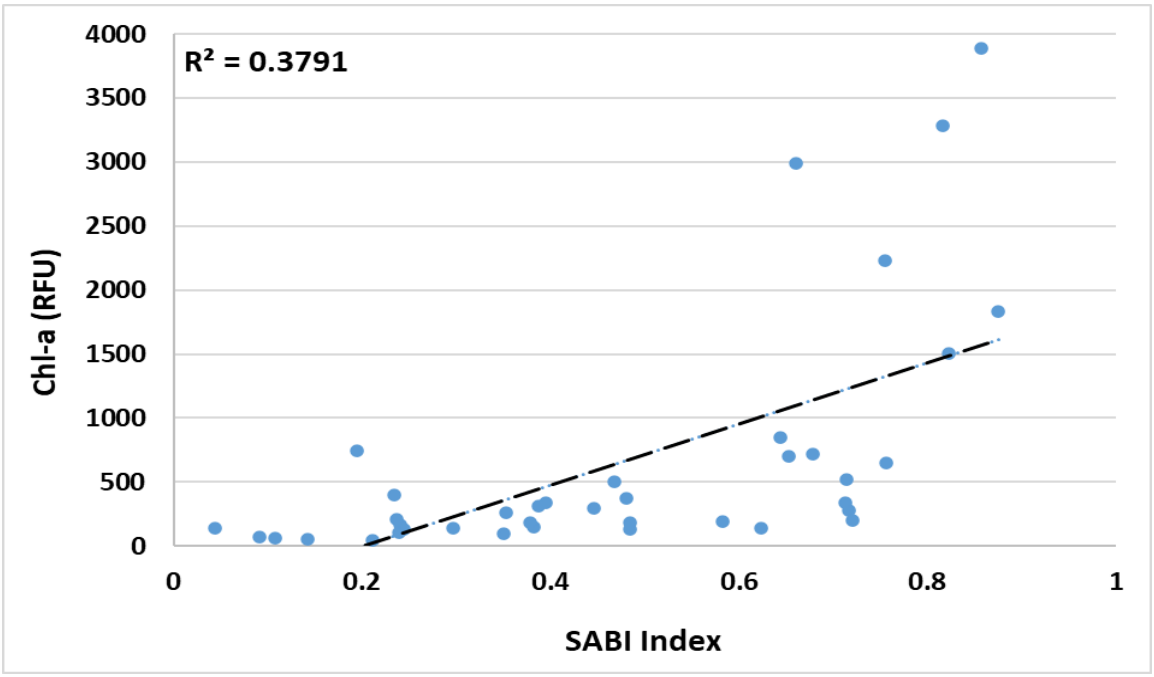

A

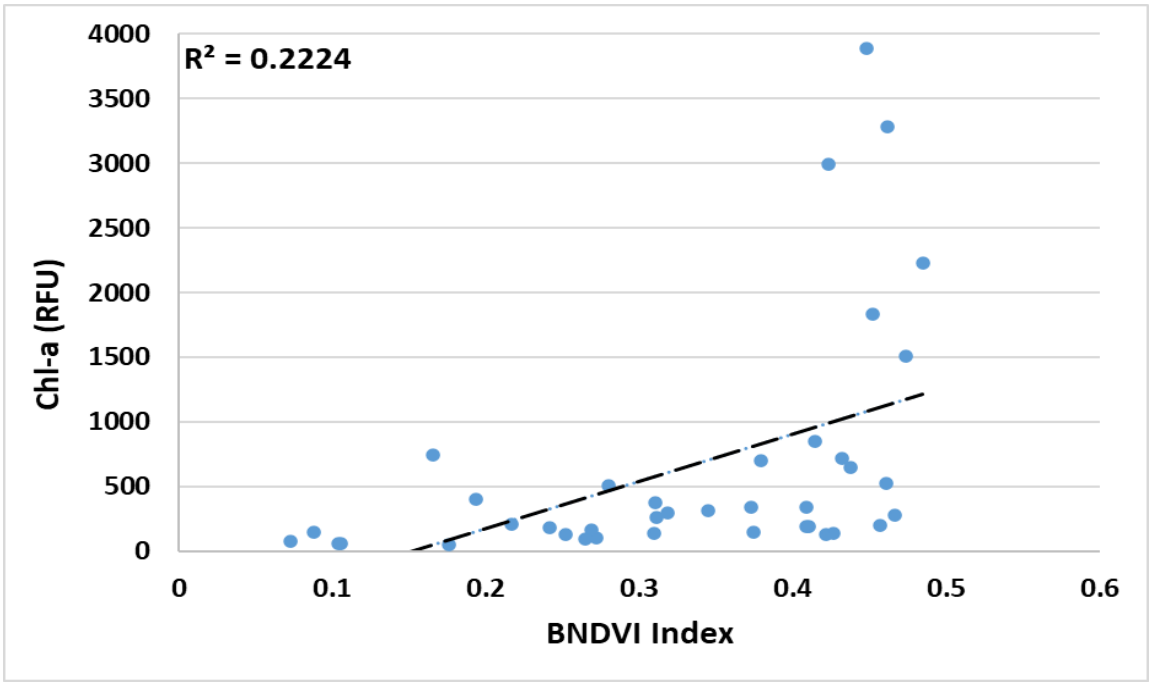

B

Figure 3.3 Scatter plots for the best performing models for retrieving chl-a when using a 3.5m buffer and non-transformed chl-a data, A) SABI, and B) BNDVI.

All algorithms showed better fits with Ln transformed chl-a data. SABI showed the best fit, with R^2 values greater than 0.53 (p-value < 0.001). Additionally, the best results were obtained when using a 3.5 m buffer. As with non-transformed chl-a data, BNDVI was the second-best performing algorithm, with the highest R^2 and Pearson correlation coefficient obtained when using the 3.5 m buffer. NDVI showed slight improvement when using Ln transformed chl-a data, but linear fit parameters were still quite low. NDRE was mostly unaffected by the data transformation, and still produced poor results. KIVU was the only algorithm that produced the worst results when regressed with Ln transformed chl-a data, showing a decrease in all linear fit parameters (Table 3.7, Figure 3.4).

Table 3.7 Linear fit parameters for all algorithms tested for the retrieval of chl-a. These results are with Ln transformed chl-a (N=39). (*) p < 0.1, (**) p < 0.05, (***) p< 0.01, (****) p < 0.001.

Algorithm	Buffer Size	R^2	Pearson r	p-value	Significance Level
NDVI	2.5	0.14	0.37	0.11	
	3.0	0.13	0.37	0.020	*
	3.5	0.13	0.36	0.020	*
BNDVI	2.5	0.38	0.62	0.000030	****
	3.0	0.39	0.62	0.000020	****
	3.5	0.40	0.63	0.000020	****
KIVU	2.5	0.060	0.21	0.20	
	3.0	0.050	0.21	0.20	
	3.5	0.050	0.22	0.18	
SABI	2.5	0.53	0.73	0.00000010	****
	3.0	0.55	0.74	0.000000080	****
	3.5	0.56	0.75	0.000000080	****
NDRE	2.5	0.040	-0.20	0.22	
	3.0	0.050	-0.21	0.18	
	3.5	0.060	-0.24	0.14	

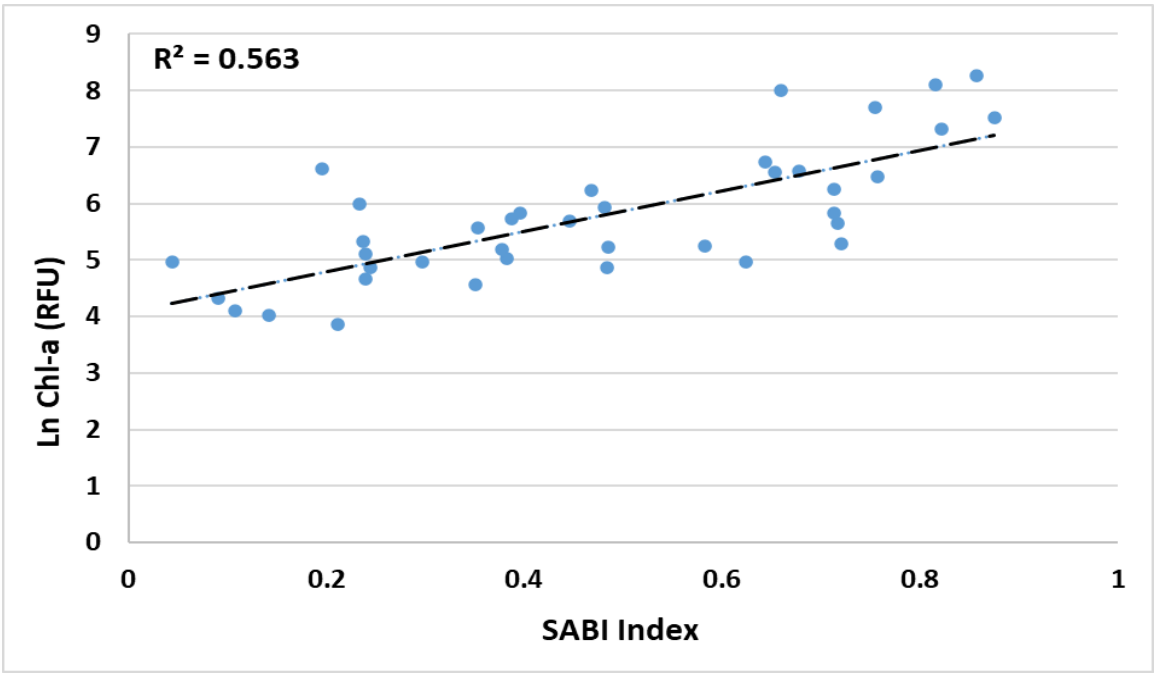

A

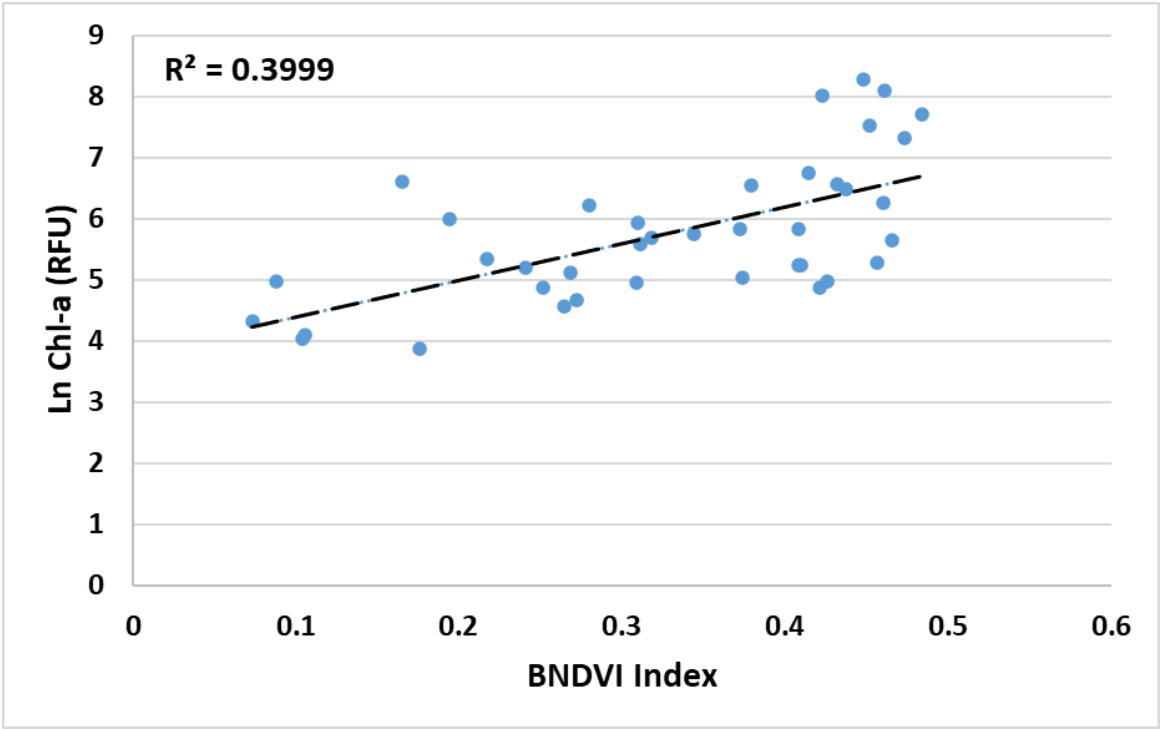

B

Figure 3.4 Scatter plots for the best performing models using a 3.5 m buffer and Ln transformed chl-a data, A) SABI, and B) BNDVI.

As with non-transformed chl-a data, SABI preformed best out of all algorithms when regressed with non-transformed PC data. The highest R^2 value and Pearson correlation coefficient was obtained with the 3.5m buffer (R^2=0.26, r = 0.51). The next best performing algorithm was BNDVI, although it showed poor regression metrics (highest R^2=0.16 and r = 0.4). All other algorithms showed poor regression metrics, with NDVI being the worst (R^2 < 0.02 and r = 0.04). A summary of all non-transformed PC regression metrics can be viewed in Table 3.8, and scatter plots of the two best performing algorithms in Figure 3.5.

Table 3.8 Linear fit parameters for all algorithms tested for the retrieval of PC. These results are with non-transformed PC values (N=39). (*) p < 0.1, (**) p < 0.05, (***) p< 0.01, (****) p < 0.001.

Algorithm	Buffer Size	R^2	Pearson r	p-value	Significance Level
NDVI	2.5	0.020	0.040	0.78	
	3.0	0.0010	0.040	0.80	
	3.5	0.0010	0.040	0.80	
BNDVI	2.5	0.15	0.39	0.020	
	3.0	0.16	0.40	0.010	***
	3.5	0.16	0.40	0.010	***
KIVU	2.5	0.070	0.27	0.050	**
	3.0	0.080	0.28	0.090	
	3.5	0.080	0.29	0.060	
SABI	2.5	0.24	0.49	0.0020	***
	3.0	0.25	0.50	0.0010	****
	3.5	0.26	0.51	0.00080	****
NDRE	2.5	0.020	-0.13	0.45	
	3.0	0.020	-0.15	0.36	
	3.5	0.030	-0.17	0.27	

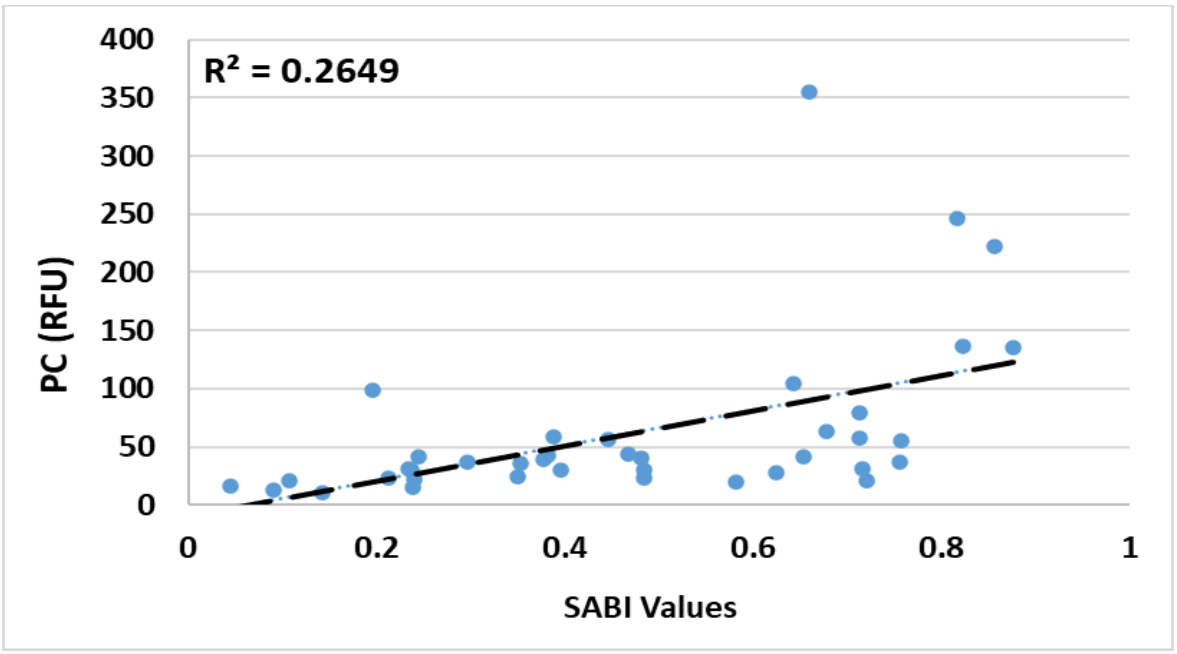

A

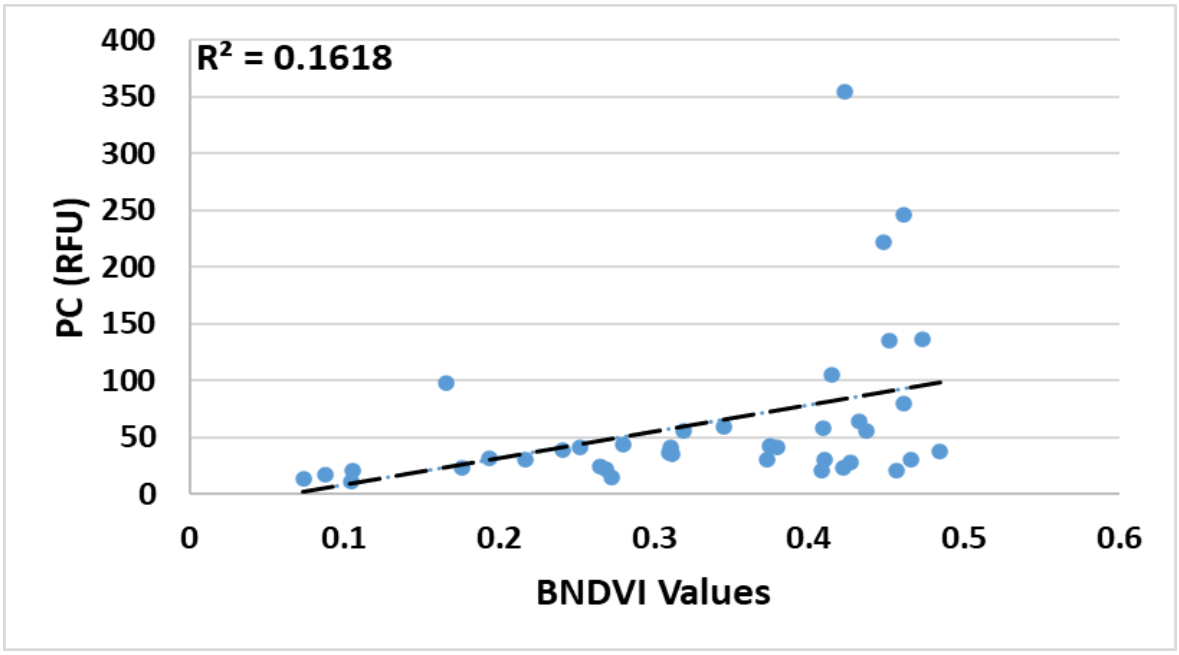

B

Figure 3.5 Scatter plots for the best performing models using a 3.5 m buffer and PC data, A) SABI, and B) BNDVI.

Ln transforming PC data improved linear fit parameters for SABI, BNDVI, and NDVI. SABI and BNDVI produced the best linear parameters. For SABI, the 3.5m buffer produced the highest R^2 and Pearson correlation coefficient (R^2=0.42, r = 0.65), while the 3m buffer produced the best results for the BNDVI algorithm (R^2=0.29, r = 0.54) (Figure 3.6). NDVI values did not show any variation with different buffer sizes and were only slightly improved when regressed with Ln transformed PC data (R^2=0.05, r=0.22). Both KIVU and NDRE produced lower R^2 and Pearson correlation coefficients when applied to the transformed PC data (Table 3.9). Overall, the best performing algorithms were SABI and BNDVI. These produced the best linear fit parameters for all data and showed the best results when applied to Ln transformed chl-a data.

Table 3.9 Linear fit parameters for all algorithms tested for the retrieval of PC. These results are with Ln transformed PC values (N=39). (*) p < 0.1, (**) p < 0.05, (***) p< 0.01, (****) p < 0.001.

Algorithm	Buffer Size	R^2	Pearson r	p-value	Significance Level
NDVI	2.5	0.050	0.22	0.17	
	3.0	0.050	0.22	0.17	
	3.5	0.050	0.22	0.18	
BNDVI	2.5	0.15	0.52	0.020	*
	3.0	0.29	0.54	0.00040	****
	3.5	0.28	0.54	0.00060	****
KIVU	2.5	0.060	0.24	0.14	
	3.0	0.060	0.25	0.12	
	3.5	0.070	0.26	0.11	
SABI	2.5	0.38	0.62	0.000030	****
	3.0	0.40	0.64	0.000010	****
	3.5	0.42	0.65	0.0000090	****
NDRE	2.5	0.010	-0.11	0.52	
	30	0.020	-0.13	0.44	
	3.5	0.020	-0.15	0.36	

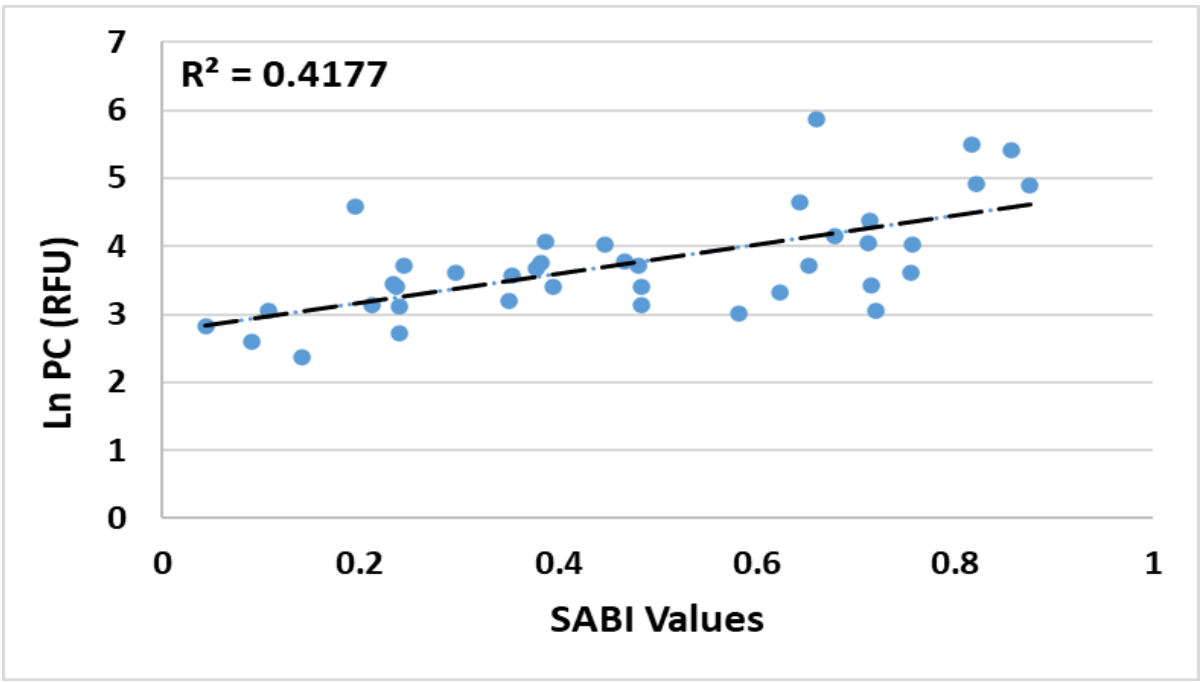

A

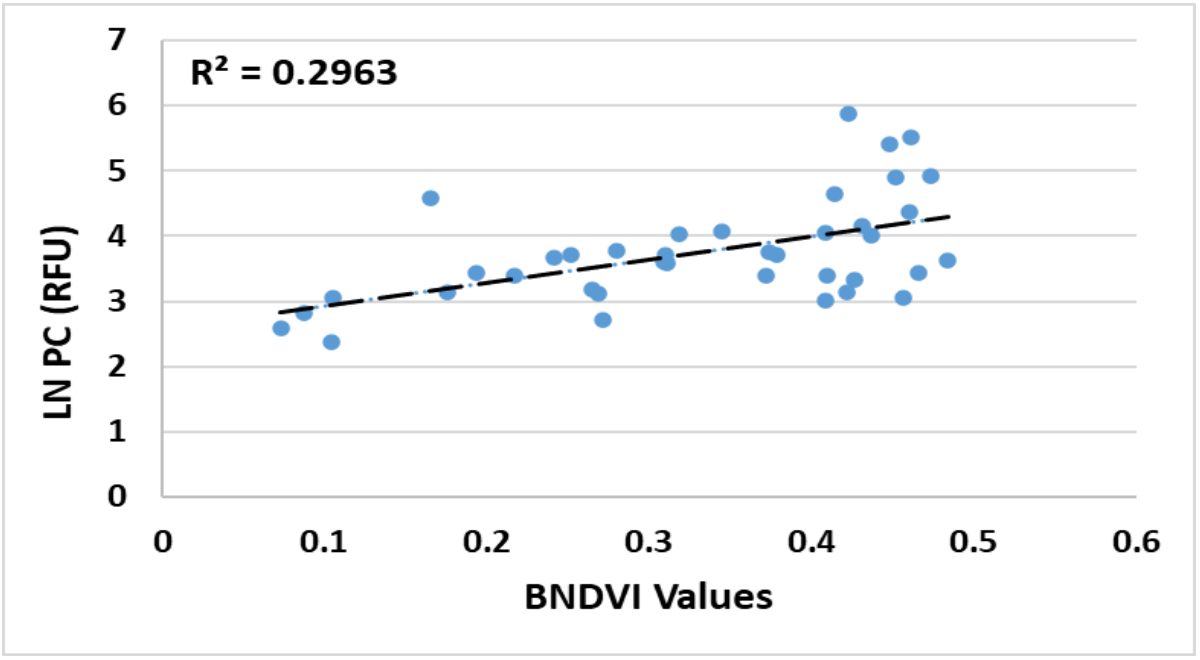

B

Figure 3.6 Scatter plots for the best performing models using a 3.5 m buffer and Ln transformed PC data, A) SABI, and B) BNDVI.

5. Discussion

Overall, the UAV system and flight planning methodologies implemented in this study performed well. All field sampling campaigns were completed with a single flight. After flights, images were manually checked for irregularities, and no images ever exhibited blur or other inconsistencies. This indicates the “hover and capture” mode is a useful technique for reducing inconsistencies that may arise during image acquisition. Although, the trade off to this is longer flight times, and consequently the need for more UAV batteries. Additionally, during the pre-processing steps, all images aligned with no failures indicating the overlap values were adequate. It is important to use the optimal overlap to ensure efficient flight times and avoid issues during pre-processing. Additionally, the use of the DJI skyport streamlined image acquisition and allowed for monitoring of the sensor while the UAV was in flight. Using an integrated UAV system can result in more efficient and accurate data acquisition.

Compared to other bodies of water, the study site was highly eutrophic for the entire sampling period. This could be one explanation for the relatively low correlations between UAV data and in-situ sampling values represented in this study. Peaks in chl-a and PC were observed in late June and in early July. Additionally, secchi disc measurements support this, as the average value was 29.22 cm. Furthermore, secchi disc depth is a measure of turbidity. Multiple studies have indicated that high turbidity levels make it difficult to extract desired data from UAV imagery (El-Alem et al., 2021, McEliece et al., 2020). Prior research has indicated that hypereutrophic bodies of water are difficult to quantify using UAV imagery. For example, Cheng et al., 2020 reported that model prediction was less satisfactory for chl-a values greater than 15 µg/l. Additionally, Tóth et al., 2021 and Cillero Castro et al., 2020 found it necessary to

implement different models for certain ranges of chl-a values. Sampling for longer periods of time and from waterbodies with different eutrophication levels is a possible solution for mitigating this problem (El-Alem et al., 2021). Furthermore, deeper integration of UAVs with other technologies such as artificial intelligence and automation technologies could aid in mitigating these issues (Wu et al., 2019).

Although out of the scope of this study, UAV imagery processing techniques are far from mature, and future research is needed to improve these (Shang et al., 2017). No advanced post-processing was implemented in this study, which could account for the low regression analysis results, however this study did show that Ln transformation of chl-a and PC data significantly improved estimations. This is implemented to address the non-normal distribution of chl-a and PC data values (Cillero Castro et al., 2020). Another interesting finding is that band algorithms using the green and blue bands performed much better than those relying on the red, NIR, or red-edge bands. In this study the SABI and BNDVI algorithms performed the best, especially when applied to Ln transformed data. SABI produced the best results for both chl-a and PC estimation. This makes sense, as this algorithm was designed for surface algal blooms, and for most of the sampling period the water body was highly eutrophic, with algal mats on the surface. Similar results, regarding band combinations were found by Tóth et al., 2021, where a simple blue/green band combination performed the best. Cillero Castro et al., 2020 found that band ratio algorithms correlated better with Ln transformed data as well. These results could indicate that UAV imagery data collected in highly eutrophic water bodies could be better analyzed using blue and green band ratios in combination with Ln data transformations. Furthermore, differing buffer

sizes did not significantly alter data acquired from UAV images in this study. On average, a larger buffer size improved regression result.

We acknowledge the following shortcomings in this experiment, as well as provide recommendations for future studies. The first is that data loss occurred during the removal of shadows and overhanging vegetation. This resulted in samples being dropped for further analysis. In addition, sun glint was not corrected during imagery post processing. This is because the areas where *in-situ* sampling took place did not exhibit high sun glint effects upon visual inspection. In addition, an objective of this study was to assess the accuracy of a simple methodology for UAV imagery acquisition that could be implemented by non-geospatial experts. Nevertheless, a sun glint correction technique could have improved UAV imagery data and is worth investigating in future research. Furthermore, *in-situ* fluorometer measurements were taken using an older technology, and more accurate sensors are now available. A newer sensor, less affected by biomass in the water could potentially improve the results. Also, samples were taken from the shore as boats are not permitted in the lake. *In-situ* samples scattered throughout the lake could have also produced better results. Future research should focus on implementing more sophisticated techniques, such as machine and deep learning, to aid in analysis. Also, there is a need to standardize UAV imagery processing so results from research can be compared directly.

6. Conclusion

The SABI algorithm performed well, indicating the UAVs could be a useful tool for water resource managers. The UAV system implemented in this study would require little training, as it is autonomous and conducts flights without the need for manual control. This can

increase the safety of UAV flights, as well as make the data acquired during flights more consistent. Our analysis indicates that the SABI algorithm performed best, confirming our original hypothesis. Buffer size did not really affect UAV imagery data as much as anticipated. Originally, we hypothesized that the 3 m buffer would provide the best results, as this would account for any error in the GPS unit. However, the results indicate that the largest buffer size, 3.5 m, provided the best results. Overall, this study indicates that could be a beneficial tool for water resource managers, but more work is needed on imagery processing techniques.

Bibliography

16S rRNA Gene Sequencing for Bacterial Identification in the Diagnostic Laboratory: Pluses, Perils, and Pitfalls. (n.d.). https://doi.org/10.1128/jcm.01228-07

Aguirre-Gómez, R., Salmerón-García, O., Gómez-Rodríguez, G., & Peralta-Higuera, A. (2017). Use of unmanned aerial vehicles and remote sensors in urban lakes studies in Mexico. *International Journal of Remote Sensing*, *38*(8–10), 2771–2779. https://doi.org/10.1080/01431161.2016.1264031

Ahari Hamed *, Nowruzi Bahareh, Anvar Ali Amir and Porzani Jafari Samaneh , The Toxicity Testing of Cyanobacterial Toxins *In vivo* and *In vitro* by Mouse Bioassay: A Review, Mini-Reviews in Medicinal Chemistry 2022; 22(8) . https://dx.doi.org/10.2174/1389557521666211101162030

Ai, Y., Lee, S., & Lee, J. (2020a). Drinking water treatment residuals from cyanobacteria bloom-affected areas: Investigation of potential impact on agricultural land application. *Science of The Total Environment*, *706*, 135756. https://doi.org/10.1016/j.scitotenv.2019.135756

Ai, Y., Lee, S., & Lee, J. (2020b). Drinking water treatment residuals from cyanobacteria bloom-affected areas: Investigation of potential impact on agricultural land application. *Science of The Total Environment*, *706*, 135756. https://doi.org/10.1016/j.scitotenv.2019.135756

Almuhtaram, H., Kibuye, F. A., Ajjampur, S., Glover, C. M., Hofmann, R., Gaget, V., Owen, C., Wert, E. C., & Zamyadi, A. (2021a). State of knowledge on early warning tools for cyanobacteria detection. *Ecological Indicators*, *133*, 108442. https://doi.org/10.1016/j.ecolind.2021.108442

Amin, N., Schwarzkopf, S., Tröscher-Mußotter, J., Camarinha-Silva, A., Dänicke, S., Huber, K., Frahm, J., & Seifert, J. (2023). Host metabolome and faecal microbiome shows potential interactions impacted by age and weaning times in calves. *Animal Microbiome*, *5*(1), 12. https://doi.org/10.1186/s42523-023-00233-z

Amorim, C. A., & Moura, A. D. N. (2021). Ecological impacts of freshwater algal blooms on water quality, plankton biodiversity, structure, and ecosystem functioning. *Science of The Total Environment*, *758*, 143605. https://doi.org/10.1016/j.scitotenv.2020.143605

Anderson, D. M., Hoagland, P., Kaoru, Y., & White, A. W. (2000). *Estimated annual economic impacts from harmful algal blooms (HABs) in the United States*. Woods Hole Oceanographic Institution. https://doi.org/10.1575/1912/96

Andersson, A., Höglander, H., Karlsson, C., & Huseby, S. (2015). Key role of phosphorus and nitrogen in regulating cyanobacterial community composition in the northern Baltic Sea. *Estuarine, Coastal and Shelf Science*, *164*, 161–171. https://doi.org/10.1016/j.ecss.2015.07.013

Arango, J. G., & Nairn, R. W. (2019). Prediction of Optical and Non-Optical Water Quality Parameters in Oligotrophic and Eutrophic Aquatic Systems Using a Small Unmanned Aerial System. *Drones*, *4*(1), 1. https://doi.org/10.3390/drones4010001

Awasthi, B., Karki, S., Regmi, P., Dhami, D. S., Thapa, S., & Panday, U. S. (2020). Analyzing the Effect of Distribution Pattern and Number of GCPs on Overall Accuracy of UAV Photogrammetric Results. In K. Jain, K. Khoshelham, X. Zhu, & A. Tiwari (Eds.), *Proceedings of UASG 2019* (pp. 339–354). Springer International Publishing. https://doi.org/10.1007/978-3-030-37393-1_29

Baek, J.-Y., Jo, Y.-H., Kim, W., Lee, J.-S., Jung, D., Kim, D.-W., & Nam, J. (2019). A New Algorithm to Estimate Chlorophyll-A Concentrations in Turbid Yellow Sea Water Using a Multispectral Sensor in a Low-Altitude Remote Sensing System. *Remote Sensing*, *11*(19), 2257. https://doi.org/10.3390/rs11192257

Ballesté, E., Blanch, A. R., Mendez, J., Sala-Comorera, L., Maunula, L., Monteiro, S., Farnleitner, A. H., Tiehm, A., Jofre, J., & García-Aljaro, C. (2021). Bacteriophages Are Good Estimators of Human Viruses Present in Water. *Frontiers in Microbiology*, *12*, 619495. https://doi.org/10.3389/fmicb.2021.619495

Banack, S. A., Caller, T. A., & Stommel, E. W. (2010). The Cyanobacteria Derived Toxin Beta-N-Methylamino-L-Alanine and Amyotrophic Lateral Sclerosis. *Toxins*, *2*(12), 2837–2850. https://doi.org/10.3390/toxins2122837

Barton, S., Jenkins, J., Buckling, A., Schaum, C.-E., Smirnoff, N., Raven, J. A., & Yvon-Durocher, G. (2020). Evolutionary temperature compensation of carbon fixation in marine phytoplankton. *Ecology Letters*, *23*(4), 722–733. https://doi.org/10.1111/ele.13469

Barwant, M. (2022). *Environment Conservation, Challenges Threats in Conservation of Biodiversity volume -I*.

Batista, T., De Sousa, G., Suput, J. S., Rahmani, R., & Šuput, D. (2003). Microcystin-LR causes the collapse of actin filaments in primary human hepatocytes. *Aquatic Toxicology*, *65*(1), 85–91. https://doi.org/10.1016/S0166-445X(03)00108-5

Becker, R. H., Sayers, M., Dehm, D., Shuchman, R., Quintero, K., Bosse, K., & Sawtell, R. (2019). Unmanned aerial system based spectroradiometer for monitoring harmful algal blooms: A new paradigm in water quality monitoring. *Journal of Great Lakes Research*, *45*(3), 444–453. https://doi.org/10.1016/j.jglr.2019.03.006

Beiko, R. G., Hsiao, W., & Parkinson, J. (Eds.). (2018a). *Microbiome Analysis: Methods and Protocols* (Vol. 1849). Springer New York. https://doi.org/10.1007/978-1-4939-8728-3

Beiko, R. G., Hsiao, W., & Parkinson, J. (Eds.). (2018b). *Microbiome Analysis: Methods and Protocols* (Vol. 1849). Springer New York. https://doi.org/10.1007/978-1-4939-8728-3

Bernard, É., Friedt, J. M., Tolle, F., Griselin, M., Marlin, Ch., & Prokop, A. (2017). Investigating snowpack volumes and icing dynamics in the moraine of an Arctic catchment using UAV photogrammetry. *The Photogrammetric Record*, *32*(160), 497–512. https://doi.org/10.1111/phor.12217

Best practices: Collecting Data with MicaSense Sensors. (2023, May 25). MicaSense Knowledge Base. https://support.micasense.com/hc/en-us/articles/224893167-Best-practices-Collecting-Data-with-MicaSense-Sensors

Bilyeu, L., Bloomfield, B., Hanlon, R., González-Rocha, J., Jacquemin, S. J., Ault, A. P., Birbeck, J. A., Westrick, J. A., Foroutan, H., Ross, S. D., Powers, C. W., & Schmale, D. G. (2022). Drone-based particle monitoring above two harmful algal blooms (HABs) in the USA. *Environmental Science: Atmospheres*, *2*(6), 1351–1363. https://doi.org/10.1039/D2EA00055E

Blondel, V. D., Guillaume, J.-L., Lambiotte, R., & Lefebvre, E. (2008). Fast unfolding of communities in large networks. *Journal of Statistical Mechanics: Theory and Experiment*, *2008*(10), P10008. https://doi.org/10.1088/1742-5468/2008/10/P10008

Bodilis, J., Nsigue-Meilo, S., Besaury, L., & Quillet, L. (2012). Variable Copy Number, Intra-Genomic Heterogeneities and Lateral Transfers of the 16S rRNA Gene in Pseudomonas. *PLoS ONE*, *7*(4), e35647. https://doi.org/10.1371/journal.pone.0035647

Bolyen, E., Rideout, J. R., Dillon, M. R., Bokulich, N. A., Abnet, C. C., Al-Ghalith, G. A., Alexander, H., Alm, E. J., Arumugam, M., Asnicar, F., Bai, Y., Bisanz, J. E., Bittinger, K., Brejnrod, A., Brislawn, C. J., Brown, C. T., Callahan, B. J., Caraballo-Rodríguez, A. M., Chase, J., … Caporaso, J. G. (2019). Reproducible, interactive, scalable and extensible microbiome data science using QIIME 2. *Nature Biotechnology*, *37*(8), 852–857. https://doi.org/10.1038/s41587-019-0209-9

Bone, T. (n.d.). *Recommendations for Cyanobacteria and Cyanotoxin Monitoring in Recreational Waters*.

Boon, M. A., Drijfhout, A. P., & Tesfamichael, S. (2017). COMPARISON OF A FIXED-WING AND MULTI-ROTOR UAV FOR ENVIRONMENTAL MAPPING APPLICATIONS: A CASE STUDY. *The International Archives of the Photogrammetry, Remote Sensing and Spatial Information Sciences*, *XLII-2-W6*, 47–54. https://doi.org/10.5194/isprs-archives-XLII-2-W6-47-2017

Boucher, J., Weathers, K. C., Norouzi, H., & Steele, B. (2018). Assessing the effectiveness of Landsat 8 chlorophyll a retrieval algorithms for regional freshwater monitoring. *Ecological Applications*, *28*(4), 1044–1054. https://doi.org/10.1002/eap.1708

Brivio, P. A., Giardino, C., & Zilioli, E. (2001). Determination of chlorophyll concentration changes in Lake Garda using an image-based radiative transfer code for Landsat TM images. *International Journal of Remote Sensing*, *22*(2–3), 487–502. https://doi.org/10.1080/014311601450059

Brown, K. P., Gerber, A., Bedulina, D., & Timofeyev, M. A. (2021). Human impact and ecosystemic health at Lake Baikal. *WIREs Water*, *8*(4), e1528. https://doi.org/10.1002/wat2.1528

Callahan, B. J., McMurdie, P. J., Rosen, M. J., Han, A. W., Johnson, A. J. A., & Holmes, S. P. (2016). DADA2: High-resolution sample inference from Illumina amplicon data. *Nature Methods*, *13*(7), 581–583. https://doi.org/10.1038/nmeth.3869

Camera Parameters for Mission Planning apps (DJI Pilot, GS Pro, etc.). (2023, May 10). MicaSense Knowledge Base. https://support.micasense.com/hc/en-us/articles/4420561840023-Camera-Parameters-for-Mission-Planning-apps-DJI-Pilot-GS-Pro-etc-

Cani, P. D., Amar, J., Iglesias, M. A., Poggi, M., Knauf, C., Bastelica, D., Neyrinck, A. M., Fava, F., Tuohy, K. M., Chabo, C., Waget, A., Delmée, E., Cousin, B., Sulpice, T., Chamontin, B., Ferrières, J., Tanti, J.-F., Gibson, G. R., Casteilla, L., … Burcelin, R. (2007). Metabolic Endotoxemia Initiates Obesity and Insulin Resistance. *Diabetes*, *56*(7), 1761–1772. https://doi.org/10.2337/db06-1491

Carmichael, W. W., & An, J. (1999). Using an enzyme linked immunosorbent assay (ELISA) and a protein phosphatase inhibition assay (PPIA) for the detection of microcystins and nodularins. *Natural Toxins*, *7*(6), 377–385. https://doi.org/10.1002/1522-7189(199911/12)7:6<377::AID-NT80>3.0.CO;2-8

Casero, M. C., Velázquez, D., Medina-Cobo, M., Quesada, A., & Cirés, S. (2019). Unmasking the identity of toxigenic cyanobacteria driving a multi-toxin bloom by high-throughput sequencing of cyanotoxins genes and 16S rRNA metabarcoding. *Science of The Total Environment*, *665*, 367–378. https://doi.org/10.1016/j.scitotenv.2019.02.083

Chaffin, J. D., Davis, T. W., Smith, D. J., Baer, M. M., & Dick, G. J. (2018). Interactions between nitrogen form, loading rate, and light intensity on Microcystis and Planktothrix growth and microcystin production. *Harmful Algae*, *73*, 84–97. https://doi.org/10.1016/j.hal.2018.02.001

Che, S., Du, G., Wang, N., He, K., Mo, Z., Sun, B., Chen, Y., Cao, Y., Wang, J., & Mao, Y. (2021). Biomass estimation of cultivated red algae Pyropia using unmanned aerial platform based multispectral imaging. *Plant Methods*, *17*(1), 12. https://doi.org/10.1186/s13007-021-00711-y

Chen, J., Liu, H., Bai, Y., Qi, J., Qi, W., Liu, H., Peng, J., & Qu, J. (2022). Mixing regime shapes the community assembly process, microbial interaction and proliferation of cyanobacterial species Planktothrix in a stratified lake. *Journal of Environmental Sciences*, *115*, 103–113. https://doi.org/10.1016/j.jes.2021.07.001

Chen, J., & Xie, P. (2005a). Seasonal dynamics of the hepatotoxic microcystins in various organs of four freshwater bivalves from the large eutrophic lake Taihu of subtropical China and the risk to human consumption. *Environmental Toxicology*, *20*(6), 572–584. https://doi.org/10.1002/tox.20146

Chen, J., & Xie, P. (2005b). Tissue distributions and seasonal dynamics of the hepatotoxic microcystins-LR and -RR in two freshwater shrimps, Palaemon modestus and Macrobrachium nipponensis, from a large shallow, eutrophic lake of the subtropical China. *Toxicon*, *45*(5), 615–625. https://doi.org/10.1016/j.toxicon.2005.01.003

Chen, L., Chen, J., Zhang, X., & Xie, P. (2016). A review of reproductive toxicity of microcystins. *Journal of Hazardous Materials*, *301*, 381–399. https://doi.org/10.1016/j.jhazmat.2015.08.041

Cheng, K. H., Chan, S. N., & Lee, J. H. W. (2020). Remote sensing of coastal algal blooms using unmanned aerial vehicles (UAVs). *Marine Pollution Bulletin*, *152*, 110889. https://doi.org/10.1016/j.marpolbul.2020.110889

Cheung, M. Y., Liang, S., & Lee, J. (2013). Toxin-producing cyanobacteria in freshwater: A review of the problems, impact on drinking water safety, and efforts for protecting public health. *Journal of Microbiology*, *51*(1), 1–10. https://doi.org/10.1007/s12275-013-2549-3

Choo, Y., Kang, G., Kim, D., & Lee, S. (2018). A study on the evaluation of water-bloom using image processing. *Environmental Science and Pollution Research*, *25*(36), 36775–36780. https://doi.org/10.1007/s11356-018-3578-6

Chorus, I. (n.d.). *Toxic Cyanobacteria in Water; A Guide to Their Public Health Consequences, Monitoring and Management; Second Edition*.

Christensen, V. G., & Khan, E. (2020). Freshwater neurotoxins and concerns for human, animal, and ecosystem health: A review of anatoxin-a and saxitoxin. *Science of The Total Environment*, *736*, 139515. https://doi.org/10.1016/j.scitotenv.2020.139515

Cillero Castro, C., Domínguez Gómez, J. A., Delgado Martín, J., Hinojo Sánchez, B. A., Cereijo Arango, J. L., Cheda Tuya, F. A., & Díaz-Varela, R. (2020). An UAV and Satellite Multispectral Data Approach to Monitor Water Quality in Small Reservoirs. *Remote Sensing*, *12*(9), 1514. https://doi.org/10.3390/rs12091514

Climate Data Online (CDO)—The National Climatic Data Center's (NCDC) Climate Data Online (CDO) provides free access to NCDC's archive of historical weather and climate data in

addition to station history information. | National Climatic Data Center (NCDC). (n.d.). Retrieved June 28, 2023, from https://www.ncei.noaa.gov/cdo-web/

Coombes, M., Fletcher, T., Chen, W.-H., & Liu, C. (2020). Decomposition-based mission planning for fixed-wing UAVs surveying in wind. *Journal of Field Robotics*, *37*(3), 440–465. https://doi.org/10.1002/rob.21928

Corbel, S., Mougin, C., & Bouaïcha, N. (2014). Cyanobacterial toxins: Modes of actions, fate in aquatic and soil ecosystems, phytotoxicity and bioaccumulation in agricultural crops. *Chemosphere*, *96*, 1–15. https://doi.org/10.1016/j.chemosphere.2013.07.056

Cracknell, A. P. (2017). UAVs: Regulations and law enforcement. *International Journal of Remote Sensing*, *38*(8–10), 3054–3067. https://doi.org/10.1080/01431161.2017.1302115

Díez, B., & Ininbergs, K. (2014). Ecological importance of cyanobacteria. In *Cyanobacteria* (pp. 41–63). John Wiley & Sons, Ltd. https://doi.org/10.1002/9781118402238.ch3

Ding, X., Gong, F., Li, J., Zhao, M., Li, H., Bai, R., & Wang, X. (2023). High-frequency monitoring of Secchi-disk depth in Taihu Lake using Himawari-8/AHI data. *Optics Express*, *31*(10), 15966. https://doi.org/10.1364/OE.484390

DJI - Official Website. (n.d.). DJI Official. Retrieved June 24, 2023, from https://www.dji.com

Dodds, W. K. (n.d.). *Freshwater ecology: Concepts and environmental applications of limnology*.

Dolman, A. M., Rücker, J., Pick, F. R., Fastner, J., Rohrlack, T., Mischke, U., & Wiedner, C. (2012). Cyanobacteria and Cyanotoxins: The Influence of Nitrogen versus Phosphorus. *PLoS ONE*, *7*(6), e38757. https://doi.org/10.1371/journal.pone.0038757

Douglas Greene, S. B., LeFevre, G. H., & Markfort, C. D. (2021). Improving the spatial and temporal monitoring of cyanotoxins in Iowa lakes using a multiscale and multi-modal monitoring approach. *Science of The Total Environment*, *760*, 143327. https://doi.org/10.1016/j.scitotenv.2020.143327

Downwelling Light Sensor (DLS) Basics. (2022, January 25). MicaSense Knowledge Base. https://support.micasense.com/hc/en-us/articles/115002782008-Downwelling-Light-Sensor-DLS-Basics

Drobac, D., Tokodi, N., Simeunović, J., Baltić, V., Stanić, D., & Svirčev, Z. (2013). Human Exposure to Cyanotoxins and their Effects on Health. *Archives of Industrial Hygiene and Toxicology*, *64*(2), 305–316. https://doi.org/10.2478/10004-1254-64-2013-2320

Duffy, J. P., Cunliffe, A. M., DeBell, L., Sandbrook, C., Wich, S. A., Shutler, J. D., Myers-Smith, I. H., Varela, M. R., & Anderson, K. (2018). Location, location, location: Considerations when using lightweight drones in challenging environments. *Remote Sensing in Ecology and Conservation*, *4*(1), 7–19. https://doi.org/10.1002/rse2.58

Ebadi, L., & Shafri, H. Z. M. (2015). A stable and accurate wavelet-based method for noise reduction from hyperspectral vegetation spectrum. *Earth Science Informatics*, *8*(2), 411–425. https://doi.org/10.1007/s12145-014-0168-0

El-Alem, A., Chokmani, K., Venkatesan, A., Rachid, L., Agili, H., & Dedieu, J.-P. (2021). How Accurate Is an Unmanned Aerial Vehicle Data-Based Model Applied on Satellite Imagery for Chlorophyll-a Estimation in Freshwater Bodies? *Remote Sensing*, *13*(6), 1134. https://doi.org/10.3390/rs13061134

Elhadary, A., Rabah, M., Ghanim, E., Mohie, R., & Taha, A. (2022). The influence of flight height and overlap on UAV imagery over featureless surfaces and constructing formulas predicting the

geometrical accuracy. *NRIAG Journal of Astronomy and Geophysics*, *11*(1), 210–223. https://doi.org/10.1080/20909977.2022.2057148
Eltner, A., Kaiser, A., Castillo, C., Rock, G., Neugirg, F., & Abellán, A. (2016). Image-based surface reconstruction in geomorphometry – merits, limits and developments. *Earth Surface Dynamics*, *4*(2), 359–389. https://doi.org/10.5194/esurf-4-359-2016
Escobar-Zepeda, A., Vera-Ponce de León, A., & Sanchez-Flores, A. (2015). The Road to Metagenomics: From Microbiology to DNA Sequencing Technologies and Bioinformatics. *Frontiers in Genetics*, *6*, 348. https://doi.org/10.3389/fgene.2015.00348
Eskandari, R., Mahdianpari, M., Mohammadimanesh, F., Salehi, B., Brisco, B., & Homayouni, S. (2020). Meta-analysis of Unmanned Aerial Vehicle (UAV) Imagery for Agro-environmental Monitoring Using Machine Learning and Statistical Models. *Remote Sensing*, *12*(21), 3511. https://doi.org/10.3390/rs12213511
Falconer, I. R., & Humpage, A. R. (2001). Preliminary evidence for in vivo tumour initiation by oral administration of extracts of the blue-green algaCylindrospermopsis raciborskii containing the toxin cylindrospermopsin. *Environmental Toxicology*, *16*(2), 192–195. https://doi.org/10.1002/tox.1024
Fayad, P. B., Roy-Lachapelle, A., Duy, S. V., Prévost, M., & Sauvé, S. (2015). On-line solid-phase extraction coupled to liquid chromatography tandem mass spectrometry for the analysis of cyanotoxins in algal blooms. *Toxicon*, *108*, 167–175. https://doi.org/10.1016/j.toxicon.2015.10.010
Ferrão-Filho, A. D. S., & Kozlowsky-Suzuki, B. (2011). Cyanotoxins: Bioaccumulation and Effects on Aquatic Animals. *Marine Drugs*, *9*(12), 2729–2772. https://doi.org/10.3390/md9122729
Ferrão-Filho, A. D. S., Kozlowsky-Suzuki, B., & Azevedo, S. M. F. O. (2002). Accumulation of microcystins by a tropical zooplankton community. *Aquatic Toxicology*, *59*(3–4), 201–208. https://doi.org/10.1016/S0166-445X(01)00253-3
Fontanillo, M., & Köhn, M. (2018). Microcystins: Synthesis and structure–activity relationship studies toward PP1 and PP2A. *Bioorganic & Medicinal Chemistry*, *26*(6), 1118–1126. https://doi.org/10.1016/j.bmc.2017.08.040
Gad, M., Hou, L., Cao, M., Adyari, B., Zhang, L., Qin, D., Yu, C.-P., Sun, Q., & Hu, A. (2022). Tracking microeukaryotic footprint in a peri-urban watershed, China through machine-learning approaches. *Science of The Total Environment*, *806*, 150401. https://doi.org/10.1016/j.scitotenv.2021.150401
Gaffey, C., & Bhardwaj, A. (2020). Applications of Unmanned Aerial Vehicles in Cryosphere: Latest Advances and Prospects. *Remote Sensing*, *12*(6), 948. https://doi.org/10.3390/rs12060948
Gaget, V., Lau, M., Sendall, B., Froscio, S., & Humpage, A. R. (2017). Cyanotoxins: Which detection technique for an optimum risk assessment? *Water Research*, *118*, 227–238. https://doi.org/10.1016/j.watres.2017.04.025
Garmin, & subsidiaries, G. L. or its. (n.d.). *Garmin GPSMAP® 66s | Handheld GPS | Outdoor*. Garmin. Retrieved June 28, 2023, from https://www.garmin.com/en-US/p/598455
Ghoul, M., & Mitri, S. (2016). The Ecology and Evolution of Microbial Competition. *Trends in Microbiology*, *24*(10), 833–845. https://doi.org/10.1016/j.tim.2016.06.011
Gibbs, M. M., Roygard, J., Patterson, M., Brown, L., & Brown, D. (2022). Factors influencing cyanobacteria blooms: Review of the historical monitoring data to assess management options

for Lake Horowhenua. *New Zealand Journal of Marine and Freshwater Research*, 1–27. https://doi.org/10.1080/00288330.2022.2107028
Gierhart, D. L. (n.d.). *NUTRIENTS, FOR PROTECTING EYE HEALTH AND TREATING EYE DSORDERS*.
Gitelson, A. (1992). The peak near 700 nm on radiance spectra of algae and water: Relationships of its magnitude and position with chlorophyll concentration. *International Journal of Remote Sensing*, *13*(17), 3367–3373. https://doi.org/10.1080/01431169208904125
Gitelson, A. A., Schalles, J. F., & Hladik, C. M. (2007). Remote chlorophyll-a retrieval in turbid, productive estuaries: Chesapeake Bay case study. *Remote Sensing of Environment*, *109*(4), 464–472. https://doi.org/10.1016/j.rse.2007.01.016
Gons, H. J. (2002). A chlorophyll-retrieval algorithm for satellite imagery (Medium Resolution Imaging Spectrometer) of inland and coastal waters. *Journal of Plankton Research*, *24*(9), 947–951. https://doi.org/10.1093/plankt/24.9.947
Grey, J., Jones, R. I., & Sleep, D. (2000). Stable isotope analysis of the origins of zooplankton carbon in lakes of differing trophic state. *Oecologia*, *123*(2), 232–240. https://doi.org/10.1007/s004420051010
Grogan, A. E., Alves-de-Souza, C., Cahoon, L. B., & Mallin, M. A. (2023). Harmful Algal Blooms: A Prolific Issue in Urban Stormwater Ponds. *Water*, *15*(13), 2436. https://doi.org/10.3390/w15132436
Gupana, R. S., Odermatt, D., Cesana, I., Giardino, C., Nedbal, L., & Damm, A. (2021). Remote sensing of sun-induced chlorophyll-a fluorescence in inland and coastal waters: Current state and future prospects. *Remote Sensing of Environment*, *262*, 112482. https://doi.org/10.1016/j.rse.2021.112482
Hachicha, R., Elleuch, F., Ben Hlima, H., Dubessay, P., De Baynast, H., Delattre, C., Pierre, G., Hachicha, R., Abdelkafi, S., Michaud, P., & Fendri, I. (2022). Biomolecules from Microalgae and Cyanobacteria: Applications and Market Survey. *Applied Sciences*, *12*(4), 1924. https://doi.org/10.3390/app12041924
Hamilton, D. P., Wood, S. A., Dietrich, D. R., & Puddick, J. (2013). Costs of harmful blooms of freshwater cyanobacteria. In N. K. Sharma, A. K. Rai, & L. J. Stal (Eds.), *Cyanobacteria* (pp. 245–256). John Wiley & Sons, Ltd. https://doi.org/10.1002/9781118402238.ch15
Hanlon, R., Jacquemin, S. J., Birbeck, J. A., Westrick, J. A., Harb, C., Gruszewski, H., Ault, A. P., Scott, D., Foroutan, H., Ross, S. D., González-Rocha, J., Powers, C., Pratt, L., Looney, H., Baker, G., & Schmale, D. G. (2022). Drone-based water sampling and characterization of three freshwater harmful algal blooms in the United States. *Frontiers in Remote Sensing*, *3*, 949052. https://doi.org/10.3389/frsen.2022.949052
Harada K-i, Kondo F, Lawton L. Laboratory analysis of cyanotoxins. In: Chorus I, Bartram J, editors. Toxic cyanobacteria in water: a guide to their public health consequences, monitoring and management. London, UK: E & FN Spon; 1999. p. 369–405.
Harder, P., Schirmer, M., Pomeroy, J., & Helgason, W. (2016). Accuracy of snow depth estimation in mountain and prairie environments by an unmanned aerial vehicle. *The Cryosphere*, *10*(6), 2559–2571. https://doi.org/10.5194/tc-10-2559-2016
Hart, J. J., Jamison, M. N., McNair, J. N., Woznicki, S. A., Jordan, B., & Rediske, R. R. (2023). Using watershed characteristics to enhance fecal source identification. *Journal of Environmental Management*, *336*, 117642. https://doi.org/10.1016/j.jenvman.2023.117642

Herrero, A., Muro-Pastor, A. M., & Flores, E. (2001). Nitrogen Control in Cyanobacteria. *Journal of Bacteriology*, *183*(2), 411–425. https://doi.org/10.1128/JB.183.2.411-425.2001
Ho, J. C., & Michalak, A. M. (2015). Challenges in tracking harmful algal blooms: A synthesis of evidence from Lake Erie. *Journal of Great Lakes Research*, *41*(2), 317–325. https://doi.org/10.1016/j.jglr.2015.01.001
Holík, L., Hlisnikovský, L., Honzík, R., Trögl, J., Burdová, H., & Popelka, J. (2019). Soil Microbial Communities and Enzyme Activities after Long-Term Application of Inorganic and Organic Fertilizers at Different Depths of the Soil Profile. *Sustainability*, *11*(12), 3251. https://doi.org/10.3390/su11123251
Hong, S. M., Baek, S.-S., Yun, D., Kwon, Y.-H., Duan, H., Pyo, J., & Cho, K. H. (2021). Monitoring the vertical distribution of HABs using hyperspectral imagery and deep learning models. *Science of The Total Environment*, *794*, 148592. https://doi.org/10.1016/j.scitotenv.2021.148592
Hosokawa, S., Momota, K., Chariton, A. A., Naito, R., & Nakamura, Y. (2021). The use of diversity indices for local assessment of marine sediment quality. *Scientific Reports*, *11*(1), 14991. https://doi.org/10.1038/s41598-021-94636-0
Hudnell, H. K. (2010). The state of U.S. freshwater harmful algal blooms assessments, policy and legislation. *Toxicon*, *55*(5), 1024–1034. https://doi.org/10.1016/j.toxicon.2009.07.021
Ibekwe, M. A., Murinda, S. E., Park, S., Obayiuwana, A., Murry, M. A., Schwartz, G., & Lundquist, T. (2020). Comparative Use of Quantitative PCR (qPCR), Droplet Digital PCR (ddPCR), and Recombinase Polymerase Amplification (RPA) in the Detection of Shiga Toxin-Producing E. coli (STEC) in Environmental Samples. *Water*, *12*(12), 3507. https://doi.org/10.3390/w12123507
Ibelings, B. W., Bruning, K., De Jonge, J., Wolfstein, K., Pires, L. M. D., Postma, J., & Burger, T. (2005). Distribution of Microcystins in a Lake Foodweb: No Evidence for Biomagnification. *Microbial Ecology*, *49*(4), 487–500. https://doi.org/10.1007/s00248-004-0014-x
Ibelings, B.W., Mur, L.R., Walsby, A.E., 1991. Diurnal changes in buoyancy and vertical distribution in populations of Microcystis in two shallow lakes. Journal of Plankton Research 13, 419e436.
Isacsson, M. (n.d.). *Snow layer mapping by remote sensing from Unmanned Aerial Vehicles*.
J. William Schopf Bonnie M. Packer ,Early Archean (3.3-Billion to 3.5-Billion-Year-Old) Microfossils from Warrawoona Group, Australia.Science237,70-73(1987).DOI:10.1126/science.11539686
Kahru, M., Leppanen, J.-M., & Rud, O. (1993). Cyanobacterial blooms cause heating of the sea surface. *Marine Ecology Progress Series*, *101*, 1–7. https://doi.org/10.3354/meps101001
Kaushik, R., & Balasubramanian, R. (2013). Methods and Approaches Used for Detection of Cyanotoxins in Environmental Samples: A Review. *Critical Reviews in Environmental Science and Technology*, *43*(13), 1349–1383. https://doi.org/10.1080/10643389.2011.644224
Kay, S., Hedley, J., & Lavender, S. (2009a). Sun Glint Correction of High and Low Spatial Resolution Images of Aquatic Scenes: A Review of Methods for Visible and Near-Infrared Wavelengths. *Remote Sensing*, *1*(4), 697–730. https://doi.org/10.3390/rs1040697
Kay, S., Hedley, J., & Lavender, S. (2009b). Sun Glint Correction of High and Low Spatial Resolution Images of Aquatic Scenes: A Review of Methods for Visible and Near-Infrared Wavelengths. *Remote Sensing*, *1*(4), 697–730. https://doi.org/10.3390/rs1040697
Kelly, L. T., Bouma-Gregson, K., Puddick, J., Fadness, R., Ryan, K. G., Davis, T. W., & Wood, S. A. (2019). Multiple cyanotoxin congeners produced by sub-dominant cyanobacterial taxa in riverine

cyanobacterial and algal mats. *PLOS ONE*, *14*(12), e0220422. https://doi.org/10.1371/journal.pone.0220422
Kim, T. W., Yun, H. S., Kim, K. B., & Hong, S. B. (2019). Development of Real-time HABs Detection Technique Using Unmanned Aerial Vehicle (UAV). *Journal of Coastal Research*, *91*(sp1), 391. https://doi.org/10.2112/SI91-079.1
Kim, Y.-J., Park, H.-K., & Kim, I.-S. (2022). Assessment of the Appearance and Toxin Production Potential of Invasive Nostocalean Cyanobacteria Using Quantitative Gene Analysis in Nakdong River, Korea. *Toxins*, *14*(5), Article 5. https://doi.org/10.3390/toxins14050294
Kimura, F., Morinaga, A., Fukushima, M., Ishiguro, T., Sato, Y., Sakaguchi, A., Kawashita, T., Yamamoto, I., & Kobayashi, T. (2019). Early Detection System of Harmful Algal Bloom Using Drones and Water Sample Image Recognition. *Sensors and Materials*, *31*(12), 4155. https://doi.org/10.18494/SAM.2019.2417
Kislik, C., Dronova, I., & Kelly, M. (2018). UAVs in Support of Algal Bloom Research: A Review of Current Applications and Future Opportunities. *Drones*, *2*(4), Article 4. https://doi.org/10.3390/drones2040035
Konopka, A. (2009). What is microbial community ecology? *The ISME Journal*, *3*(11), 1223–1230. https://doi.org/10.1038/ismej.2009.88
Koreivienė, J., & Belous, O. (2012). Methods for Cyanotoxins detection. *Botanica Lithuanica*, *18*(1), 58–65. https://doi.org/10.2478/v10279-012-0008-4
Kozlowsky-Suzuki, B., Wilson, A. E., & Ferrão-Filho, A. D. S. (2012). Biomagnification or biodilution of microcystins in aquatic foodwebs? Meta-analyses of laboratory and field studies. *Harmful Algae*, *18*, 47–55. https://doi.org/10.1016/j.hal.2012.04.002
Kuiper-Goodman T, Falconer I, Fitzgerald J. Human health aspects. In: Chorus I, Bartram J, editors. Toxic cyanobacteria in water: a guide to their public health consequences, monitoring and management. London, UK: E & FN Spon; 1999. p. 113–53.
Kulabhusan, P. K., & Campbell, K. (2021). Recent trends in the detection of freshwater cyanotoxins with a critical note on their occurrence in Asia. *Trends in Environmental Analytical Chemistry*, *32*, e00150. https://doi.org/10.1016/j.teac.2021.e00150
Kurtz, Z. D., Müller, C. L., Miraldi, E. R., Littman, D. R., Blaser, M. J., & Bonneau, R. A. (2015). Sparse and Compositionally Robust Inference of Microbial Ecological Networks. *PLOS Computational Biology*, *11*(5), e1004226. https://doi.org/10.1371/journal.pcbi.1004226
Kwon, Y. S., Pyo, J., Kwon, Y.-H., Duan, H., Cho, K. H., & Park, Y. (2020). Drone-based hyperspectral remote sensing of cyanobacteria using vertical cumulative pigment concentration in a deep reservoir. *Remote Sensing of Environment*, *236*, 111517. https://doi.org/10.1016/j.rse.2019.111517
Law Enforcement. (n.d.). DJI. Retrieved June 24, 2023, from https://enterprise.dji.com/public-safety/photo
Lee, C. S., Kim, M., Lee, C., Yu, Z., & Lee, J. (2016). The Microbiota of Recreational Freshwaters and the Implications for Environmental and Public Health. *Frontiers in Microbiology*, *7*, 1826. https://doi.org/10.3389/fmicb.2016.01826
Lee, J., Lee, S., & Jiang, X. (2017). Cyanobacterial Toxins in Freshwater and Food: Important Sources of Exposure to Humans. *Annual Review of Food Science and Technology*, *8*(1), 281–304. https://doi.org/10.1146/annurev-food-030216-030116

Lee, S., Kim, J., & Lee, J. (2021). Colonization of toxic cyanobacteria on the surface and inside of leafy green: A hidden source of cyanotoxin production and exposure. *Food Microbiology*, *94*, 103655. https://doi.org/10.1016/j.fm.2020.103655

Lehman, P. W., Teh, S. J., Boyer, G. L., Nobriga, M. L., Bass, E., & Hogle, C. (2010). Initial impacts of Microcystis aeruginosa blooms on the aquatic food web in the San Francisco Estuary. *Hydrobiologia*, *637*(1), 229–248. https://doi.org/10.1007/s10750-009-9999-y

Letelier, R. (1996). An analysis of chlorophyll fluorescence algorithms for the moderate resolution imaging spectrometer (MODIS). *Remote Sensing of Environment*, *58*(2), 215–223. https://doi.org/10.1016/S0034-4257(96)00073-9

Li, X., Xu, L., Zhou, W., Zhao, Q., & Wang, Y. (2016). Chronic exposure to microcystin-LR affected mitochondrial DNA maintenance and caused pathological changes of lung tissue in mice. *Environmental Pollution*, *210*, 48–56. https://doi.org/10.1016/j.envpol.2015.12.001

Lopez, C.B., Jewett, E.B., Dortch, Q., Walton, B.T., and Hudnell, H.K. 2008. Scientific Assessment of Freshwater Harmful Algal Blooms. Interagency Working Group on Harmful Algal Blooms, Hypoxia, and Human Health of the Joint Subcommittee on Ocean Science and Technology. Washington, D.C., USA.

Luo, A., Chen, H., Gao, X., Carvalho, L., Xue, Y., Jin, L., & Yang, J. (2022a). Short-term rainfall limits cyanobacterial bloom formation in a shallow eutrophic subtropical urban reservoir in warm season. *Science of The Total Environment*, *827*, 154172. https://doi.org/10.1016/j.scitotenv.2022.154172

Luo, L., Zhao, W., Wang, L., Ogashawara, I., Yang, Q., Zhou, H., Yang, R., Duan, Q., Zhou, C., & Zhuang, Y. (2021). Are the shoreline and eutrophication of desert lakes related to desert development? *Environmental Monitoring and Assessment*, *193*(1), 43. https://doi.org/10.1007/s10661-020-08806-0

Lyons, T. W., Reinhard, C. T., & Planavsky, N. J. (2014). The rise of oxygen in Earth's early ocean and atmosphere. *Nature*, *506*(7488), 307–315. https://doi.org/10.1038/nature13068

Lyu, P., Malang, Y., Liu, H. H. T., Lai, J., Liu, J., Jiang, B., Qu, M., Anderson, S., Lefebvre, D. D., & Wang, Y. (2017). Autonomous cyanobacterial harmful algal blooms monitoring using multirotor UAS. *International Journal of Remote Sensing*, *38*(8–10), 2818–2843. https://doi.org/10.1080/01431161.2016.1275058

Marmen, S., Fadeev, E., Al Ashhab, A., Benet-Perelberg, A., Naor, A., Patil, H. J., Cytryn, E., Viner-Mozzini, Y., Sukenik, A., Lalzar, M., & Sher, D. (2021). Seasonal Dynamics Are the Major Driver of Microbial Diversity and Composition in Intensive Freshwater Aquaculture. *Frontiers in Microbiology*, *12*, 679743. https://doi.org/10.3389/fmicb.2021.679743

Matrice 200 Series—Download Center—DJI. (n.d.). DJI Official. Retrieved July 5, 2023, from https://www.dji.com/downloads/products/matrice-200-series

Mazur-Marzec, H., Meriluoto, J., Pliński, M., & Szafranek, J. (2006). Characterization of nodularin variants in Nodularia spumigena from the Baltic Sea using liquid chromatography/mass spectrometry/mass spectrometry. *Rapid Communications in Mass Spectrometry*, *20*(13), 2023–2032. https://doi.org/10.1002/rcm.2558

McCarthy, M. J., Gardner, W. S., Lehmann, M. F., Guindon, A., & Bird, D. F. (2016). Benthic nitrogen regeneration, fixation, and denitrification in a temperate, eutrophic lake: Effects on the nitrogen budget and cyanobacteria blooms. *Limnology and Oceanography*, *61*(4), 1406–1423. https://doi.org/10.1002/lno.10306

McEliece, R., Hinz, S., Guarini, J.-M., & Coston-Guarini, J. (2020). Evaluation of Nearshore and Offshore Water Quality Assessment Using UAV Multispectral Imagery. *Remote Sensing*, *12*(14), 2258. https://doi.org/10.3390/rs12142258

Mehinto, A. C., Smith, J., Wenger, E., Stanton, B., Linville, R., Brooks, B. W., Sutula, M. A., & Howard, M. D. A. (2021). Synthesis of ecotoxicological studies on cyanotoxins in freshwater habitats – Evaluating the basis for developing thresholds protective of aquatic life in the United States. *Science of The Total Environment*, *795*, 148864. https://doi.org/10.1016/j.scitotenv.2021.148864

Meinshausen, N., & Bühlmann, P. (2006). High-dimensional graphs and variable selection with the Lasso. *The Annals of Statistics*, *34*(3). https://doi.org/10.1214/009053606000000281

Merel, S., Walker, D., Chicana, R., Snyder, S., Baurès, E., & Thomas, O. (2013). State of knowledge and concerns on cyanobacterial blooms and cyanotoxins. *Environment International*, *59*, 303–327. https://doi.org/10.1016/j.envint.2013.06.013

Meyer, A., Todt, C., Mikkelsen, N. T., & Lieb, B. (2010). Fast evolving 18S rRNA sequences from Solenogastres (Mollusca) resist standard PCR amplification and give new insights into mollusk substitution rate heterogeneity. *BMC Evolutionary Biology*, *10*(1), 70. https://doi.org/10.1186/1471-2148-10-70

Miglione, A., Napoletano, M., & Cinti, S. (2021). Electrochemical Biosensors for Tracing Cyanotoxins in Food and Environmental Matrices. *Biosensors*, *11*(9), 315. https://doi.org/10.3390/bios11090315

Millar, E. N., Surette, M. G., & Kidd, K. A. (2022). Altered microbiomes of aquatic macroinvertebrates and riparian spiders downstream of municipal wastewater effluents. *Science of The Total Environment*, *809*, 151156. https://doi.org/10.1016/j.scitotenv.2021.151156

Mills, M., Lee, S., Mollenkopf, D., Wittum, T., Sullivan, S. M. P., & Lee, J. (2022). Comparison of environmental microbiomes in an antibiotic resistance-polluted urban river highlights periphyton and fish gut communities as reservoirs of concern. *Science of The Total Environment*, *851*, 158042. https://doi.org/10.1016/j.scitotenv.2022.158042

Mohsan, S. A. H., Khan, M. A., Noor, F., Ullah, I., & Alsharif, M. H. (2022). Towards the Unmanned Aerial Vehicles (UAVs): A Comprehensive Review. *Drones*, *6*(6), Article 6. https://doi.org/10.3390/drones6060147

Moore, C., Juan, J., Lin, Y., Gaskill, C., & Puschner, B. (2016). Comparison of Protein Phosphatase Inhibition Assay with LC-MS/MS for Diagnosis of Microcystin Toxicosis in Veterinary Cases. *Marine Drugs*, *14*(3), 54. https://doi.org/10.3390/md14030054

Mowe, M. A. D., Porojan, C., Abbas, F., Mitrovic, S. M., Lim, R. P., Furey, A., & Yeo, D. C. J. (2015). Rising temperatures may increase growth rates and microcystin production in tropical Microcystis species. *Harmful Algae*, *50*, 88–98. https://doi.org/10.1016/j.hal.2015.10.011

Munir, N., Hasnain, M., Hanif, M., Waqif, H., & Sharif, N. (2022). Fungal organisms: A check for harmful algal blooms. In *Freshwater Mycology* (pp. 91–115). Elsevier. https://doi.org/10.1016/B978-0-323-91232-7.00002-7

Nagarkar, S., Williams, G. A., Subramanian, G., & Saha, S. K. (n.d.). *Cyanobacteria-dominated biofilms: A high quality food resource for intertidal grazers*.

Nalbantoglu, U., Cakar, A., Dogan, H., Abaci, N., Ustek, D., Sayood, K., & Can, H. (2014). Metagenomic analysis of the microbial community in kefir grains. *Food Microbiology*, *41*, 42–51. https://doi.org/10.1016/j.fm.2014.01.014

Nshimyimana, J. P., Cruz, M. C., Wuertz, S., & Thompson, J. R. (2019). Variably improved microbial source tracking with digital droplet PCR. *Water Research*, *159*, 192–202. https://doi.org/10.1016/j.watres.2019.04.056

O'Neil, J. M., Davis, T. W., Burford, M. A., & Gobler, C. J. (2012). The rise of harmful cyanobacteria blooms: The potential roles of eutrophication and climate change. *Harmful Algae*, *14*, 313–334. https://doi.org/10.1016/j.hal.2011.10.027

Optica Publishing Group. (n.d.). Retrieved July 11, 2023, from https://opg.optica.org/view_article.cfm?pdfKey=289b83c2-f1b1-49a3-9f3699037fab7bc2_19173

Paerl, H. W., & Otten, T. G. (2013). Harmful Cyanobacterial Blooms: Causes, Consequences, and Controls. *Microbial Ecology*, *65*(4), 995–1010. https://doi.org/10.1007/s00248-012-0159-y

Paerl, H. W., & Paul, V. J. (2012). Climate change: Links to global expansion of harmful cyanobacteria. *Water Research*, *46*(5), 1349–1363. https://doi.org/10.1016/j.watres.2011.08.002

Park, S., Rana, A., Sung, W., & Munir, M. (2021). Competitiveness of Quantitative Polymerase Chain Reaction (qPCR) and Droplet Digital Polymerase Chain Reaction (ddPCR) Technologies, with a Particular Focus on Detection of Antibiotic Resistance Genes (ARGs). *Applied Microbiology*, *1*(3), 426–444. https://doi.org/10.3390/applmicrobiol1030028

Pearson, L., Mihali, T., Moffitt, M., Kellmann, R., & Neilan, B. (2010). On the Chemistry, Toxicology and Genetics of the Cyanobacterial Toxins, Microcystin, Nodularin, Saxitoxin and Cylindrospermopsin. *Marine Drugs*, *8*(5), 1650–1680. https://doi.org/10.3390/md8051650

Peeters, F., Straile, D., Lorke, A., & Livingstone, D. M. (2007). Earlier onset of the spring phytoplankton bloom in lakes of the temperate zone in a warmer climate. *Global Change Biology*, *13*(9), 1898–1909. https://doi.org/10.1111/j.1365-2486.2007.01412.x

Pérez-Cobas, A. E., Gomez-Valero, L., & Buchrieser, C. (2020). Metagenomic approaches in microbial ecology: An update on whole-genome and marker gene sequencing analyses. *Microbial Genomics*, *6*(8). https://doi.org/10.1099/mgen.0.000409

Pons, P., & Latapy, M. (2005). *Computing communities in large networks using random walks (long version)* (arXiv:physics/0512106). arXiv. https://doi.org/10.48550/arXiv.physics/0512106

Powers, C. W., Hanlon, R., Grothe, H., Prussin, A. J., Marr, L. C., & Schmale, D. G. (2018). Coordinated Sampling of Microorganisms Over Freshwater and Saltwater Environments Using an Unmanned Surface Vehicle (USV) and a Small Unmanned Aircraft System (sUAS). *Frontiers in Microbiology*, *9*, 1668. https://doi.org/10.3389/fmicb.2018.01668

Pyo, J., Hong, S. M., Jang, J., Park, S., Park, J., Noh, J. H., & Cho, K. H. (2022). Drone-borne sensing of major and accessory pigments in algae using deep learning modeling. *GIScience & Remote Sensing*, *59*(1), 310–332. https://doi.org/10.1080/15481603.2022.2027120

Qin, B., Zhu, G., Gao, G., Zhang, Y., Li, W., Paerl, H. W., & Carmichael, W. W. (2010). A Drinking Water Crisis in Lake Taihu, China: Linkage to Climatic Variability and Lake Management. *Environmental Management*, *45*(1), 105–112. https://doi.org/10.1007/s00267-009-9393-6

Quast, C., Pruesse, E., Yilmaz, P., Gerken, J., Schweer, T., Yarza, P., Peplies, J., & Glöckner, F. O. (2013). The SILVA ribosomal RNA gene database project: Improved data processing and web-based tools. *Nucleic Acids Research*, *41*(Database issue), D590–D596. https://doi.org/10.1093/nar/gks1219

Quince, C., Walker, A. W., Simpson, J. T., Loman, N. J., & Segata, N. (2017). Shotgun metagenomics, from sampling to analysis. *Nature Biotechnology*, *35*(9), 833–844. https://doi.org/10.1038/nbt.3935

Radiometric Calibration Model for MicaSense Sensors. (2023, June 9). MicaSense Knowledge Base. https://support.micasense.com/hc/en-us/articles/115000351194-Radiometric-Calibration-Model-for-MicaSense-Sensors

Rastogi, R. P., Sonani, R. R., Madamwar, D., & Incharoensakdi, A. (2016). Characterization and antioxidant functions of mycosporine-like amino acids in the cyanobacterium Nostoc sp. R76DM. *Algal Research*, *16*, 110–118. https://doi.org/10.1016/j.algal.2016.03.009

Recommended Human Health Recreational Ambient Water Quality Criteria or Swimming Advisories for Microcystins and Cylindrospermopsin. (2019, June 6). Federal Register. https://www.federalregister.gov/documents/2019/06/06/2019-11814/recommended-human-health-recreational-ambient-water-quality-criteria-or-swimming-advisories-for

RedEdge-MX Integration Guide. (2022, November 17). MicaSense Knowledge Base. https://support.micasense.com/hc/en-us/articles/360011389334-RedEdge-MX-Integration-Guide

Rivasseau, C., Racaud, P., Deguin, A., & Hennion, M.-C. (1999). Evaluation of an ELISA Kit for the Monitoring of Microcystins (Cyanobacterial Toxins) in Water and Algae Environmental Samples. *Environmental Science & Technology*, *33*(9), 1520–1527. https://doi.org/10.1021/es980460g

Roos, J. C., & Pieterse, A. J. H. (1994). Light, temperature and flow regimes of the Vaal River at Balkfontein, South Africa. *Hydrobiologia*, *277*(1), 1–15. https://doi.org/10.1007/BF00023982

Rousso, B. Z., Bertone, E., Stewart, R., & Hamilton, D. P. (2020). A systematic literature review of forecasting and predictive models for cyanobacteria blooms in freshwater lakes. *Water Research*, *182*, 115959. https://doi.org/10.1016/j.watres.2020.115959

Ruddick, K. G., Gons, H. J., Rijkeboer, M., & Tilstone, G. (2001). Optical remote sensing of chlorophyll a in case 2 waters by use of an adaptive two-band algorithm with optimal error properties. *Applied Optics*, *40*(21), 3575. https://doi.org/10.1364/AO.40.003575

Runnegar, M. T. C., Gerdes, R. G., & Falconer, I. R. (1991). The uptake of the cyanobacterial hepatotoxin microcystin by isolated rat hepatocytes. *Toxicon*, *29*(1), 43–51. https://doi.org/10.1016/0041-0101(91)90038-S

Rushford, C. A., North, R. L., & Miller, G. L. (2022). Detection of cyanotoxins in irrigation water and potential impact on putting green health. *International Turfgrass Society Research Journal*, *14*(1), 994–996. https://doi.org/10.1002/its2.40

Rytkönen, A., Tiwari, A., Hokajärvi, A.-M., Uusheimo, S., Vepsäläinen, A., Tulonen, T., & Pitkänen, T. (2021). The Use of Ribosomal RNA as a Microbial Source Tracking Target Highlights the Assay Host-Specificity Requirement in Water Quality Assessments. *Frontiers in Microbiology*, *12*, 673306. https://doi.org/10.3389/fmicb.2021.673306

Sahu, D., Priyadarshani, I., & Rath, B. (2012). *CYANOBACTERIA - as potential biofertilizer*. *1*.

Saini, D. K., Pabbi, S., & Shukla, P. (2018). Cyanobacterial pigments: Perspectives and biotechnological approaches. *Food and Chemical Toxicology*, *120*, 616–624. https://doi.org/10.1016/j.fct.2018.08.002

Sánchez-Baracaldo, P., & Cardona, T. (2020). On the origin of oxygenic photosynthesis and Cyanobacteria. *New Phytologist*, *225*(4), 1440–1446. https://doi.org/10.1111/nph.16249

Santhakumaran, P., Kookal, S. K., Mathew, L., & Ray, J. G. (2019). Bioprospecting of Three Rapid-Growing Freshwater Green Algae, Promising Biomass for Biodiesel Production. *BioEnergy Research*, *12*(3), 680–693. https://doi.org/10.1007/s12155-019-09990-9

Sawtell, R. W., Anderson, R., Tokars, R., Lekki, J. D., Shuchman, R. A., Bosse, K. R., & Sayers, M. J. (2019). Real time HABs mapping using NASA Glenn hyperspectral imager. *Journal of Great Lakes Research*, *45*(3), 596–608. https://doi.org/10.1016/j.jglr.2019.02.007

Sayers, M., Fahnenstiel, G. L., Shuchman, R. A., & Whitley, M. (2016). Cyanobacteria blooms in three eutrophic basins of the Great Lakes: A comparative analysis using satellite remote sensing. *International Journal of Remote Sensing*, *37*(17), 4148–4171. https://doi.org/10.1080/01431161.2016.1207265

Scavia, D., David Allan, J., Arend, K. K., Bartell, S., Beletsky, D., Bosch, N. S., Brandt, S. B., Briland, R. D., Daloğlu, I., DePinto, J. V., Dolan, D. M., Evans, M. A., Farmer, T. M., Goto, D., Han, H., Höök, T. O., Knight, R., Ludsin, S. A., Mason, D., … Zhou, Y. (2014). Assessing and addressing the re-eutrophication of Lake Erie: Central basin hypoxia. *Journal of Great Lakes Research*, *40*(2), 226–246. https://doi.org/10.1016/j.jglr.2014.02.004

Segata, N., Izard, J., Waldron, L., Gevers, D., Miropolsky, L., Garrett, W. S., & Huttenhower, C. (2011). Metagenomic biomarker discovery and explanation. *Genome Biology*, *12*(6), R60. https://doi.org/10.1186/gb-2011-12-6-r60

Sekrecka, A., Wierzbicki, D., & Kedzierski, M. (2020). Influence of the Sun Position and Platform Orientation on the Quality of Imagery Obtained from Unmanned Aerial Vehicles. *Remote Sensing*, *12*(6), 1040. https://doi.org/10.3390/rs12061040

Shang, S., Lee, Z., Lin, G., Hu, C., Shi, L., Zhang, Y., Li, X., Wu, J., & Yan, J. (2017). Sensing an intense phytoplankton bloom in the western Taiwan Strait from radiometric measurements on a UAV. *Remote Sensing of Environment*, *198*, 85–94. https://doi.org/10.1016/j.rse.2017.05.036

Shardlow, T. J. (n.d.). *Identification and characterization of toxic cyanobacteria in two forested maritime watersheds in North America*.

Shi, K., Zhang, Y., Qin, B., & Zhou, B. (2019). Remote sensing of cyanobacterial blooms in inland waters: Present knowledge and future challenges. *Science Bulletin*, *64*(20), 1540–1556. https://doi.org/10.1016/j.scib.2019.07.002

Shuchman, R. A., Leshkevich, G., Sayers, M. J., Johengen, T. H., Brooks, C. N., & Pozdnyakov, D. (2013). An algorithm to retrieve chlorophyll, dissolved organic carbon, and suspended minerals from Great Lakes satellite data. *Journal of Great Lakes Research*, *39*, 14–33. https://doi.org/10.1016/j.jglr.2013.06.017

Sibanda, M., Mutanga, O., Chimonyo, V. G. P., Clulow, A. D., Shoko, C., Mazvimavi, D., Dube, T., & Mabhaudhi, T. (2021). Application of Drone Technologies in Surface Water Resources Monitoring and Assessment: A Systematic Review of Progress, Challenges, and Opportunities in the Global South. *Drones*, *5*(3), 84. https://doi.org/10.3390/drones5030084

Silvarrey Barruffa, A., Pardo, Á., Faggian, R., & Sposito, V. (2021). Monitoring cyanobacterial harmful algal blooms by unmanned aerial vehicles in aquatic ecosystems. *Environmental Science: Water Research & Technology*, *7*(3), 573–583. https://doi.org/10.1039/D0EW00830C

Sivonen K, Jones G. Cyanobacterial toxins. In: Chorus I, Bartram J, editors. Toxic cyanobacteria in water: a guide to their public health consequences, monitoring and management. London, UK: E & FN Spon; 1999. p. 41–111

Small Unmanned Aircraft Systems (UAS) Regulations (Part 107) | Federal Aviation Administration. (n.d.). Retrieved June 24, 2023, from https://www.faa.gov/newsroom/small-unmanned-aircraft-systems-uas-regulations-part-107

Smucker, N. J., Beaulieu, J. J., Nietch, C. T., & Young, J. L. (2021). Increasingly severe cyanobacterial blooms and deep water hypoxia coincide with warming water temperatures in reservoirs. *Global Change Biology*, *27*(11), 2507–2519. https://doi.org/10.1111/gcb.15618

Son, G., Kim, D., Kim, Y. D., Lyu, S., & Kim, S. (2020). A Forecasting Method for Harmful Algal Bloom(HAB)-Prone Regions Allowing Preemptive Countermeasures Based only on Acoustic Doppler Current Profiler Measurements in a Large River. *Water*, *12*(12), 3488. https://doi.org/10.3390/w12123488

Song, Q., Ma, C., Liu, J., & Wei, H. (2022). Quantifying ocean surface green tides using high-spatial resolution thermal images. *Optics Express*, *30*(20), 36592. https://doi.org/10.1364/OE.472479

Spoof, L., & Catherine, A. (2016). Appendix 3: Tables of Microcystins and Nodularins. In *Handbook of Cyanobacterial Monitoring and Cyanotoxin Analysis* (pp. 526–537). John Wiley & Sons, Ltd. https://doi.org/10.1002/9781119068761.app3

Stoyneva-Gärtner, M. P., Uzunov, B. A., Descy, J.-P., Gärtner, G., Draganova, P. H., Borisova, C. I., Pavlova, V., & Mitreva, M. (2020). Pilot application of drone observations and pigment marker detection by HPLC in studies of cyanobacterial harmful algal blooms in Bulgarian inland waters. *Marine and Freshwater Research*, *71*(5), 606. https://doi.org/10.1071/MF18383

Sun, Q., Chen, X., Liu, W., Li, S., Zhou, Y., Yang, X., & Liu, J. (2021). Effects of long-term low dose saxitoxin exposure on nerve damage in mice. *Aging (Albany NY)*, *13*(13), 17211–17226. https://doi.org/10.18632/aging.203199

Sundaravadivelu, D., Sanan, T. T., Venkatapathy, R., Mash, H., Tettenhorst, D., DAnglada, L., Frey, S., Tatters, A. O., & Lazorchak, J. (2022). Determination of Cyanotoxins and Prymnesins in Water, Fish Tissue, and Other Matrices: A Review. *Toxins*, *14*(3), Article 3. https://doi.org/10.3390/toxins14030213

Suomalainen, J., Oliveira, R. A., Hakala, T., Koivumäki, N., Markelin, L., Näsi, R., & Honkavaara, E. (2021). Direct reflectance transformation methodology for drone-based hyperspectral imaging. *Remote Sensing of Environment*, *266*, 112691. https://doi.org/10.1016/j.rse.2021.112691

Svirčev, Z., Drobac, D., Tokodi, N., Mijović, B., Codd, G. A., & Meriluoto, J. (2017). Toxicology of microcystins with reference to cases of human intoxications and epidemiological investigations of exposures to cyanobacteria and cyanotoxins. *Archives of Toxicology*, *91*(2), 621–650. https://doi.org/10.1007/s00204-016-1921-6

Thomson-Laing, G., Puddick, J., & Wood, S. A. (2020). Predicting cyanobacterial biovolumes from phycocyanin fluorescence using a handheld fluorometer in the field. *Harmful Algae*, *97*, 101869. https://doi.org/10.1016/j.hal.2020.101869

Tian, W., Zhang, H., Zhang, J., Zhao, L., Miao, M., & Huang, H. (2017). Biodiversity effects on resource use efficiency and community turnover of plankton in Lake Nansihu, China. *Environmental Science and Pollution Research*, *24*(12), 11279–11288. https://doi.org/10.1007/s11356-017-8758-2

Toporowska, M., & Pawlik-Skowrońska, B. (2014). Four-year study on phytoplankton biodiversity in a small hypertrophic lake affected by water blooms of toxigenic cyanobacteria (E. Poland). *Polish Journal of Environmental Studies*, *23*, 491–499.

Tóth, V. Z., Grósz, J., Ladányi, M., & Jung, A. (2021). A new lake algae detection method supported by a drone-based multispectral camera. *Lakes & Reservoirs: Science, Policy and Management for Sustainable Use*, *26*(3), e12377. https://doi.org/10.1111/lre.12377

UAS Remote Identification | Federal Aviation Administration. (n.d.). Retrieved June 24, 2023, from https://www.faa.gov/uas/getting_started/remote_id

Ufelmann, H., Krüger, T., Luckas, B., & Schrenk, D. (2012). Human and rat hepatocyte toxicity and protein phosphatase 1 and 2A inhibitory activity of naturally occurring desmethyl-microcystins and nodularins. *Toxicology*, *293*(1–3), 59–67. https://doi.org/10.1016/j.tox.2011.12.011

US EPA, O. (2016, October 27). *Additional Information about Cyanotoxins in Drinking Water* [Data and Tools]. https://www.epa.gov/ground-water-and-drinking-water/additional-information-about-cyanotoxins-drinking-water

US EPA, O. (2018a, August 17). *World Health Organization (WHO) 1999 Guideline Values for Cyanobacteria in Freshwater* [Overviews and Factsheets]. https://www.epa.gov/cyanohabs/world-health-organization-who-1999-guideline-values-cyanobacteria-freshwater

US EPA, O. (2018b, September 18). *EPA Drinking Water Health Advisories for Cyanotoxins* [Overviews and Factsheets]. https://www.epa.gov/cyanohabs/epa-drinking-water-health-advisories-cyanotoxins

Use of Calibrated Reflectance Panels For MicaSense Data. (2023, April 22). MicaSense Knowledge Base. https://support.micasense.com/hc/en-us/articles/115000765514-Use-of-Calibrated-Reflectance-Panels-For-MicaSense-Data

Vďačný, P., Breiner, H.-W., Yashchenko, V., Dunthorn, M., Stoeck, T., & Foissner, W. (2014). The Chaos Prevails: Molecular Phylogeny of the Haptoria (Ciliophora, Litostomatea). *Protist*, *165*(1), 93–111. https://doi.org/10.1016/j.protis.2013.11.001

Vilne, B., Grantiņa-Ieviņa, L., Ķibilds, J., Mališevs, A., Konvisers, G., Makarova, S., Pūle, D., & Valciņa, O. (2021). Investigating Bacterial and Free-Living Protozoa Diversity in Biofilms of Hot Water Pipes of Apartment Buildings in the City of Riga (Latvia). *Frontiers in Water*, *3*. https://www.frontiersin.org/articles/10.3389/frwa.2021.799840

Visser, P. M., Verspagen, J. M. H., Sandrini, G., Stal, L. J., Matthijs, H. C. P., Davis, T. W., Paerl, H. W., & Huisman, J. (2016). How rising CO2 and global warming may stimulate harmful cyanobacterial blooms. *Harmful Algae*, *54*, 145–159. https://doi.org/10.1016/j.hal.2015.12.006

Vogiazi, V., De La Cruz, A., Mishra, S., Shanov, V., Heineman, W. R., & Dionysiou, D. D. (2019). A Comprehensive Review: Development of Electrochemical Biosensors for Detection of Cyanotoxins in Freshwater. *ACS Sensors*, *4*(5), 1151–1173. https://doi.org/10.1021/acssensors.9b00376

Wang, Z., Li, B., & Li, L. (2019). Research on Water Quality Detection Technology Based on Multispectral Remote Sensing. *IOP Conference Series: Earth and Environmental Science*, *237*, 032087. https://doi.org/10.1088/1755-1315/237/3/032087

Westrick, J. A., Szlag, D. C., Southwell, B. J., & Sinclair, J. (2010). A review of cyanobacteria and cyanotoxins removal/inactivation in drinking water treatment. *Analytical and Bioanalytical Chemistry*, *397*(5), 1705–1714. https://doi.org/10.1007/s00216-010-3709-5

What is the center wavelength and bandwidth of each filter for MicaSense sensors? (2023, April 17). MicaSense Knowledge Base. https://support.micasense.com/hc/en-us/articles/214878778-What-is-the-center-wavelength-and-bandwidth-of-each-filter-for-MicaSense-sensors-

Wierzbicki, D., Kedzierski, M., & Fryskowska, A. (2015). ASSESMENT OF THE INFLUENCE OF UAV IMAGE QUALITY ON THE ORTHOPHOTO PRODUCTION. *The International*

Archives of the Photogrammetry, Remote Sensing and Spatial Information Sciences, *XL-1-W4*, 1–8. https://doi.org/10.5194/isprsarchives-XL-1-W4-1-2015

Windle, A. E., & Silsbe, G. M. (2021). Evaluation of Unoccupied Aircraft System (UAS) Remote Sensing Reflectance Retrievals for Water Quality Monitoring in Coastal Waters. *Frontiers in Environmental Science*, *9*, 674247. https://doi.org/10.3389/fenvs.2021.674247

Wu, D., Li, R., Zhang, F., & Liu, J. (2019). A review on drone-based harmful algae blooms monitoring. *Environmental Monitoring and Assessment*, *191*(4), 211. https://doi.org/10.1007/s10661-019-7365-8

Xu, F., Gao, Z., Jiang, X., Shang, W., Ning, J., Song, D., & Ai, J. (2018). A UAV and S2A data-based estimation of the initial biomass of green algae in the South Yellow Sea. *Marine Pollution Bulletin*, *128*, 408–414. https://doi.org/10.1016/j.marpolbul.2018.01.061

Xu, W., Duan, L., Wen, X., Li, H., Li, D., Zhang, Y., & Zhang, H. (2022). Effects of Seasonal Variation on Water Quality Parameters and Eutrophication in Lake Yangzong. *Water*, *14*(17), 2732. https://doi.org/10.3390/w14172732

Yan, T., Li, X.-D., Tan, Z.-J., Yu, R.-C., & Zou, J.-Z. (2022). Toxic effects, mechanisms, and ecological impacts of harmful algal blooms in China. *Harmful Algae*, *111*, 102148. https://doi.org/10.1016/j.hal.2021.102148

Yang, Y., Zheng, X., Tang, Q., Gu, J., Lei, L., & Han, B.-P. (2020). Species diversity and seasonal dynamics of filamentous cyanobacteria in urban reservoirs for drinking water supply in tropical China. *Ecotoxicology*, *29*(6), 780–789. https://doi.org/10.1007/s10646-020-02189-1

Yen, H.-K., Lin, T.-F., & Liao, P.-C. (2011). Simultaneous detection of nine cyanotoxins in drinking water using dual solid-phase extraction and liquid chromatography–mass spectrometry. *Toxicon*, *58*(2), 209–218. https://doi.org/10.1016/j.toxicon.2011.06.003

Žegura, B., Sedmak, B., & Filipič, M. (2003). Microcystin-LR induces oxidative DNA damage in human hepatoma cell line HepG2. *Toxicon*, *41*(1), 41–48. https://doi.org/10.1016/S0041-0101(02)00207-6

Zeng, C., Richardson, M., & King, D. J. (2017). The impacts of environmental variables on water reflectance measured using a lightweight unmanned aerial vehicle (UAV)-based spectrometer system. *ISPRS Journal of Photogrammetry and Remote Sensing*, *130*, 217–230. https://doi.org/10.1016/j.isprsjprs.2017.06.004

Zhang, H., Li, B., Liu, Y., Chuan, H., Liu, Y., & Xie, P. (2022). Immunoassay technology: Research progress in microcystin-LR detection in water samples. *Journal of Hazardous Materials*, *424*, 127406. https://doi.org/10.1016/j.jhazmat.2021.127406

Zhang, H., Song, B., Wang, H., & Xuan, J. (2019). A method for evaluating the wind disturbance rejection capability of a hybrid UAV in the quadrotor mode. *International Journal of Micro Air Vehicles*, *11*, 175682931986964. https://doi.org/10.1177/1756829319869647

Zhang, H., Zhang, J., Hong, Y., & Chen, Y. (2007). Evaluation of organ distribution of microcystins in the freshwater phytoplanktivorous fish Hypophthalmichthys molitrix. *Journal of Zhejiang University SCIENCE B*, *8*(2), 116–120. https://doi.org/10.1631/jzus.2007.B0116

Zhao, D., Cai, Y., Jiang, H., Xu, D., Zhang, W., & An, S. (2011). Estimation of water clarity in Taihu Lake and surrounding rivers using Landsat imagery. *Advances in Water Resources*, *34*(2), 165–173. https://doi.org/10.1016/j.advwatres.2010.08.010

Appendix A: Supplementary Data

Table A.1 Summary of all human-health related guidelines in each state for cyanotoxins as of June 2021. This table was adapted from (Mehinto et al., 2021).

Some states employ a tiered approach, while others do not. States with only one level of guidance are represented using x* and placed under Tier II (typically, the equivalent for these are tier II recreational advisories for states using a tiered approach). Tier I is a general warning that toxic cyanobacteria are present in a waterbody, and it is advised to avoid impacted bodies of water. Tier II restricts primary contact recreation (e.g., swimming) but allows for secondary contact activities such as fishing or boating. Tier III restricts all primary and secondary recreational activities on the water body, and usually results in closure of the water body.

Toxin	Water Concentration	State	Recreational Advisory Tier		
			Tier I	Tier II	Tier III
Microcystin	0.8 µg/L	California	x		
	3 µg/L	New Jersey		x*	
	<4 ug/L	Kansas	x		
	<4 ug/L	Montana	x		
	4 µg/L	Idaho		x*	
		Kansas	x		
		New York	x		
		Rhode Island			x
	6 µg/L	California		x	
		Minnesota		x*	
		Pennsylvania	x		
		Vermont		x	

Continued

Table A.1 continued

		Washington	**x**
	8 µg/L	US EPA (federal)	x*
		Arkansas	x*
		Colorado	x*
		Indiana	x
		Illinois	x*
		Iowa	x*
		Kansas	x
		Kentucky	x*
		Missouri	x*
		Nebraska	x*
		Ohio	x*
		Oregon	x*
		South Carolina	x*
		South Dakota	x*
		Virginia	x*
		Utah	
		Wisconsin	x*
		Wyoming	x
	10 µg/L	Maryland	x*
		New York (open Water)	x
		North Dakota	x
	14 µg/L	Massachusetts	x*

Continued

Table A.1 continued

	20 µg/L	California			X
		Indiana		x	
		Michigan		x*	
		New York (shore)	x		
		Oklahoma	x	x	
		Pennsylvania	x	x	
		West Virginia		x	
	>20 ug/L	Montana		x	
	2000 µg/L	Kansas			x
	2000 µg/L	Utah			x
Cylindro-spermopsin	1 µg/L	California	x		
	4 µg/L	California		x	
	4.5 µg/L	Washington		x	
	5 µg/L	Pennsylvania	x		
	N/A	West Virginia	x		
	8 µg/L	Idaho		x*	
		Oregon		x*	
		New Jersey		x*	
	10 µg/L	Vermont		x	
	15 µg/L	US EPA (federal)		x*	
		Arkansas		x*	
		Colorado		x*	

Continued

Table A.1 continued

		Illinois	x*	
		Indiana	x	
		Kentucky	x*	
		Minnesota	x*	
		Missouri	x*	
		Ohio	x*	
		Oregon	x*	
		South Carolina	x*	
		Wisconsin	x*	
		Wyoming	x	
	17 µg/L	California		x
	20 µg/L	Indiana		x
		Pennsylvania		x
		West Virginia		x
Anatoxin-a	Non-detect	Montana	x	
	≤ 1 µg/L Detection	California	x	
	Detect	Montana	x	
	1 µg/L	Washington	x	
	7 µg/L	Minnesota	x*	
	8 µg/L	Ohio	x*	
	10 µg/L	Vermont	x	
	15 µg/L	Colorado	x*	
		Oregon	x*	
		Utah	x	

Continued

Table A.1 continued

	20 µg/L	California	x	
		Missouri	x*	
	>20 ug/L	Montana		x
	80 µg/L	Indiana	x	
		Kentucky	x*	
		Pennsylvania	x	
		West Virginia	x	
	90 µg/L	California		x
		Utah		x
	300 µg/L	Indiana		x
		Pennsylvania		x
		West Virginia		x
Saxitoxin	0.8 µg/L	Ohio	x	
		Pennsylvania	x	
		West Virginia	x	
		Indiana	x	
	3 µg/L	Indiana		x
		Pennsylvania	x	
		West Virginia	x	
	8 µg/L	Colorado	x*	
		Oregon	x*	
	10 µg/L	Missouri	x*	
	75 µg/L	Washington	x	

Table A.2 Summary of studies utilizing UAVs for HAB monitoring from 2017-present. Implications for public health of each is also discussed.

UAV Platform(s)	**UAV Attachment(s)**	**Summary**	**Potential Public Health Application**	**Study**
DJI Phantom 3	RGB camera	Aimed to show the potential of using in situ and UAV aerial remote-sensing data to analyze the temporal and spatial scale of cyanobacteria	The main activities on the lake are recreational, such as rowing and boat recreation, so a tool is needed that can handle the spatial distribution of HABs.	Aguirre-Gómez et al. (2017)
Custom octocopter	Sony ILCE-6000	Exhaustively tested how UAV hardware settings affect quality of the data captured. UAV was then deployed to evaluate if UAVs are a viable tool for early and timely cyanobacteria detection.	Timely, flexible, and cost-effective tool for monitoring of HABs using novel algorithm for separating cyanobacteria from other photosynthesizing organisms.	Lyu et al. (2017)
LT-150 TOPRS Technology	AvaSpec-dual spectroradiometer	UAV assessment of a phytoplankton (Phaeocystis globosa) bloom in an estuary using hyperspectral sensors.	Weitou bay is full of fishing and aquaculture activities. HABs negatively impact human health and the health of local and regional economies, so a tool is needed for accurately quantifying HABs.	Shang et al. (2017)

Continued

Table A.2 continued

DJI Inspire 1	DJI X3 RGB camera	Green algae were identified with an UAV. A biomass estimation model was proposed for green algae biomass based on Sentinel-2A image (S2A) and UAV images.	For 10 consecutive years the world's largest green tide disaster has been occurring in the South Yellow Sea, causing nearly 10 billion RMB in economic and ecological losses, so an early warning model is needed.	Xu et al. (2018)
FireFLY6 BirdsEyeView Aerobotics	Micasense RedEdge	This study utilized remote sensing techniques using an UAV with multispectral sensor to monitor the Nakdong River.	Sincheon river experiences severe algal blooms every years effecting nearby communities, researcher sought to use UAV on body of water too small to be monitored by satellite	Choo et al. (2018)
Custom quadcopter & hexacopter	Ocean Optics STS Hyperspectral Vis-NIR Spectroradiometer	Deployed two different UAV platform configurations, utilizing Ocean Optics STS spectroradiometers, to measure optical properties of river and lake water for monitoring HAB.	Rapid deployment of this system, low initial cost, high quality of data, ability to take measurements without disturbing water's surface, and low operational costs make UAVs a useful tool for water resource managers.	Becker et al. (2019)

Continued

Table A.2 continued

Custom blimp	RGB camera	An UAV with a camera was connected to the ground by a rope to detect, determine velocity, and determine movement direction of HABs.	Real time monitoring tool for HABs allowing the location, movement velocity, and movement direction of HABs to be determined around a water desalination plant.	Kim et al. (2019)
DJI Inspire 2	Micasense RedEdge	Developed a new chl-A estimation algorithm based on multispectral camera signals.	A chl-a algorithm, more accurate than others discussed in previous research, was developed in this study, and could be used for chl-a monitoring to improve public health.	Baek et al. (2019)
ATI AgBot	Micasense RedEdge	Sought to create different predictive algorithms of trophic state for optical and non-optical water quality indicators in an oligotrophic system and a eutrophic system using images from an UAV equipped with a multispectral sensor.	UAV imagery used to create statistical models for optical and non-optical water quality properties, indicating UAVs could be a useful tool for water resource managers around the world.	Arango & Nairn (2019)

Continued

Table A.2 continued

DJI Matrice 200 & custom quadcopter named Akabot II	RGB camera & 3 bottle sampling mechanism	An early detection system for HABs using an UAV that locates anomalies in sea surface reflectance, then an aerial water sampling UAV collects a water sample.	Risk level of HAB is ranked as alert or caution based on reference values, this notification is sent to water resource managers and saved in cloud-based system and used for real-time notification.	Kimura et al. (2019)
DJI Mavic Pro	RGB Camera	The first use of aerial observations by a drone as an additional means for choosing sampling points during field studies of HABs in Bulgaria.	Ability to speed up detection and reduce sampling efforts while enabling valuable information to be gathered on HABs.	Stoyneva-Gärtner et al. (2020)
DJI Matrice 600 Pro	Nano Hyperspec hyperspecrtal imaging sensor	Generated a vertical pigment-concentration profile with a portable sensor and utilized UAV-based surface reflectance to develop an improved bio-optical remote sensing method.	Daechung reservoir supplies water to surrounding cities for domestic and industrial use, so monitoring is crucial for preserving public health.	Kwon et al. (2020)
DJI Phantom 4	RGB camera	For the first time, this study demonstrates the use of an UAV to quantitatively map surface water Chl-a distribution in coastal waters from a low altitude utilizing an estimation model for Chl-a concentration.	Blooms in this area can lead to massive fish kills within the coastal fish farms and can lead to beach closures. Research provides a tool to quantitively map HABs.	Cheng et al. (2020)

Continued

Table A.2 continued

Octocopter Atyges FV8	Micasense RedEdge	Researchers sought to combine the affordability, stability, quality and continuity of ESA and NASA missions (satellite) with the flexibility and spatial resolution provided using UAV platforms.	Since 2000, the reservoir has maintained a drinking water supply service for households and facilities in the municipality. The reservoir also has a river park and recreational areas. Tool developed to combine satellite and UAV monitoring.	Cillero Castro et al. (2020)
DJI Phantom 3 Pro	Sentera Multispectral Sensor	Aimed to evaluate the ability of UAVs equipped with multispectral sensors for inferring the spatial distribution of Chl-A concentration and turbidity in surface waters.	Provides the ability to estimate the spatial distribution of Chl-a concentrations.	McEliece et al. (2020)
DJI Phantom 4	RGB camera	Aimed to develop a practical and rapid countermeasure to HABs by identifying HAB prone regions with acoustic doppler current profiler measurements and visually inspecting HAB prone regions with UAV.	The Chilseo WTP is in operation downstream providing water to Daegu and Busan, and is affected by these blooms, harmful microcystins could affect the public water drinking system. Began developing rapid countermeasure for HABs.	Son et al. (2020)

Continued

Table A.2 continued

DJI Phantom 4 Pro	Parrot Sequoia multispectral (Parrot SA)	Used a UAV equipped with multispectral sensor to estimate Chl-a and cc concentrations using many different band combinations.	De Los Cisnes Lagoon supplies drinking water to more than 95 percent of the fixed population. This study shows it is possible to identify cyanobacteria among other photosynthetic organisms using an UAV equipped with a four-band multispectral camera.	Silvarrey Barruffa et al. (2021)
Mavic 2 Enterprise	Thermal dual camera & BD2Vision LaQuinta multipsectral	Developed a new methodology to determine algal concentrations in lakes, utilizing a UAV equipped with a multispectral camera.	The quick-process measurements obtained in this study can be done as frequently as required with a markedly lower budget.	Tóth et al. (2021)
DJI Inspire 1	Zenmus X3 optical camera	The seasonal shoreline and eutrophication of a desert lake were monitored using an UAV and water sampling during three crop growth stages.	Desert lakes cover a small portion of the desert landscape but provide important ecological services and benefits to residents. UAVs can be a tool for better understanding the eutrophication of these water resources.	Luo et al. (2021)

Continued

Table A.2 continued

DJI Inspire 1	Micasense Rededge-3	Proposed the use of a multiscale, multimethod approach using near-range imaging, bioassay, and chromatography methods to best capture bloom dynamics.	Sought to generate multi-platform framework for predicting microcystins in water sources.	Douglas Greene et al. (2021)
Custom hexacopter	Hyperspectral Pika 2 & Pika NIR	Presented a development effort for a regional/local EBS-based model for Chl-a estimates in freshwater bodies that can be run on both data acquired by an UAV and Sentinel-2 data.	An algorithm is developed that can be applied to both sentinel-2 data and UAV imagery; Satellite data could be used for analysis at regional scale while water managers could utilize UAVs at a local scale.	El-Alem et al. (2021)
DJI Phantom 4 Pro	Micasense RedEdge-MX	Presents a comparison of four approaches to remove sun glint and surface reflected light that can be applied to UAS remote sensing to derive water quality parameters such as Chl-A concentration.	Improved water quality monitoring of coastal and inland water bodies to effectively track trends, identify and mitigate pollution sources, and discern potential human health risks.	Windle & Silsbe (2021)

Continued

Table A.2 continued

Matrice 600 Pro	Nano Hyperspec hyperspecrtal imaging sensor	Applied a deep neural network model to monitor the vertical distribution of Chl-A, PC, and turbidity using drone borne hyperspectral imagery, in-situ measurements, and meteoroidal data.	Deep learning models could be used to better understand and predict vertical migration of HABs. This could allow for more informed early warning systems.	Hong et al. (2021)
Ecodrone UAS-8 m	Micasense RedEdge-M & FireFly 8 s camera	Aimed to establish an algorithm model of biomass based on multispectral imaging data, which could be used for estimating P. yezoensis biomass in an accurate, high-throughput, and non-destructive way.	Accurate estimations of macroalgae production are economically important for providing food, medicine, cosmetics, and biofuel.	Che et al. (2021)
DJI Inspire 2	Impinging device & optical particle counter	An Airborne DROne Particle-monitoring System (AirDROPS) was developed and used to monitor, collect, and characterize airborne particles over two HABs.	Lake spray aerosols can contain toxins, which can be transported inland to communities, negatively impacting public health. UAVs could be a new tool for evaluating the toxicity of HAB aerosols.	Bilyeu et al. (2022)

Continued

Table A.2 continued

DJI Phantom 4	RGB camera & water sampling tube	Utilized drone-based water sampling methods to characterize cyanotoxins, PC, and nutrients in three freshwater lakes in the United States with active HABs.	Demonstrates the potential for drone-based water sampling technologies to be used by public health and water quality experts to provide critical and timely information for regulatory decisions and health advisories.	Hanlon et al. (2022)
Matrice 600 Pro	Nano Hyperspec hyperspecrtal imaging sensor	Evaluated the potential of deep learning models to estimate biomass pigments (i.e. Chl-a and PC) and accessory pigments (i.e. lutein, fucoxanthin, and zeaxanthin).	Deep learning model could accurately analyze algal phenomenon quantitatively and qualitatively when using UAV imagery spatial information input of HABs.	Pyo et al. (2022)

Table A.3 Bio-Rad C1000 PCR thermal cycler conditions used for DNA amplification of cyanotoxin-producing cyanobacteria.

Note: “Infinite” refers to the holding temperature for samples after amplification is complete. In each process there is a “return to” portion. This denotes what step must be returned to, and the value beside this (i.e. 37 X) denotes how many times those steps must be repeated.

Targeted Gene	Step	Temperature (C°)	Time
mcyE *Microcystis*	1	95	10 minutes
	2	94	30 seconds
	3	56	30 seconds
	4	60	30 seconds
	5	Return to step 2	37 X
	6	98	10 minutes
	7	4	Infinite
mcyE *Planktothrix*	1	95	10 min
	2	94	30 sec
	3	59	30 sec
	4	60	30 sec
	5	Return to 2	37 x
	6	98	10 min
	7	4	infinite
PC-IGS	1	95	10 minutes
	2	94	30 seconds
	3	59	30 seconds
	4	60	30 seconds
	5	Return to step 2	37 x
	6	98	10 minutes
	7	4	Infinite
anaC	1	95	5 min
	2	95	30 sec
	3	57	30 sec
	4	60	30 sec
	5	Return to 2	37 x
	6	4	5 min
	7	90	5 min
	8	4	infinite

Continued

Table A.3 continued

sxtA	1	95	5 min
	2	95	30 sec
	3	57	30 sec
	4	60	30 sec
	5	Return to 2	37 x
	6	4	5 min
	7	90	5 min
	8	4	infinite

Table A.4 Bio-Rad C1000 PCR thermal cycler conditions used for DNA amplification of MSTs

Note: "Infinite" refers to the holding temperature for samples after amplification is complete. In each process there is a "return to" portion. This denotes what step must be returned to, and the value beside this (i.e. 37 X) denotes how many times those steps must be repeated.

Targeted Gene	**Step**	**Temperature (C°)**	**Time**
GFD	**1**	**95**	**10:00**
	2	95	0:30
	3	56	0:30
	4	60	0:30
	5	Return to 2	39x
	6	90	5:00
	7	4	infinite
BacCan	1	95	10:00
	2	94	0:30
	3	60	1:00
	4	Return to 2	44x
	5	98	10:00
HF183	1	95	10:00
	2	94	0:30
	3	60	1:00
	4	Return to 2	44x
	5	98	10:00
	6	4	infinite

Bacterial 16S

V1-V3 domains (27F & 519R)

27F_A	TCGTCGGCAGCGTCAGATGTGTATAAGAGACAG	TCGATCGGAAKRGTTYGATYNTGGCTCAG
27F_B	TCGTCGGCAGCGTCAGATGTGTATAAGAGACAG	ATCTGTCATGGAAKRGTTYGATYNTGGCTCAG
27F_C	TCGTCGGCAGCGTCAGATGTGTATAAGAGACAG	CGAGCAATCCACTCGAAKRGTTYGATYNTGGCTCAG
27F_D	TCGTCGGCAGCGTCAGATGTGTATAAGAGACAG	GATCAGTCGTCTCACTCGAAKRGTTYGATYNTGGCTCAG
519R_A	GTCTCGTGGGCTCGGAGATGTGTATAAGAGACAG	CGGACTTGATGTACGAACGTNTBACCGCDGCTGCTG
519R_B	GTCTCGTGGGCTCGGAGATGTGTATAAGAGACAG	TCAGTAGCTACGCACGTNTBACCGCDGCTGCTG
519R_C	GTCTCGTGGGCTCGGAGATGTGTATAAGAGACAG	GATTAGCTGCACGTNTBACCGCDGCTGCTG
519R_D	GTCTCGTGGGCTCGGAGATGTGTATAAGAGACAG	ATCAGCAACGTNTBACCGCDGCTGCTG

V4-V5 domains (515F & 806R) (also detect Archeal 16S)

515F_A	TCGTCGGCAGCGTCAGATGTGTATAAGAGACAG	TCGATCGGAGTGCCAGCMGCCGCGGTAA
515F_B	TCGTCGGCAGCGTCAGATGTGTATAAGAGACAG	ATCTGTCATGGAGTGCCAGCMGCCGCGGTAA
515F_C	TCGTCGGCAGCGTCAGATGTGTATAAGAGACAG	CGAGCAATCCACTCGAGTGCCAGCMGCCGCGGTAA
515F_D	TCGTCGGCAGCGTCAGATGTGTATAAGAGACAG	GATCAGTCGTCTCACTCGAGTGCCAGCMGCCGCGGTAA
806R_A	GTCTCGTGGGCTCGGAGATGTGTATAAGAGACAG	CGGACTTGATGTACGAACGGACTACHVGGGTWTCTAAT
806R_B	GTCTCGTGGGCTCGGAGATGTGTATAAGAGACAG	TCAGTAGCTACGCACGGACTACHVGGGTWTCTAAT
806R_C	GTCTCGTGGGCTCGGAGATGTGTATAAGAGACAG	GATTAGCTGCACGGACTACHVGGGTWTCTAAT
806R_D	GTCTCGTGGGCTCGGAGATGTGTATAAGAGACAG	ATCAGCAACGGACTACHVGGGTWTCTAAT

V3-V4 domains	TCGTCGGCAGCGTCAGATGTGTATAAGAGACAG	CCTACGGGNGGCWGCAG
Bac341F	GTCTCGTGGGCTCGGAGATGTGTATAAGAGACAG	GACTACHVGGGTATCTAATCC
Bac785R		
Fungal ITS	TCGTCGGCAGCGTCAGATGTGTATAAGAGACAG	CTTGGTCATTTAGAGGAAGTAA
ITS1F	GTCTCGTGGGCTCGGAGATGTGTATAAGAGACAG	GCTGCGTTCTTCATCGATGC
ITS2R		
Protozoal 18S (V3-V4)		
P-SSU-316F	TCGTCGGCAGCGTCAGATGTGTATAAGAGACAG	GCTTTCGWTGGTAGTGTATT
GIC758R	GTCTCGTGGGCTCGGAGATGTGTATAAGAGACAG	CAACTGTCTCTATKAAYCG

in black: overhangs for appending the Illumina Nextera adaptor sequences
In red: spacers
in bue: target sequence
* all the primers have been modified from their original sources to be compatible with the Illumina platform

Figure A.5 List of primers for 16S/TS rRNA genes amplicons for bacteria, archea, fungi and protozoa. Figure was obtained from (https://mcic.osu.edu/sites/mcic/files/imce/documents/MicrobialrRNAgenesAmpliconPrimers_MCIC.pdf.)

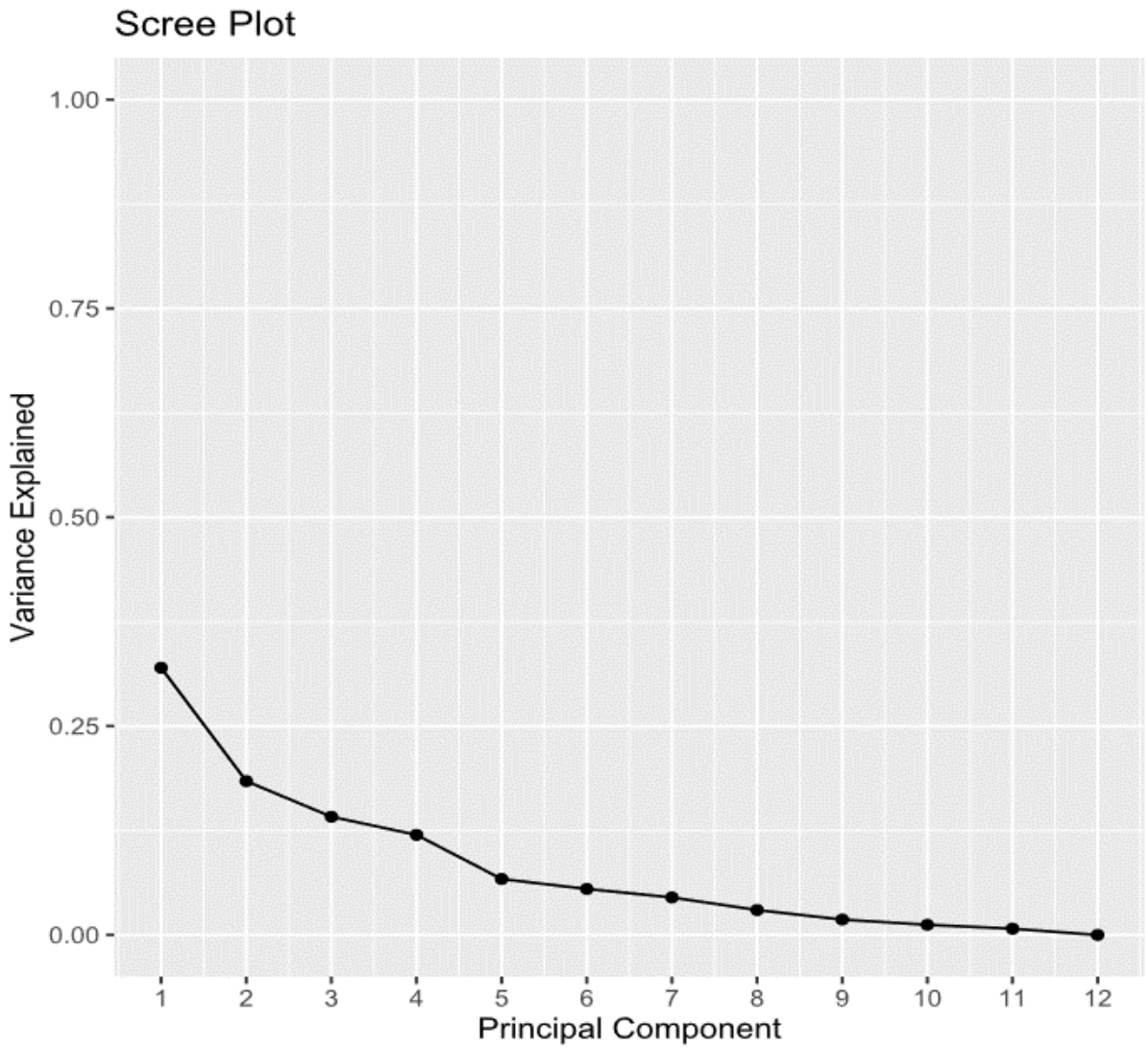

Figure A.6 Scree plot showing the percentage of variance explained by all 12 principal components.